CALVAL-TP
SALP/lot2.C
CLS.DOS/NT/04.280
SALP-RP-MA-EA-21233-CLS

Ramonville, March, 9th 2004

TOPEX/Poseidon validation activities

12 years of T/P data (GDR-Ms)

Contract No 03/CNES/1340/00-DSO310 - lot2.C

	AUTHORS	COMPANY	DATE	INITIALS
PREPARED BY	M.Ablain F.Mertz	CLS CLS		
APPROVED BY	J.Dorandeu	CLS		
QUALITY VISA	M.Destouesse	CLS		
APPROVED BY	P.Vincent N.Picot	CNES CNES		

CLS 810 Rue Hermès Parc Technologoque du Canal 31526 Ramonville StAgne FRANCE
Telephone 33 5 61 39 47 00 / Fax 33 5 61 75 10 14

DISTRIBUTION LIST		
COMPANY	**NAMES**	**COPIES**
CLS/DOS	M.ABLAIN	1 electonic copy
	P.Y.LE TRAON	1 electonic copy
	F.MERTZ	1 electonic copy
	J.DORANDEU	1 electonic copy
	G.DIBARBOURE	1 electonic copy
	F.BRIOL	1 electonic copy
	Y.FAUGERE	1 electonic copy
	V.ROSMORDUC	1 electonic copy
	F.MERCIER	1 electonic copy
DOC/CLS	Documentation	1 electonic copy
CNES	N.PICOT	1 electonic copy
CNES	P.VINCENT	1 electonic copy
CNES	S.COUTIN-FAYE	1 electonic copy
CNES	P.SNINI	1 electonic copy
CNES	J.NOUBEL	1 electonic copy

CLS 810 Rue Hermès Parc Technologoque du Canal 31526 Ramonville StAgne FRANCE
Telephone 33 5 61 39 47 00 / Fax 33 5 61 75 10 14

DOCUMENT STATUS SHEET			
Project Control Initials	**ISSUE**	**DATE**	**REASON FOR CHANGE**
	1.1	December, 23th 2004	Creation
	1.1	March, 9th 2004	Revision

Contents

1 Introduction **2**

2 Missing and edited measurements **4**
2.1 Missing measurements . . . 4
2.2 Edited measurements . . . 6
2.2.1 Editing criteria definition . . . 6
2.2.2 Flagging quality criteria: Radiometer land flag . . . 7
2.2.3 Flagging quality criteria: Ice flag . . . 8
2.2.4 Threshold criteria: Global . . . 9
2.2.5 Threshold criteria: Number and standard deviation of elementary TOPEX altimeter measurements . . . 10
2.2.6 Threshold criteria: Significant Wave Height . . . 11
2.2.7 Threshold criteria: Backscatter coefficient . . . 13
2.2.8 Threshold criteria: TMR wet troposphere correction . . . 14

3 Statistical monitoring **16**
3.1 Background . . . 16
3.2 Comparison of cnes and nasa orbits . . . 16
3.3 Comparison of tidal models . . . 18
3.4 Wet troposphere corrections . . . 19
3.4.1 TMR wet troposphere correction . . . 19
3.4.2 TMR brightness temperatures . . . 20
3.4.3 Comparison of TMR and ECMWF wet troposphere corrections . . . 21
3.5 Ionosphere corrections . . . 23
3.5.1 TOPEX dual-frequency ionosphere correction . . . 23
3.5.2 Comparison of TOPEX dual-frequency and DORIS ionosphere corrections . . . 24
3.6 Significant wave height monitoring . . . 26
3.6.1 Ku-band SWH . . . 26
3.6.2 Comparison of Ku-band and C-band SWH . . . 27
3.7 Backscatter coefficient monitoring . . . 28
3.7.1 Ku-Band Sigma0 . . . 28
3.7.2 Comparison of Ku-band and C-band Sigma0 . . . 29
3.8 Sea state bias corrections (SSB) . . . 30
3.8.1 BM4 and BM3 SSB . . . 30
3.8.2 Non Parametric and BM4 SSB . . . 32
3.9 Waveform-deduced off-nadir angle . . . 33

4 Crossover analysis **34**
4.1 Overall results . . . 34
4.2 Comparison of NASA and CNES orbits . . . 38
4.3 Comparison of tidal models . . . 40
4.3.1 CSR3.0 and FES95.2 . . . 40
4.3.2 GOT99 and CSR3.0 . . . 40
4.4 Comparison of radiometer (TMR) and model (ECMWF) wet troposphere corrections . . . 41
4.5 Comparison of Topex dual-frequency and Doris ionosphere corrections . . . 43
4.6 Comparison of sea state bias corrections (SSB) . . . 45

4.6.1 BM3 and BM4 SSB . . . 45
4.6.2 BM4 and Non-Parametric SSB . . . 46

5 Topex/Poseidon / ERS cross-calibration 47
5.1 SWH cross-calibration . . . 47
5.2 Sigma0 cross-calibration . . . 49
5.3 Topex / ERS radiometer cross-calibration . . . 50

6 Repeat-track analysis 51
6.1 Ocean variability . . . 51
6.2 Mean sea level variations . . . 52
6.2.1 Main results . . . 52
6.2.2 Impact of orbit calculation . . . 55
6.3 Topex/Poseidon relative altimeter bias . . . 56
6.4 Sea level seasonal variations . . . 57

7 Mean Sea Level (MSL) and Sea Surface Temperature (SST) comparisons 70
7.1 SSH definition for each mission . . . 70
7.2 MSL and SST time series over main oceanic areas . . . 71
7.2.1 Methodology . . . 71
7.2.2 Global ocean . . . 72
7.2.3 Monitoring over the Indian Ocean . . . 73
7.2.4 Monitoring on the Northern hemisphere . . . 74
7.2.5 Monitoring on Southern hemisphere . . . 75
7.2.6 Monitoring over the North Atlantic Ocean . . . 76
7.2.7 Monitoring over the South Atlantic Ocean . . . 77
7.2.8 Monitoring over the North Pacific Ocean . . . 78
7.2.9 Monitoring over the South Pacific Ocean . . . 79
7.2.10 Monitoring over the Mediterranean Sea . . . 80
7.2.11 Monitoring over the Black Sea . . . 81
7.3 Spatial MSL and SST slopes . . . 82
7.3.1 Methodology . . . 82
7.3.2 Spatial MSL slopes over Jason-1 period . . . 83
7.3.3 Spatial MSL slopes over Envisat period . . . 84
7.3.4 Spatial SST and MSL slopes for T/P . . . 86

8 Conclusion 87

List of Figures

1 *Percentage of missing measurements relative to a nominal track* 4
2 *Percentage of missing measurements edited by radiometer land flag* 7
3 *Percentage of missing measurements edited by ice flag* 8
4 *Map of edited measurements by ice flag criterion on cycle 370* 8
5 *Cycle per cycle percentage of edited measurements by threshold criteria* 9
6 *Number of TOPEX edited measurements due to too low (< 5) number of valid 10Hz-elementary measurements* 11
7 *Number of TOPEX edited measurements due to too high (> 100 mm) RMS of 10-Hz elementary measurements* 11
8 *Number of TOPEX edited measurements due to too high values of SWH (SWH > 11 m)* . 12
9 *Number of edited measurements due to invalid Sigma0 values* 13
10 *Number of edited measurements due to invalid TMR wet troposphere correction values* . 14
11 *Number of edited measurements due to differences between TMR and ECMWF model greater than 20 cm* 15
12 *Cycle mean (left) and standard deviation (right) of differences between CNES and NASA orbits* 17
13 *Cycle mean (left) and standard deviation (right) of differences between CSR3.0 and GOT99 tide model values* 18
14 *Cycle mean (left) and standard deviation (right) of TMR wet troposphere correction values* 19
15 *Cycle means of 18 GHz (top left), 21 GHZ (top right) and 37 GHz (buttom) TMR brightness temperatures. Annual signals have been filtered out* 20
16 *Cycle mean (left) and standard deviation (right) of differences between TMR and ECMWF wet troposphere corrections* 21
17 *Daily mean of differences between TMR and ECMWF wet troposphere corrections* . . . 22
18 *Cycle mean (left) and standard deviation (right) of TOPEX dual frequency ionosphere correction* 23
19 *Cycle mean (left) and standard deviation (right) of differences between raw TOPEX ionosphere values and filtered values (300 km low pass filter)* 24
20 *Cycle mean (left) and standard deviation (right) of differences between DORIS and TOPEX ionosphere corrections* 24
21 *Differences between DORIS and TOPEX ionosphere corrections as a function of local time* 25
22 *Cycle mean (left) and standard deviation (right) of Ku-band TOPEX SWH* 26
23 *Cycle mean (left) and standard deviation (right) of differences between Ku-band and C-band TOPEX SWH values* 27
24 *Cycle mean (left) and standard deviation (right) of Ku-band TOPEX Sigma0 (10-2 dB)* . 29
25 *Cycle mean (left) and standard deviation (right) of differences (10-2 dB) between Ku-band and C-band TOPEX Sigma0 values* 29
26 *Cycle means of BM3 SSB (top left), BM4 SSB (top right) and Non Parametric SSB correction (bottom)* 30
27 *Cycle mean (left) and standard deviation (right) of differences between BM3 and BM4 SSB corrections* 31
28 *Cycle mean (left) and standard deviation (right) of differences between BM4 and Non Parametric SSB corrections* 32
29 *Cycle mean (left) and standard deviation (right) of waveform-deduced offnadir angle values* 33

30 *TOPEX/Poseidon crossover cycle standard deviation, from cycle 11 to cycle 444. Only crossover differences less than 30 cm are selected* . . . 35
31 *TOPEX/Poseidon crossover standard deviation, when selecting:latitudes between 50S and +50N; low ocean variability areas (ocean variability $< 20cm$); open ocean areas ($depth < -1000m$)* . . . 36
32 *TOPEX/Poseidon crossover standard deviation when using the DORIS ionosphere correction (same as Figure 30 but with DORIS instead of TOPEX ionosphere correction)* . . 36
33 *Geographical pattern (4x4 degree bins) of TOPEX/Poseidon crossover standard deviation (cm), from cycle 11 to cycle 444* . . . 37
34 *Geographical pattern (4x4 degree bins) of the mean of crossover differences, from cycle 11 to cycle 444.* . . . 38
35 *Gain in crossover variance (cm2) when using NASA orbit rather than CNES orbit* . . . 39
36 *Difference in crossover variance (cm2) when using NASA orbit rather than CNES orbit, before use of the ITRF97 set of coordinates in the CNES orbit (top left), with the use of ITRF97 (top right) and with ITRF2000 before (bottom left) and after the orbit change (bottom right)* . . . 40
37 *Difference in crossover means obtained when using NASA and CNES orbits* . . . 41
38 *Gain in crossover variance (cm2) when using the GOT99 tidal correction rather than the CSR3 tidal correction* . . . 41
39 *Gain in crossover variance (cm2) when using the TMR wet troposphere correction rather than the ECMWF correction* . . . 42
40 *Gain in crossover variance (cm2) when using the TMR wet troposphere correction rather than the ECMWF correction* . . . 42
41 *Difference in terms of crossover variance (cm2) when using the TOPEX ionosphere correction rather than DORIS* . . . 43
42 *Comparison of mean crossover differences obtained when using DORIS and TOPEX ionosphere corrections (DORIS TOPEX), with Alt-A cycles (left) and Alt-B cycles (right)* 44
43 *Gain in crossover variance (cm2) when using BM4 SSB correction rather than BM3* . . . 45
44 *Gain in crossover variance (bottom) when using non-parametric SSB correction rather than BM4 SSB with Alt-A cycles (left) and Alt-B cycles (right)* . . . 46
45 *Differences of SWH at 1 hour crossovers between ERS and TP. Except for Poseidon, each point is obtained averaging differences over 12 TOPEX cycles* . . . 48
46 *Differences of Sigma0 at 1 hour crossovers between ERS and TP. Except for Poseidon, each point is obtained averaging differences over 12 TOPEX cycles* . . . 49
47 *Differences of Sigma0 at 1 hour crossovers between ERS and TP. Except for Poseidon, each point is obtained averaging differences over 12 TOPEX cycles* . . . 50
48 *Map of SLA variability (cm) from collinear analysis of T/P data from cycles 11 to 444.* . . . 52
49 *Cycle per cycle monitoring of SLA variability (cm) from collinear analysis of T/P data from cycles 11 to 444.* . . . 52
50 *Mean Sea Level obtained from AVISO M-GDR data (with additive correction). Inverse barometer correction is applied. TMR drift up to beginning of 1997: 1.0 mm/year; Additive Alt-A/B bias value: 0.5 cm; Correction for (DORIS-TOPEX) ionosphere correction drift, for Poseidon cycles after cycle 209* . . . 53
51 *Mean Sea Level obtained from AVISO M-GDR data (with additive correction). Inverse barometer correction is not applied. TMR drift up to beginning of 1997: 1.0 mm/year; Additive Alt-B/Alt-A bias value: 0.5 cm; Correction for (DORIS-TOPEX) ionosphere correction drift, for Poseidon cycles after cycle 209* . . . 54

52 *Difference in MSL estimations using respectively CNES and NASA orbits* 55
53 *(TOPEX Poseidon) SSH relative bias from AVISO M-GDRs (no other correction applied)* 56
54 *Seasonal variations of Jason SLA (cm) for year 1993 relative to a MSS CLS 2001* 58
55 *Seasonal variations of Jason SLA (cm) for year 1994 relative to a MSS CLS 2001* 59
56 *Seasonal variations of Jason SLA (cm) for year 1995 relative to a MSS CLS 2001* 60
57 *Seasonal variations of Jason SLA (cm) for year 1996 relative to a MSS CLS 2001* 61
58 *Seasonal variations of Jason SLA (cm) for year 1997 relative to a MSS CLS 2001* 62
59 *Seasonal variations of Jason SLA (cm) for year 1998 relative to a MSS CLS 2001* 63
60 *Seasonal variations of Jason SLA (cm) for year 1999 relative to a MSS CLS 2001* 64
61 *Seasonal variations of Jason SLA (cm) for year 2000 relative to a MSS CLS 2001* 65
62 *Seasonal variations of Jason SLA (cm) for year 2001 relative to a MSS CLS 2001* 66
63 *Seasonal variations of Jason SLA (cm) for year 2002 relative to a MSS CLS 2001* 67
64 *Seasonal variations of Jason SLA (cm) for year 2003 relative to a MSS CLS 2001* 68
65 *Seasonal variations of Jason SLA (cm) for year 2004 relative to a MSS CLS 2001* 69
66 *MSL and SST over global ocean and over the T/P period* 72
67 *MSL and SST over global ocean and over the Jason-1 period* 72
68 *MSL and SST over the Indian Ocean and over the T/P period* 73
69 *MSL and SST over the Indian Ocean and over the Jason-1 period* 73
70 *MSL and SST on the Northern hemisphere and over the T/P period* 74
71 *MSL and SST on the Northern hemisphere and over the Jason-1 period* 74
72 *MSL and SST on the Southern hemisphere and over the T/P period* 75
73 *MSL and SST on the Southern hemisphere and over the Jason-1 period* 75
74 *MSL and SST over the North Atlantic Ocean and over the T/P period* 76
75 *MSL and SST over the North Atlantic Ocean and over the Jason-1 period* 76
76 *MSL and SST over the South Atlantic Ocean and over the T/P period* 77
77 *MSL and SST over the South Atlantic Ocean and over the Jason-1 period* 77
78 *MSL and SST over the North Pacific Ocean and over the T/P period* 78
79 *MSL and SST over the North Pacific Ocean and over the Jason-1 period* 78
80 *MSL and SST over the South Pacific Ocean and over the T/P period* 79
81 *MSL and SST over the South Pacific Ocean and over the Jason-1 period* 79
82 *MSL and SST over the Mediterranean Sea and over the T/P period* 80
83 *MSL and SST over the Mediterranean Sea and over the Jason-1 period* 80
84 *MSL and SST over the Black Sea and over the T/P period* 81
85 *MSL and SST over the Black Sea and over the Jason-1 period* 81
86 *MSL slopes over Jason-1 period for T/P (left) and Jason-1 (right), MSL slope differences between Jason-1 and T/P (bottom)* 83
87 *MSL slopes over Envisat period for T/P (left), Jason-1 (right) and Envisat (bottom)* . . . 84
88 *MSL slopes differences over Envisat period between Jason-1 and Envisat (left), T/P and Envisat (right) and T/P and Jason-1 (bottom)* 85
89 *T/P MSL and SST slopes over 12 years* 86
90 *Adjustment errors of T/P MSL and SST slopes over 12 years* 86

List of Tables

1 *E*diting criteria 6

1 Introduction

This document presents the synthesis report concerning validation activities of TOPEX/Poseidon under SALP contract (N° 03/CNES/1340/00-DSO310 Lot 2.C) supported by CNES at the CLS Space Oceanography Division.

Since the beginning of the mission, TOPEX/Poseidon data have been analyzed and monitored in order to assess the quality of AVISO M-GDR products (AVISO handbook, 1996 [1]) for oceanographic applications.

This report is basically concerned with long-term monitoring of both instrumental and geophysical parameter statistics, system and algorithm performances, homogeneity between TOPEX and Poseidon altimeters, for more than 12 years of data. Overall results from Sea Surface Height (SSH) analyses (Sea Level Variability (SLA) and Mean Sea Level (MSL) estimations) are also reported, as they are the main objectives of the mission.

T/P and ERS-2 Cross-calibration results are also presented. Indeed, the two altimeter series can be compared on the long term. These results are obtained from OPR-2 data (CERSAT User Manual [17]) and are derived from data quality assessment and intercalibration activities conducted at CLS, under IFREMER/CERSAT contract.
The comparisons with Jason-1 and Envisat measurements are not presented here. These results are included in specific reports to, as part of the CNES/SSALTO activities. However a study about the mean sea level comparisons between T/P, Jason-1, Envisat and Geosat Follow-on has been presented in this document.

The Side-B TOPEX altimeter has been switched on since February 1999 (cycle 236), because Side-A Point Target Response (PTR) changes made the altimeter measurement progressively degrading (Hayne and Hancock, 1998 [23]). It is thus important to compare measurements from A and B TOPEX altimeters in terms of biases, drifts and performances.
Moreover, the 15th of August 2002 (cycle 365), a maneuver sequence was conducted over a period of about 30 days to move T/P to the new Tandem Mission orbit at one half the TP/Jason-1 track spacing to the West of Jason-1. As a result, the T/P orbit is not repetitive from cycle 365 (pass 111 included) to cycle 368 (pass 172 included) and no nominal track is available during this period.

Finally, after the successful launch of Jason-1, a synthesis study about the whole T/P mission seems particularly useful. More than 12 years of T/P data represent the reference altimeter mission, with the objective of continuous SSH observations for the long term. All results (except data coverage analysis) are obtained after data selection corresponding to editing criteria described in Le Traon et al., 1994 [31]. However, T/P data have been updated with new corrections (applied on Jason-1 products), but with no change in the threshold criteria:

- GOT99 tidal correction used instead of CSR3 tidal.
- Time variable reference pressure used for the Inverse Barometer (IB) correction.

Moreover a new criterion has been added to take into account the interpolation anomalies of the TMR

correction (section 2.2.8). The number of edited measurements, for each criterion, is first analyzed as a function of time. Then a statistical monitoring of different parameters is achieved. Crossover analysis allows estimations of system performances and comparisons of redundant corrections. Finally repeat-track analysis allows performing MSL estimations, to compute the relative bias between TOPEX and Poseidon altimeters and to estimate the ocean variability.

2 Missing and edited measurements

2.1 Missing measurements

Missing measurements relative to the nominal track have been monitored during the last years. It allows detection of coverage anomalies, particularly due to altimeter problems.
The number of missing measurements over ocean has been plotted on figure 1 from cycle 10) to cycle 444. This figure also includes events as Single Event Upsets (SEU) or altimeter tests, appearing as isolated peaks of missing measurements. Notice that the number of missing measurements is not computed from cycle 365 to 368 because no reference track can be used during the T/P orbit change.

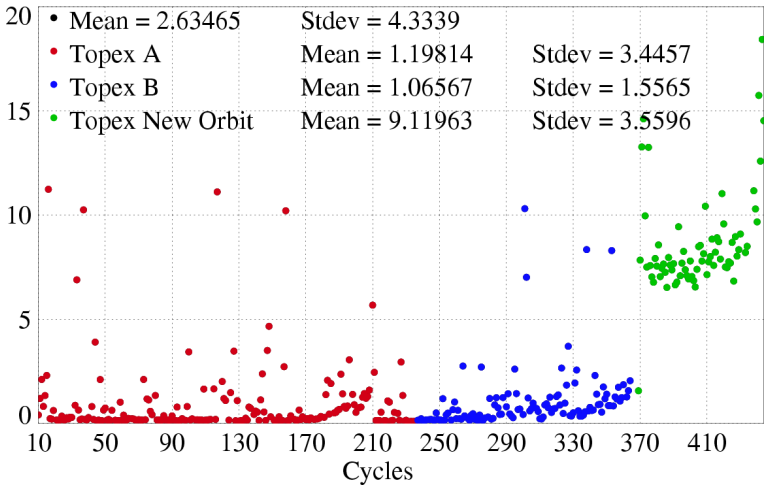

Figure 1: *Percentage of missing measurements relative to a nominal track*

The figure shows a first large increase of the number of missing measurements until cycle 212. From cycle 178 to cycle 212, one of the three tape recorders onboard the satellite (B tape recorder) exhibited anomalous behavior and caused data losses. Then it was decided to not use this tape recorder, switching to a 2-tape recorder functioning mode. Unfortunately, short missing portions of tracks began again to be detected in missing measurements plots (AVISO/CALVAL report, cycle 267 [2]) and the A tape recorder was identified as the cause of these failures (T/P daily status [43]). In order to ensure a proper data acquisition, it was decided to conduct some engineering tests on tape recorder B (TR-B). It has been demonstrated that the unit will operate well within a certain range of tape speeds. This could enable data storage for a two to four hour period on this recorder (T/P daily status [44]). During the past year, tape recorder functioning has continued to degrade. Tape recorder A (TR-A) operations were modified on July 2001 (T/P daily status [45]) as it was previously the case for TR-B. In September 2001, after performance of TR-B had degraded to the point that it could no longer be used in a normal operation mode, it was decided not to use it (T/P daily status [46]).
Then TR-B was again used in low tape speed mode, but other degradations on both TR-A and B (see above) has caused the number of missing measurements remain at a higher level during the year 2001. However, in the worst case of cycle 210, the number of missing measurements does not exceed 1.3 % of

valid data.
From about cycle 340 onwards, the number of missing measurements rises slightly up to the same level as during cycles 190-210. This is due once again to degradations of tape recorders. But from September 2002 (cycle 370 onwards), more significant anomalies with tape recorders are observed. As a result, a lot of data gaps are present, especially in the Indian Ocean and in the Pacific Ocean close to the South America. From cycle 370 to 375, the number of missing measurements increases up to 14 %, and between 375 and 400, it remains almost stable between 7% and 8%. From cycle 400 to 444, the tape recorder performances has continued to decline. Thus it was decided on cycle 444 to remove from service the tape recorder. Science data recovery requirements will now be met through increased TDRSS (Data relay Satellite System) real-time contacts.
Notice that no data is available for cycle 118, 430 and 431 due to 2 safe hold modes. These missing measurements have not been taken into account in the figure 1 and in the global percentage of missing measurements.

2.2 Edited measurements

2.2.1 Editing criteria definition

Editing criteria (Le Traon, 1994 [31]) have been used to select valid measurements over ocean. For each criterion, the percentage of edited measurements (relative to the total number of present measurements) has been monitored. This allows us to detect trends in the number of removed data, which could come from instrumental, geophysical or algorithmic changes.
The editing criteria are divided into 3 parts. First, the quality criteria concern the flags. Secondly, threshold criteria are applied on altimeter, radiometer and geophysical parameters and are described in the table 1 for TOPEX . Moreover, a spline criterion is applied to remove the remaining spurious data. These criteria are also defined in AVISO and PODAAC User handbook for the GDR product.

Parameter	Min thresholds	Max thresholds	mean removed
Sea surface height	$-130\ m$	$100\ m$	0.18%
number measurements of range	5	$Not\ applicable$	0.33%
standard deviation of range	0	$0.1\ m$	1.13%
Off nadir angle	$0\ deg$	$4\ deg$	3.52%
Dry troposphere correction	$-2.5\ m$	$-1.9\ m$	0.00%
Inverted barometer correction	$-2.0\ m$	$2.0\ m$	0.001%
TMR wet troposphere correction	$-0.5m$	$-0.001\ m$	0.97%
Ionosphere correction	$-0.4\ m$	$0.04\ m$	0.66%
Significant waveheight	$0.0\ m$	$11.0\ m$	0.13%
Sea State Bias	$-0.5\ m$	$0.0\ m$	0.28%
Ku-band Sigma0	$7\ dB$	$30\ dB$	0.30%
Ocean tide	$-5.0\ m$	$5.0\ m$	0.14%
Earth tide	$-1.0\ m$	$1.0\ m$	0.00%
Pole tide	$-15.0\ m$	$15.0\ m$	0.00%
TMR and ECMWF model differences	$-0.2\ m$	$0.2\ m$	0.32%

Table 1: *E*diting criteria

2.2.2 Flagging quality criteria: Radiometer land flag

The percentage of edited measurements using the radiometer land flag is plotted as a function of the cycle number in figure 2. The mean percentage is close to 29% with a dominant annual signal.
Probably due to the interpolation problem with the TMR (see section 2.2.8), some measurements have radiometer land flag unset over land. This has no impact on the valid data because these measurements have been edited by the altimetric parameter criteria. However, this anomaly leads to wrong statistics of the edited measurements. Therefore a new criterion has been added to the editing procedure to remove all the measurements for which the radiometer land flag is set to ocean when the altimeter land flag is set to land. This can be explained why the percentage of edited measurements has been decreased by 1% from cycle 370 and the percentage of edited measurements higher than usual on cycle 437 (35%).

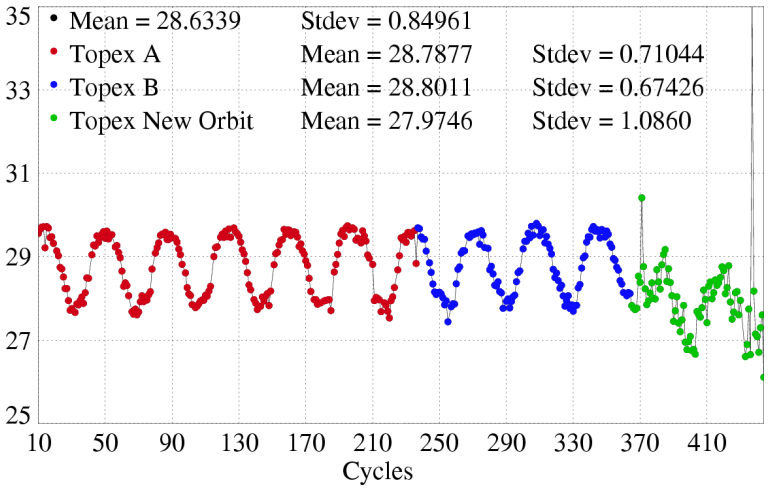

Figure 2: *Percentage of missing measurements edited by radiometer land flag*

2.2.3 Flagging quality criteria: Ice flag

The same kind of plot has been performed for the ice flag (figure 3 3). It shows no anomalous trend but a dominant annual cycle : the maximum number of points over ice is reached during the northern fall.
The ice flag edited measurements are plotted in Figure 4 for one cycle.

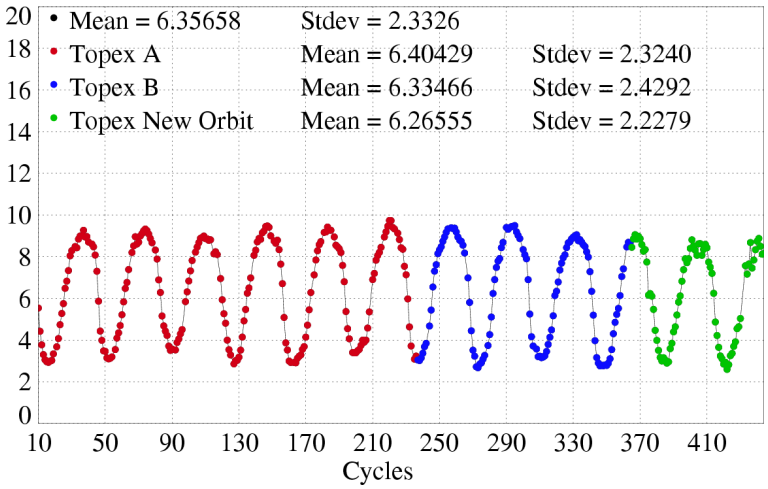

Figure 3: *Percentage of missing measurements edited by ice flag*

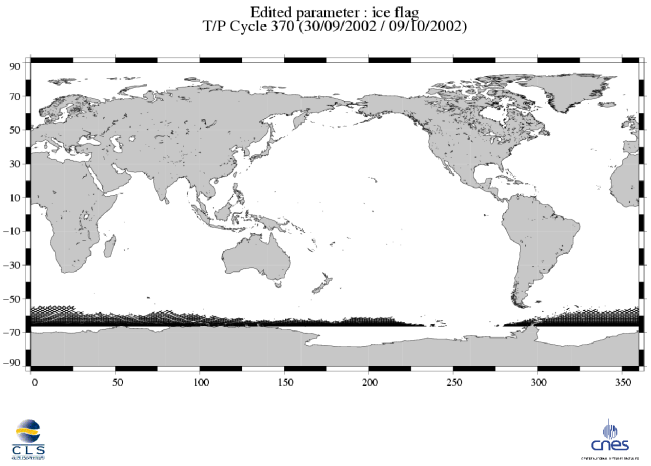

Figure 4: *Map of edited measurements by ice flag criterion on cycle 370*

2.2.4 Threshold criteria: Global

Instrumental parameters have also been analysed from comparison with thresholds, after having applied flagging quality criteria (land and ice flag). Notice that no measurements are edited by the following corrections : dry troposphere correction, inverted barometer correction, equilibrium tide, earth tide pole tide and earth tide pole tide.
The percentage of measurements edited using each criterion has been monitored on a cycle per cycle basis (figure **??**). The mean percentage of edited measurements is about 4.2% from cycle 10 to cycle 369. The percentage increases to about 7% from cycle 370 onwards due to the radiometer wet tropospheric correction (see section 2.2.8).
The percentage of edited measurements is higher than 10% from cycle 433 to 437. This is due to a pitch wheel event linked to the T/P safehold mode occurred from cycle 430 to 432 (see electonic communication : T/P Daily Status (26/07/2004). Consequently, the satellite had a strong mispointing during this period and the altimeter mesurements were impacted.
Besides, an annual cycle is visible due to the seasonal sea ice coverage in the northern hemisphere. Inddeed most of northern hemisphere coasts are without ice during northern hemisphere summer. Consequently some of these coastal measurements are edited by the thresholds criteria in summer instead of the ice flag in winter. This seasonal effect visible in the statistics is not balanced by the southern hemisphere coasts due to the shore distibution between both hemispheres.

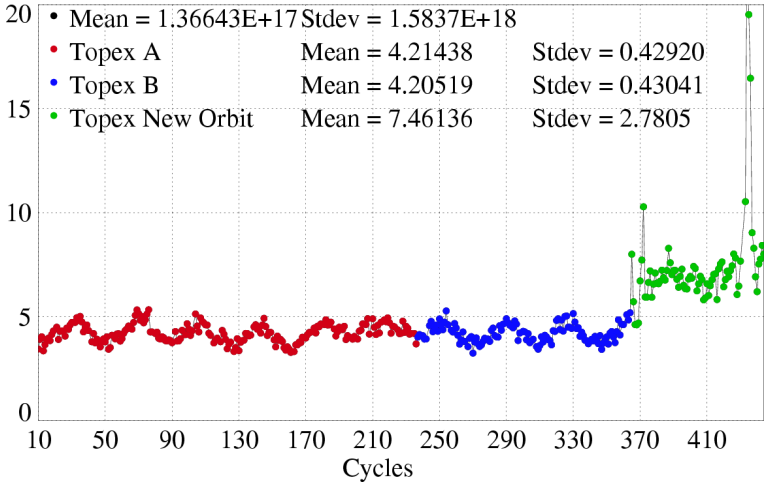

Figure 5: *Cycle per cycle percentage of edited measurements by threshold criteria*

2.2.5 Threshold criteria: Number and standard deviation of elementary TOPEX altimeter measurements

Figure 6 and figure 7 respectively show the percentage of removed measurements due to the number and the standard deviation of elementary TOPEX altimeter measurements.
The number of edited points due to too few (< 5) 10-Hz elementary measurements increases from around cycle 150 to the last Alt-A cycle (235). This reveals altimeter changes, and can be attributed to observed modifications in the Alt-A PTR.
In the first Alt-B cycles, high variations are observed in the percentage of edited measurements due to this criterion. Then the value abruptly decreases to the same level as the one obtained in the first Alt-A cycles. This could be explained by land/sea transition problems detected in the first Alt-B cycles with non negligible portions of passes impacted (Dorandeu et al., 2001 [14]). During the first Alt-B cycles, some small differences in the Side-B noise signal caused the Alt-B not to recognize it has lost the signal as quickly as Alt-A (David Hancock, internet communications [20] and [21]). Flight tracker software and parameters were the same for both Side-A and Side-B, whereas different tuning of Alt-B parameters should have been performed.
During cycle 256 (Poseidon cycle), a safe-hold incident occurred on the TOPEX/Poseidon platform with the result that the TOPEX altimeter was powered off during most of this cycle. This event seems to have made the Alt-B characteristics evolve, according to the number of edited measurements after the incident. Indeed after cycle 256, such land/sea transitions problems do not occur anymore (Hayne and Hancock 2000 [24]). Note that the percentage of edited measurements is higher than usual for cycles 365, 366 and 368. This might be due to the maneuvers to change the T/P orbit. Then the value remains stable with the new T/P orbit from cycle 369 onwards, at the same level as in the beginning of the mission.
Approximately the same behavior is noticed for the standard deviation of 10 Hz elementary measurements (Figure 7): increase of Alt-A edited measurements after cycles 130-150, high values for the first Alt-B cycles, then lower values after the platform safe-hold. An annual signal is observed due to ice seasonal variations.
As previously, the percentage of edited measurements is higher than usual from cycle 433 to 437 : this is due to a strong mispointing as a result of a pitch wheel event (see section 2.2.4).

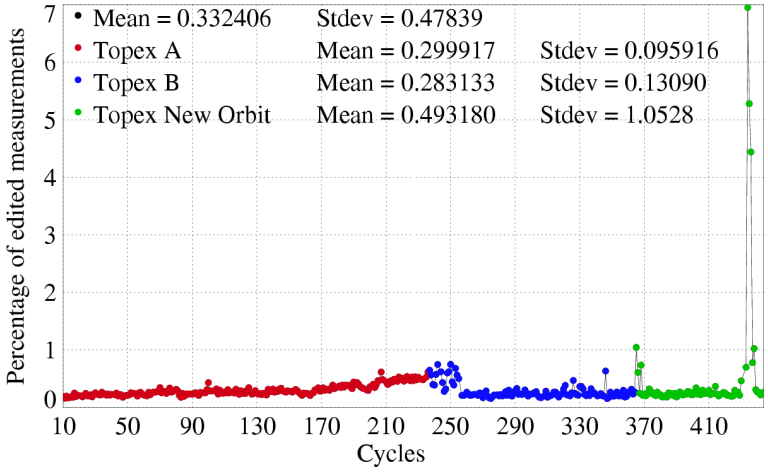

Figure 6: *Number of TOPEX edited measurements due to too low (< 5) number of valid 10Hz-elementary measurements*

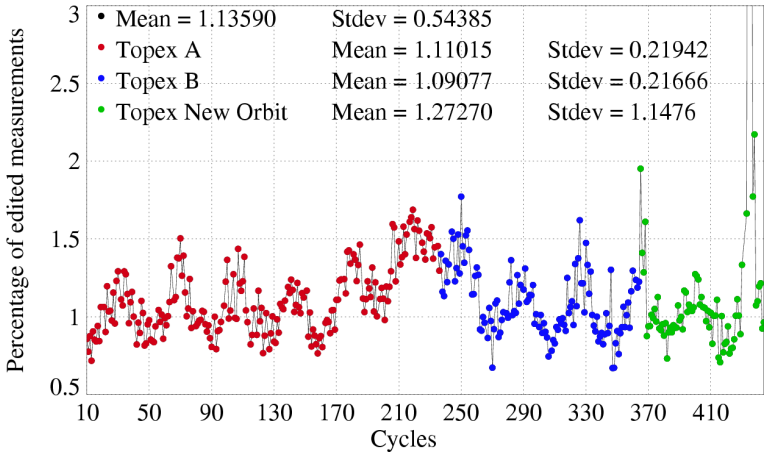

Figure 7: *Number of TOPEX edited measurements due to too high (> 100 mm) RMS of 10-Hz elementary measurements*

2.2.6 Threshold criteria: Significant Wave Height

Significant Wave Heights higher than 11 m are removed during the editing process. The number of edited measurements using this criterion has been plotted on Figure 8. The Alt-A SWH has increased from early in the mission, as it was first detected by Queffeulou (1998) [38] in his comparison of TOPEX and ERS SWH. This instrumental problem has been described in (Hayne and Hancock, 1998 [24]): the Point Target Response (PTR) changes account for most of the increase in the TOPEX SWH estimate. Though low values of SWH are more impacted than high values, it explains why more data are edited in the last Alt-A cycles. With Alt-B, the number of edited measurements due to SWH value recovers the same level as Alt-A in the beginning of the mission. Notice that Alt-B land/sea transition problems from cycle 236 to cycle 255 are less sensitive for this criterion, since SWH values are set to zero for these

anomalous measurements. Note that slightly higher percentages of edited measurements are obtained from cycle 365 to 368, probably due to the maneuvers to change the T/P orbit.
As previously, for the number and standard deviation of elementary altimeter measurements, the percentage of edited measurements is higher than usual from cycle 433 to 437 : this is due to a strong mispointing as a result of a pitch wheel event (see section 2.2.4).

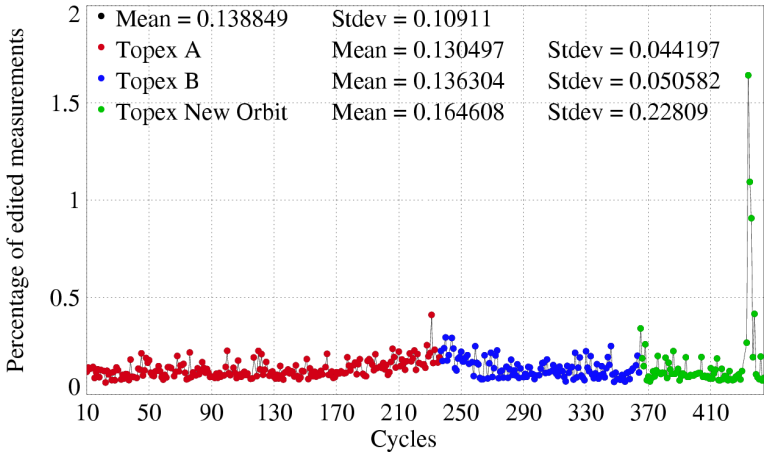

Figure 8: *Number of TOPEX edited measurements due to too high values of SWH (SWH > 11 m)*

2.2.7 Threshold criteria: Backscatter coefficient

The same kind of statistical monitoring has been performed for the Ku-band Backscatter Coefficient (Ku Sigma0) (Figure 9) : it shows again a particularly high number of edited measurements during Alt-B land/sea transition failures, because the Sigma0 parameter is set to a default value in the M-GDR product during these events. Like for the other altimeter criteria, more anomalous Sigma0 values are detected during the T/P orbit transitions (cycles 365-368) and as a result of a pitch event between cycles 433 and 437.

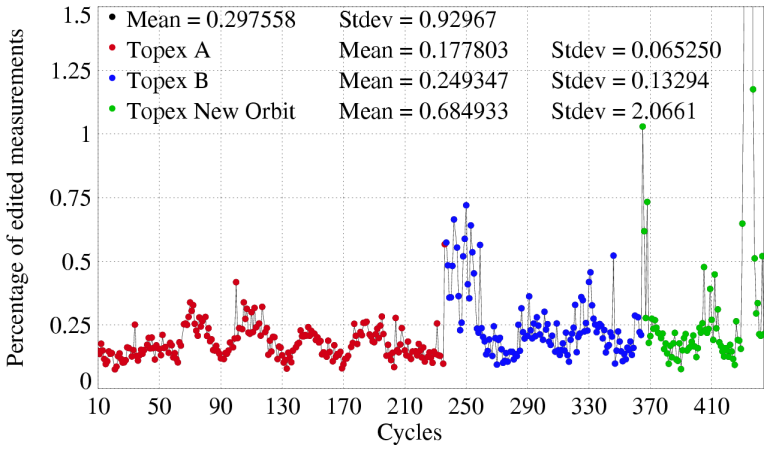

Figure 9: *Number of edited measurements due to invalid Sigma0 values*

2.2.8 Threshold criteria: TMR wet troposphere correction

The number of edited measurements using the radiometer wet tropospheric correction criterion is plotted on Figure 10. Apart from seasonal variations, larger numbers are obtained and those are correlated with the number of missing measurements. Indeed, data gaps cause anomalous values of brightness temperatures and wet correction at the altimeter time tag, because of bad interpolation in the TMR processing, when data are missing. This explains why the number of edited measurements due to the wet troposphere criterion increases during tape recorder problems.

The first anomalies appear between cycle 190 and 210 with a percentage of edited measurements about twice higher than usual (0.8 %). As mentioned previously, one of the three tape recorders onboard the satellite (B tape recorder) exhibited anomalous behavior and caused data losses. Then, during year 2001, some cycles exhibit a percentage of edited measurements just below 1%. This is due to other degradations on both TR-A and B (see section 2.1). But the more important anomalies appear from cycle 370 onwards. Indeed the percentage of edited measurements reaches 6% on cycle 370, then remains stable, around 3-4%. These significant figures can still be explained by tape recorder failures occurring more often than in the past.

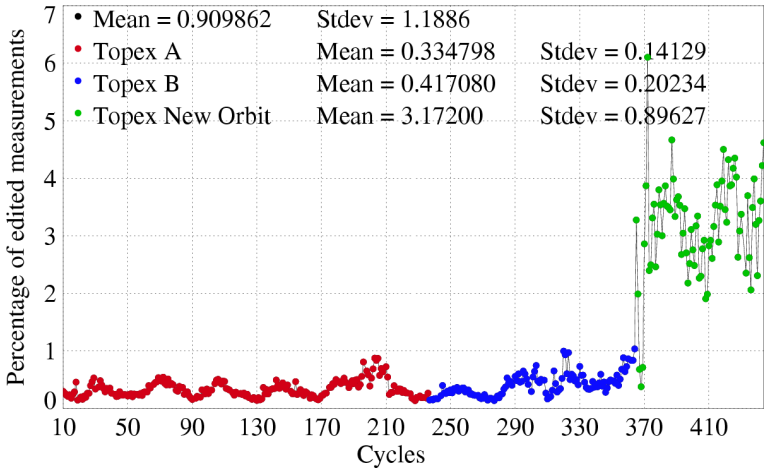

Figure 10: *Number of edited measurements due to invalid TMR wet troposphere correction values*

Despite the comparison to thresholds, some bad TMR corrections are still present in the selected dataset. Thus, since cycle 365, a new criterion has been added in the editing procedure to remove all measurements for which the difference between the TMR and the ECMWF model wet troposphere corrections is greater than 20 cm. 0.3% of the measurements are edited on average by this new criterion (Figure 11). After applying this procedure, only a few bad TMR corrections remain. Notice that positive values of TMR wet tropospheric correction are flagged (Geo_Bad flag) in the new TOPEX processing system (version 6.3) since cycle 218. It is recommended to discard zero values also (Callahan, 1998 [5]).

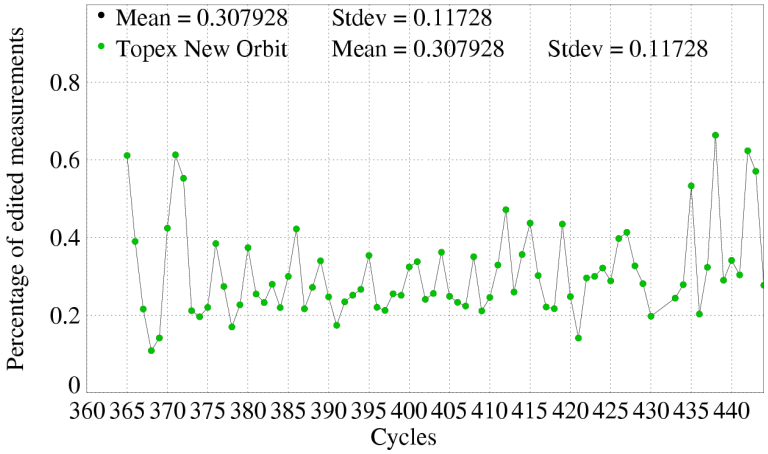

Figure 11: *Number of edited measurements due to differences between TMR and ECMWF model greater than 20 cm*

3 Statistical monitoring

3.1 Background

Both mean and standard deviation of T/P data main parameters have been monitored since the beginning of the mission. In particular, it is important to analyze the differences between corrections of the same type as a function of time, and to estimate the differences between Alt-A and Alt-B TOPEX altimeters. Only valid points (according to editing criteria) are used to analyze the behavior of these parameters over a long time series.

3.2 Comparison of cnes and nasa orbits

Figure 12 displays comparisons between the two types of the radial components of the GDRM precise orbits. The mean and the standard deviation of (CNES orbit NASA orbit) differences are plotted as a function of the cycle number.
The cycle mean of the difference remains almost constant (about 5 mm) until around cycles 120-130. Then, a trend is observed up to cycle 246. Finally the mean difference returns to lower values after cycle 247. The differences are particularly low after cycle 320.

Different strategies have been applied by the two entities in terms of reference frame: in the NASA processing, horizontal velocities have been accounted for to allow station positions evolving with time, while the CNES processing, estimating at the beginning of 1996 that horizontal velocities were not sufficiently well known, chose to work with a fixed reference frame during a given period (with the open possibility to change the reference frame in accordance with oceanographic requirements). From cycle 247 to cycle 320, the ITRF97 set of station coordinates has been taken into account in the CNES orbit computation, explaining the jump on cycle 247. Following the recommendation of the Miami SWT POD meeting, the reference frame was again switched from ITRF97 to ITRF2000 starting with cycle 320. Advantage of this transition was also taken to turn on the albedo model in the CNES orbit calculation. This reduces the mean radial differences between CNES ad NASA orbits (Berthias, 2001 [3]).

The non homogeneity of the terrestrial reference frames explains the trend detected in the difference between the two orbits (Morel et al., 1998 [36]). It can be roughly expressed as a z-axis coordinate drift between the two orbits (Dorandeu, 1998 [11]). Note that global (that is, with no land/sea mask applied) differences between the two orbits would not lead to such a result since northern and southern hemispheres should compensate each other. In our analysis, only ocean data are considered and the Southern hemisphere is thus more sampled. The actual impact of orbit differences in terms of Mean Sea Level (MSL) estimation will be analyzed in the dedicated MSL section (section 6.2.2).

The same features can also be noticed in the standard deviation of the difference. While it was less than 1.5 cm RMS during the first 3 years, it raised through the 3 following years, up to 2.5 cm RMS around cycle 220. One part of this greater value can be attributed to the z-axis coordinate drift between the two orbits. Indeed, after the ITRF97 set of coordinates is used in the CNES orbit calculation, the standard deviation of the differences between the two orbits ranges again between 1 and 2 cm RMS. The particular value of cycle 256 is mainly due to some NASA orbit degradation (after the satellite safe hold mode). After the use of both ITRF2000 reference frame and albedo model in the CNES orbit, differences

between the two orbits are now reduced to less than 1.5 cm rms.

From cycle 360 onwards, ITRF2000 reference frame has been applied on NASA orbit and the two orbits have been particularly consistent as of this cycle.

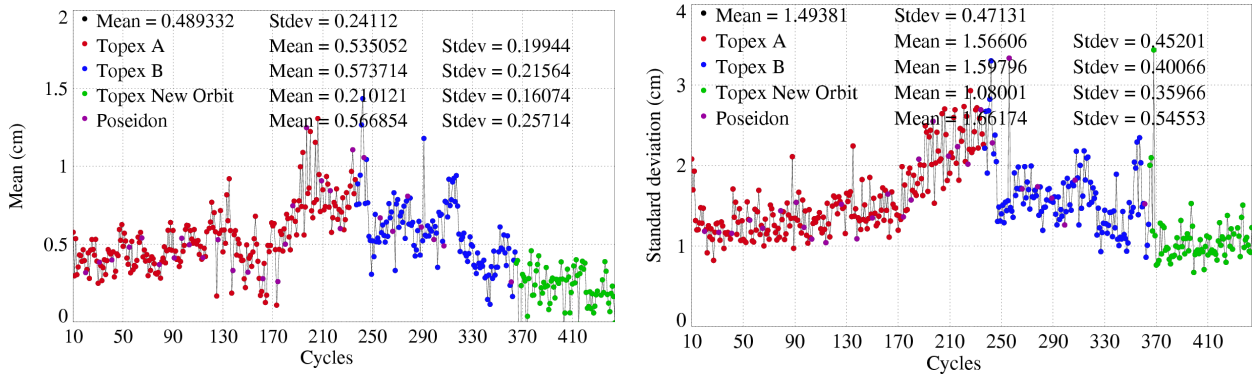

Figure 12: *Cycle mean (left) and standard deviation (right) of differences between CNES and NASA orbits*

3.3 Comparison of tidal models

The GOT99 tidal model has been computed to update the T/P product. Both cycle mean and standard deviation of the (CSR3.0 GOT99) differences are plotted on Figure 13. It shows a very close to zero mean difference. Thus using either of the two models introduces no bias. The standard deviation is about 3 cm RMS, with annual variations probably due to seasonal coverage of areas where tide models are less efficient (AVISO/CALVAL yearly report, 1997 [12]). The performances of the two models for correcting T/P altimeter data are analyzed in the dedicated section 4.3.2.

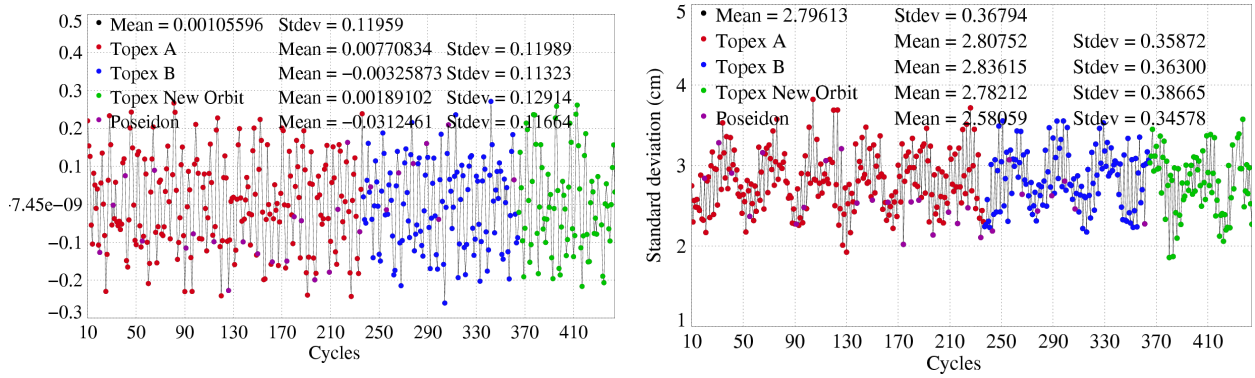

Figure 13: *Cycle mean (left) and standard deviation (right) of differences between CSR3.0 and GOT99 tide model values*

3.4 Wet troposphere corrections

3.4.1 TMR wet troposphere correction

The mean and the standard deviation of the correction are plotted on Figure 14. Apart from large seasonal variations, the long data series allows to notice some general features in the correction. The mean correction seems to drift by about 1.2 mm/year from the beginning to early 1997 (cycle 160). Then one year of data seems to be affected by a moisture increase (greater correction in absolute value). The last 5 years remain approximately at the same level as before the particular 1997-1998 episode, even though the mean decreases at the end.

The standard deviation evolution also reveals a particular behavior from mid-1997 to the end of 1998. As both mean and standard deviation recover the same values as before, these changes might be attributed to geophysical modifications (during the last 1997-1998 El Niño).

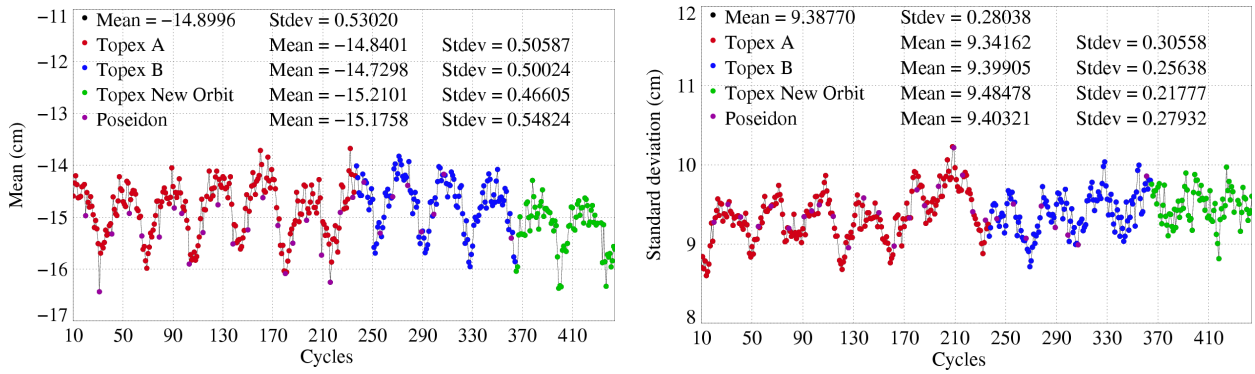

Figure 14: *Cycle mean (left) and standard deviation (right) of TMR wet troposphere correction values*

Many studies from different authors have been carried out on TMR troposphere correction. A synthesis of preliminary conclusions from these different works can be found in Keihm et al., 2000 [30], in addition to own studies based on comparisons relative to SSMI measurements, radiosonde comparisons and an analysis of the coldest measured TMR antenna temperatures. Keihm et al. concluded that a drift of about 1.3-1.4 mm/year is present in the TMR correction from the beginning of the mission to late 1996. This is corroborated by others studies and simple statistics (this study). They also detected some changes probably due to the 1997-1998 El-Niño event, SSMI and TMR measurements being somewhat differently impacted during this period. The authors checked the origin of the drift analyzing the coldest measured TMR antenna temperatures. They identified this trend as a hardware drift in the TMR 18-GHz channel.

3.4.2 TMR brightness temperatures

It is thus interesting to plot the cycle mean of the three TMR brightness temperatures (Figure 15) after removing annual variations. These global averages account for all brightness temperature scales and then potentially reflects any possible trend in either atmospheric or ocean surface parameters, contrary to what has been done by Keihm et al. with their cold data subset. However, Figure 15 (top on the feft) clearly shows a drift in the 18-GHz channel, consistent to the previously cited study. Drifts can be deduced from 21 and 37 GHz channels, probably also linked to geophysical changes.

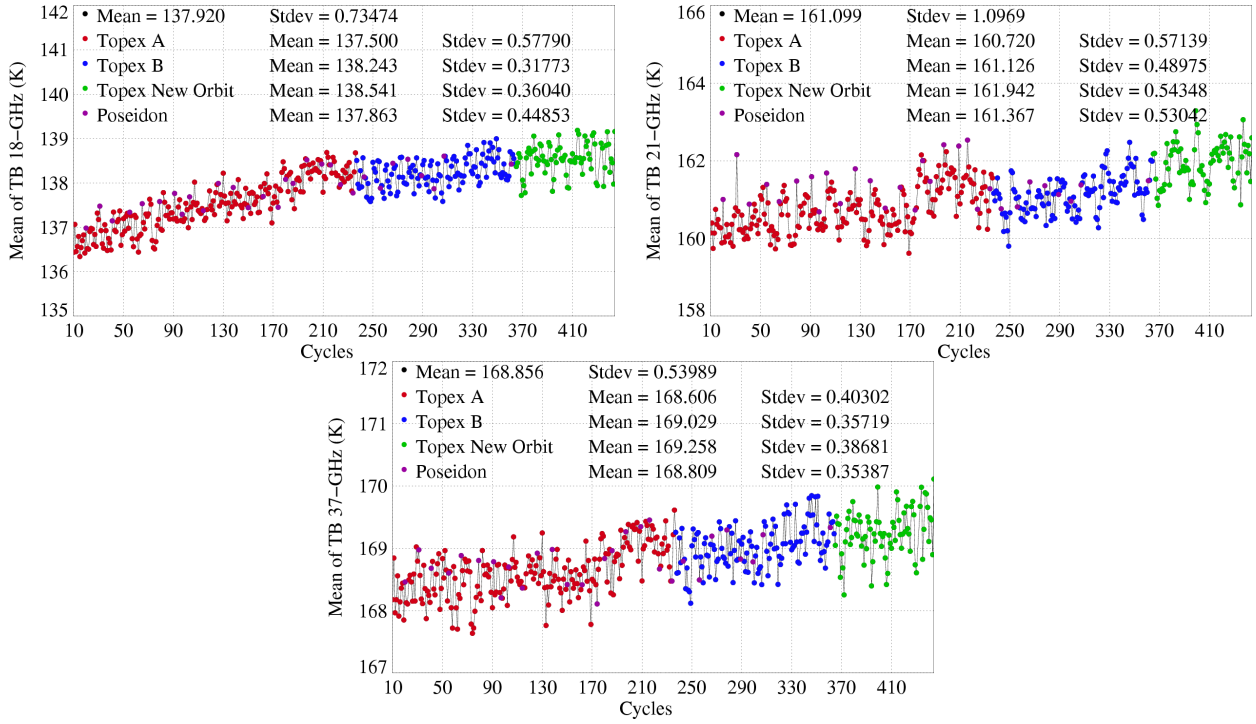

Figure 15: *Cycle means of 18 GHz (top left), 21 GHZ (top right) and 37 GHz (buttom) TMR brightness temperatures. Annual signals have been filtered out*

3.4.3 Comparison of TMR and ECMWF wet troposphere corrections

Figure 16 compares the two types of troposphere corrections. Significant variations are observed on the long term monitoring of the cycle mean.
The first change that occurred at cycle 82 is due to the assimilation of TOVS data during modeling.
Secondly, a gap is observed at cycle 192 and is due to the improvement of the wet troposphere correction calculation at Météo-France, that allowed to minimize a scale error. After this processing change, the cycle mean difference between TMR and ECMWF corrections is about zero. Notice that because of the use of a simplified formula for the refraction index in the model correction computation, the GDR-M model wet correction should be multiplied by 3.815 / 3.746 to recover a correct value. But this would only change the model values by less than 2% (about 3 mm on average).
Then, another gap is observed at cycle 340. The change is due to an improvement of the ECMWF model. After this processing change, the cycle mean difference between TMR and ECMWF corrections is about 7 mm. But notice if the TMR drift correction from Ruf is applied (Ruf, 2002 [39]), the bias is close to 0.

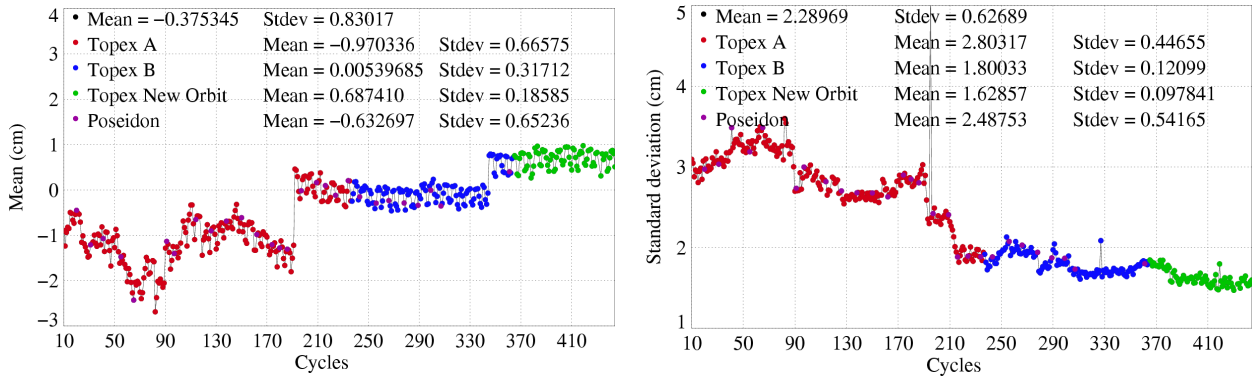

Figure 16: *Cycle mean (left) and standard deviation (right) of differences between TMR and ECMWF wet troposphere corrections*

These major processing changes in the model correction calculation are also noticed in the standard deviation of the difference between the two corrections. The standard deviation has continuously decreased for the whole T/P mission from about 3-3.5 cm rms at the beginning to 1.5 cm rms at the end, showing the improvements made to the model.

Moreover, irregular variations are observed between the two corrections. Yaw mode transitions impact the TMR correction since the beginning of the mission. The long term monitoring of the daily differences during 18 months (plotted on Figure 17) illustrates the impact of the "yaw modes". Note that the amplitude of the signal is about 5 mm with a period of 2 months.

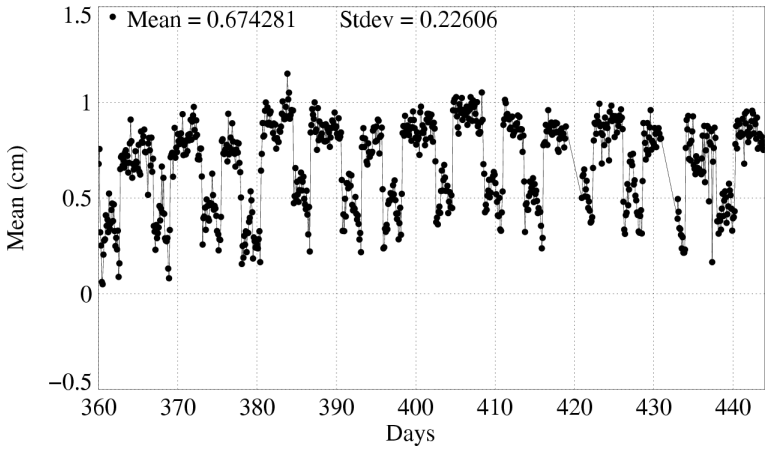

Figure 17: *Daily mean of differences between TMR and ECMWF wet troposphere corrections*

3.5 Ionosphere corrections

3.5.1 TOPEX dual-frequency ionosphere correction

Cycle by cycle statistics of the dual frequency ionosphere correction are presented on Figure 18. Apart from annual variability, the rises and falls in the mean and standard deviation are mainly due to sunspot activity variations. Last years, from 2001, exhibit large solar activity (Blusson, 2002, [4]). This directly impacts the ionospheric correction.

Notice that there is no gap between Alt-A and Alt-B cycle means (before cycle 235 and after cycle 236), as it was one of the goals of the Alt-B calibration phase (AVISO/CALVAL SideB TOPEX altimeter evaluation, 1999 [13]).

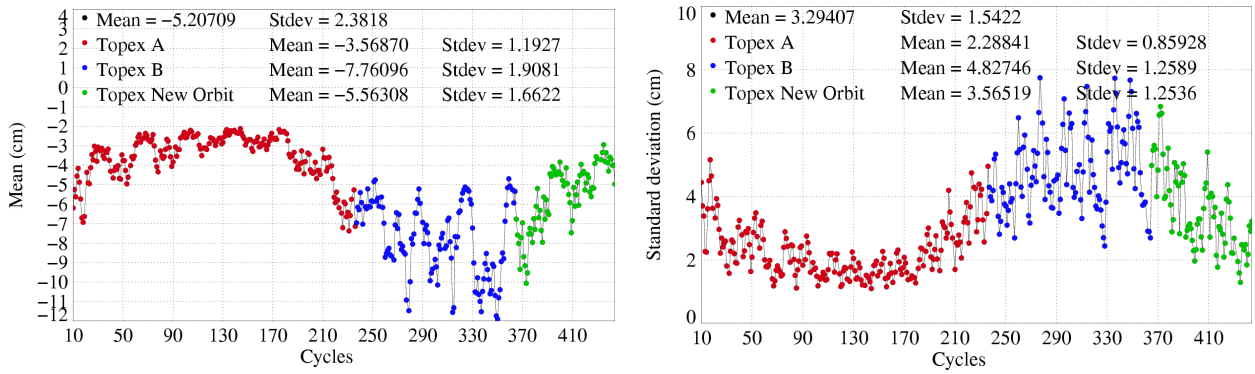

Figure 18: *Cycle mean (left) and standard deviation (right) of TOPEX dual frequency ionosphere correction*

Furthermore, note that the orbit change from cycle 365 onwards has no impact on the dual-frequency ionosphere correction. The dual-frequency ionosphere correction is routinely filtered, with a 300 Km wavelength cut-off (low-pass filter), in order to reduce the noise of the correction. Statistics of the difference between before filtering and after filtering are plotted on Figure 19. The standard deviation increases until cycle 235 (last Alt-A cycle), from 6.3 to 7.2 mm RMS. It denotes a rising noise of the dual-frequency correction, probably linked to altimeter degradation. After the Alt-B switching on, same values as in the beginning of the mission are obtained for both mean and standard deviation. No trend can be detected in the Alt-B statistics from cycle 236 to cycle 444.

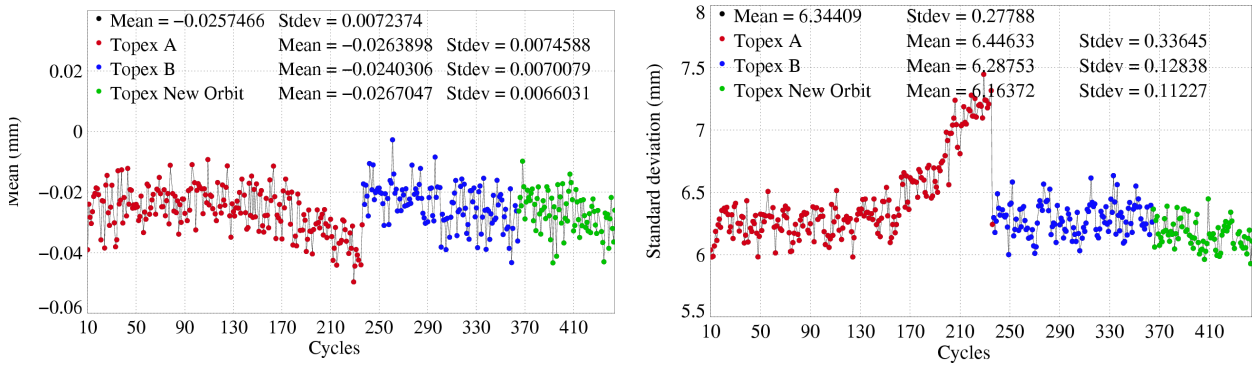

Figure 19: *Cycle mean (left) and standard deviation (right) of differences between raw TOPEX ionosphere values and filtered values (300 km low pass filter)*

3.5.2 Comparison of TOPEX dual-frequency and DORIS ionosphere corrections

Both mean and standard deviation of the difference between DORIS and TOPEX dualfrequency corrections are plotted on Figure 20. A mean value of about 1 cm is obtained during the first 5 years. But after, the cycle mean difference exhibits larger variations and increases (in absolute value) by about 0.5 cm. The mean difference between TOPEX and DORIS corrections is correlated to the sunspot activity : the mean difference increases when the ionosphere correction increases and conversely. This may be explained by a lower ability of the DORIS correction to retrieve large and quick variations which are more intense in case of high solar activity. The end of the period (after cycle 350) corresponds to the beginning of the solar activity decrease, the two kinds of corrections becoming more consistent.

The standard deviation of the difference is also impacted: it increases by about 1 cm RMS in high solar activity periods, showing that variations between the two corrections are not a simple increasing bias.

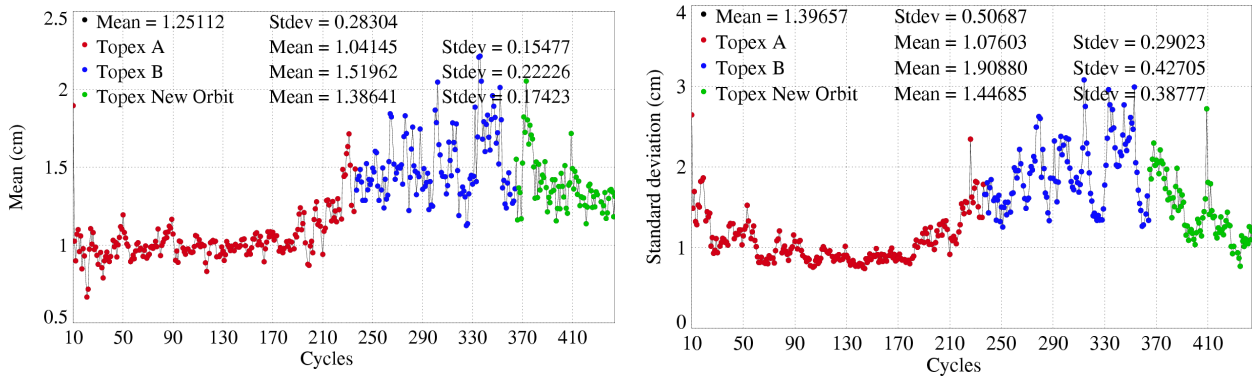

Figure 20: *Cycle mean (left) and standard deviation (right) of differences between DORIS and TOPEX ionosphere corrections*

In order to assess the evolution of the discrepancies between the two corrections, the mean differences have been computed according to several local time intervals of 4 hours. The computation has been performed through the entire mission. Each cycle gives an estimate of the mean difference between DORIS and TOPEX corrections for every local time interval. Averages each year have been computed and leads to the results plotted in figure 21.
While differences between DORIS and TOPEX corrections remain almost stable in the years 1993 1997 for all local times, the differences increase since 1997, particularly for local times ranging from 10 a.m. to 6 p.m. In 2000 and 2001, the mean difference has increased by about 8 mm for local times between 10 a.m. and 2 p.m. In 2004 and 2003, the mean difference has decreased for local times between 6 a.m. and 18 p.m. In 2004, the difference remain almost stable for all local times.
The shape of the increase in the mean difference follows the shape of the Total Electronic Content, as a function of local time. Thus it seems to show that the variations in the mean difference between DORIS and TOPEX corrections are mainly due to the DORIS correction for high solar activity conditions. At global scale, taking all local times into account, this translates into a mean increase of about 0.5 cm of the (DORIS TOPEX) difference.
It is important to notice that this non constant difference between DORIS and TOPEX ionosphere corrections directly impacts the relative bias between TOPEX Sea Surface Height (SSH) and Poseidon SSH estimations. After the 5 first years, the relative bias between the two altimeters may thus increase and is expected to be 0.5 cm higher in the last cycles than in the first part of the mission. Moreover, seasonal variations as large as 0.5 cm are observed in the (DORIS TOPEX) ionosphere differences. They also add uncertainties in the relative bias between the two altimeters.

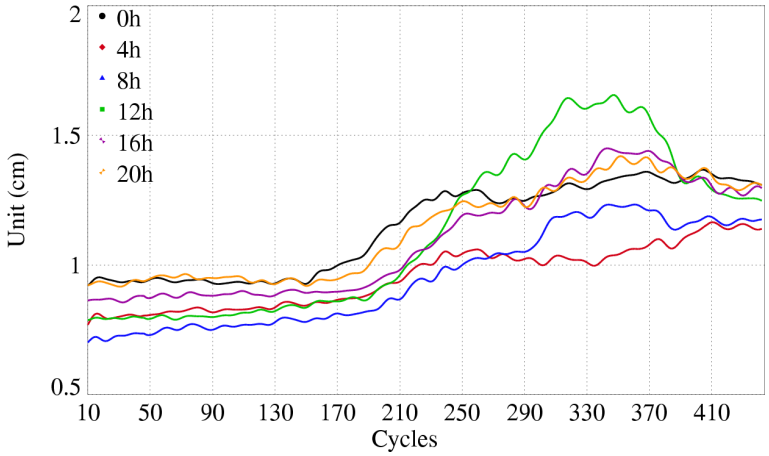

Figure 21: *Differences between DORIS and TOPEX ionosphere corrections as a function of local time*

3.6 Significant wave height monitoring

3.6.1 Ku-band SWH

The cycle mean of Ku-band SWH is plotted as a function of the cycle number on Figure 22. The Alt-A SWH has experienced a large increase (of about 30-35 cm) after approximately cycle 130. Alt-B values (after cycle 236) are consistent to usual values of Alt-A before the change. TOPEX altimeter drifts are responsible of these changes (Hayne et Hancock, 1998 [23]). No trend can be detected from the Alt-B estimates and after the orbit change, through cycles 236-444.
The standard deviation only reflects sea state variations, with higher variability during the austral winter. Alt-B values are consistent with Alt-A.

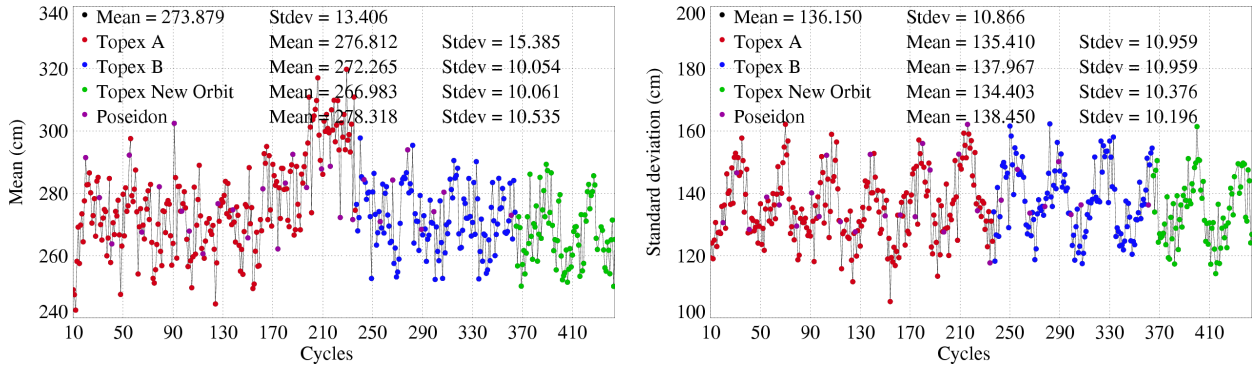

Figure 22: *Cycle mean (left) and standard deviation (right) of Ku-band TOPEX SWH*

3.6.2 Comparison of Ku-band and C-band SWH

The difference between the two bands in terms of SWH is represented on Figure 23. The figure shows an evolution of the Side-A altimeter from the very beginning of the mission, though the mean difference between the two bands only varies by about 2.5 cm. Alt-B values are now very close to those of last Alt-A cycles. The cycle standard deviation also points out this continuous evolution, probably due to Alt-A instrument degradation. The standard deviation of the (Ku C) SWH differences is dramatically reduced on Alt-B cycles which lead to low values, even lower than Alt-A values in the beginning.

Some very slight consistent trend can also be observed in the Alt-B mean difference, but the difference between Ku and C Alt-B SWH measurements do not vary by more than 0.5 cm in average.

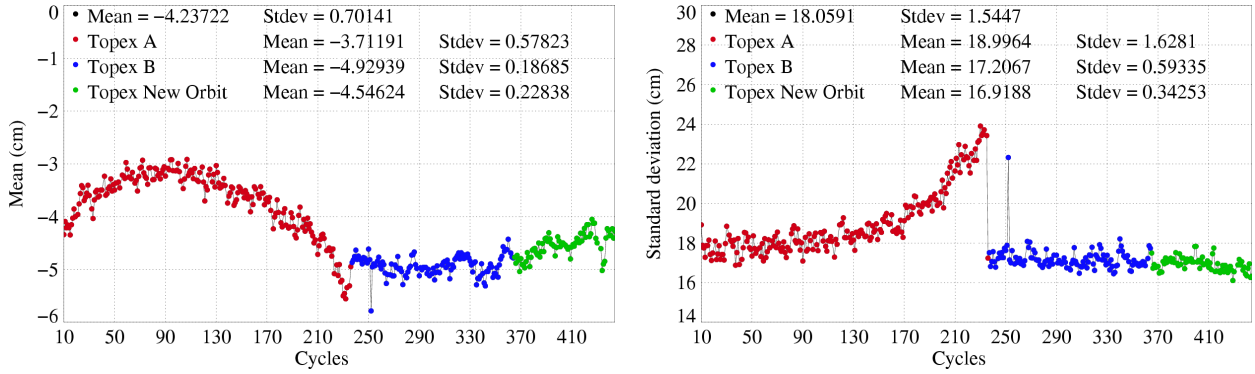

Figure 23: *Cycle mean (left) and standard deviation (right) of differences between Ku-band and C-band TOPEX SWH values*

3.7 Backscatter coefficient monitoring

3.7.1 Ku-Band Sigma0

Statistics have been computed for the Ku-band Sigma0 (Figure 24). The cycle mean remains more or less constant in the first part of the mission, maybe because the last version of MGDR includes Sigma0 reprocessed values, accounting for updated calibration tables. After cycle 132, higher variability of the parameter is observed, though calibration corrections are routinely applied in the processing (Hayne and Hancock, 1997 [26], Hayne and Hancock, 1999 [27]).

Note that all the results presented in this report are only based on M-GDRs, even though some improvements are now proposed by Hayne and Hancock, 1999 [27] and Hayne and Hancock, 2002 [28] with new calibration tables for both TOPEX Alt-A and Alt-B.

Given the variability of the Ku Sigma0, there is no significant bias between Alt-A and Alt-B. Notice that biases between the two altimeters for both Ku and C bands have been estimated during the Alt-B calibration phase and actually applied to Alt-B data (Dorandeu, 1999 [13]).

After cycle 236 (first Alt-B cycle), Ku Sigma0 variations seem consistent to what was previously observed with Alt-A. However, two reprocessing steps have been necessary during the Alt-B M-GDR operational production. In fact, Sigma0 trends are adjusted to uncorrected values to compute the correction table, so it was not easy to determine a long term correction based on a short Alt-B period of observation:

- The first reprocessing seems to be due to the platform event (at cycle 256) after which the TOPEX Ku band sigma0 mean value experienced an unexplained increase (Hayne and Hancock, 2000 [24]). Cycles 259 trough 265 were reprocessed (Callahan, 2000 [6], Hayne, 2000 [29]). But Cycles 257 and 258 have been left apart from this correction. Another reprocessing was decided on cycle 277-284 (Callahan, 2000 [6]) in order to correct Sigma0 values for errors of about 0.06 dB in Ku band and 0.12 dB in C band. This corresponds to updated correction tables, once again.
- The study from Hayne and Hancock, 2002 [28] shows that the TOPEX first calibration mode (Cal 1) could only provide a basis for correcting the Side B Ku-band Sigma0 in the first cycles. In operational mode, both Ku and C band calibration tables are actually computed from long term trends adjusted on Sigma0 observations.

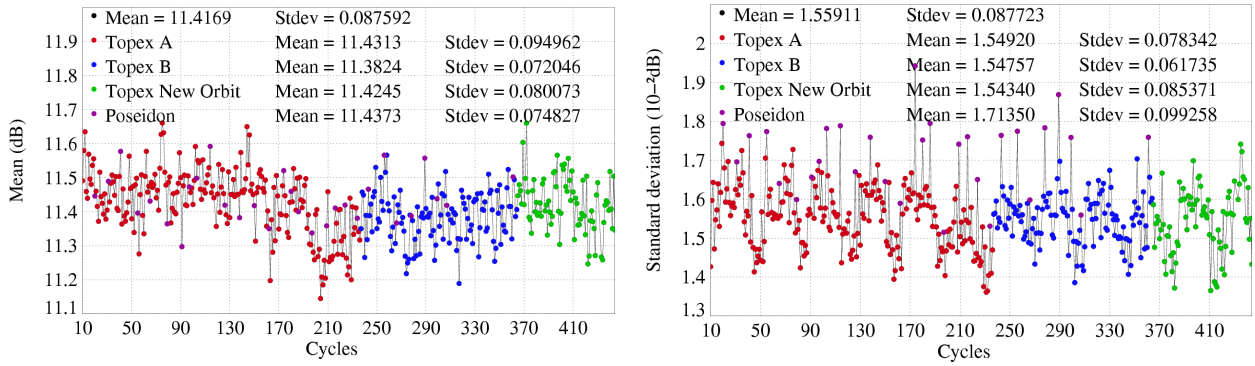

Figure 24: *Cycle mean (left) and standard deviation (right) of Ku-band TOPEX Sigma0 (10-2 dB)*

3.7.2 Comparison of Ku-band and C-band Sigma0

Figure 25 shows the cycle mean and standard deviation of the difference between Ku and C bands in terms of Sigma0. The figure accounts for Sigma0 modifications of the calibration tables described above. Cycles 257 and 258 mean values are too higher (by about 0.2 dB) because these two cycles have not been corrected in the first reprocessing.

As far as the standard deviation is concerned, the difference between the two bands is now consistent with first values of Alt-A. This parameter had continuously decreased on Alt-A along the mission, maybe due to altimeter changes.

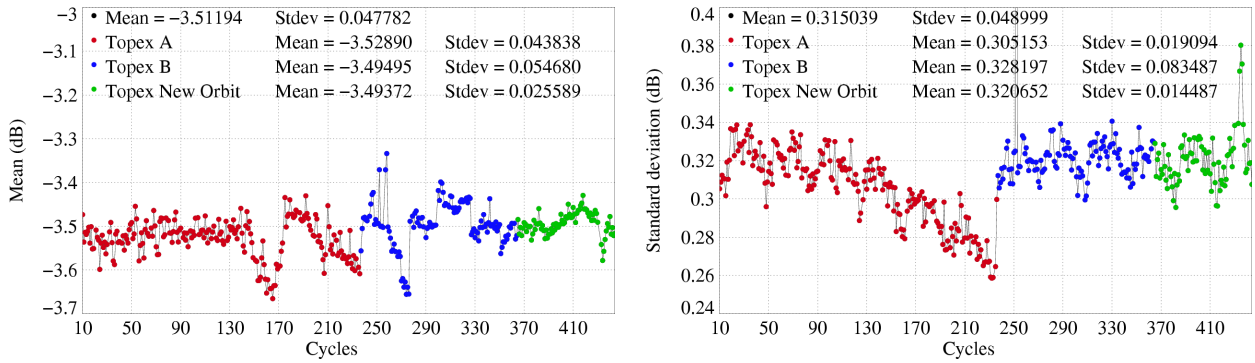

Figure 25: *Cycle mean (left) and standard deviation (right) of differences (10-2 dB) between Ku-band and C-band TOPEX Sigma0 values*

3.8 Sea state bias corrections (SSB)

3.8.1 BM4 and BM3 SSB

Because of the Sea State Bias (SSB) dependency on SWH (3 or 4-parameter models), both corrections are affected by a downward trend for increasing mean SWH (Figure 26) as it was the case in the last years of TOPEX Alt-A, as mentioned previously. Up to cycle 235, the SWH trend in Alt-A measurements translates into nearly 1 cm in terms of SSB correction. Note that this 1 cm variation creates an unrealistic trend in Mean Sea Level estimations (MSL rise becoming overestimated) due to the SSB correction alone. It also impacts the estimation of the relative bias between TOPEX and Poseidon (also overestimated). But the effect of altimeter drifts on the range itself also adds uncertainty on MSL estimations, and the two effects are partly compensating each other (Hayne and Hancock, 1998 [23]). As the Alt-B SWH values nearly recover those of Alt-A at the beginning of the mission, the Alt-B SSB cycle means also return to the level of first Alt-A cycles.

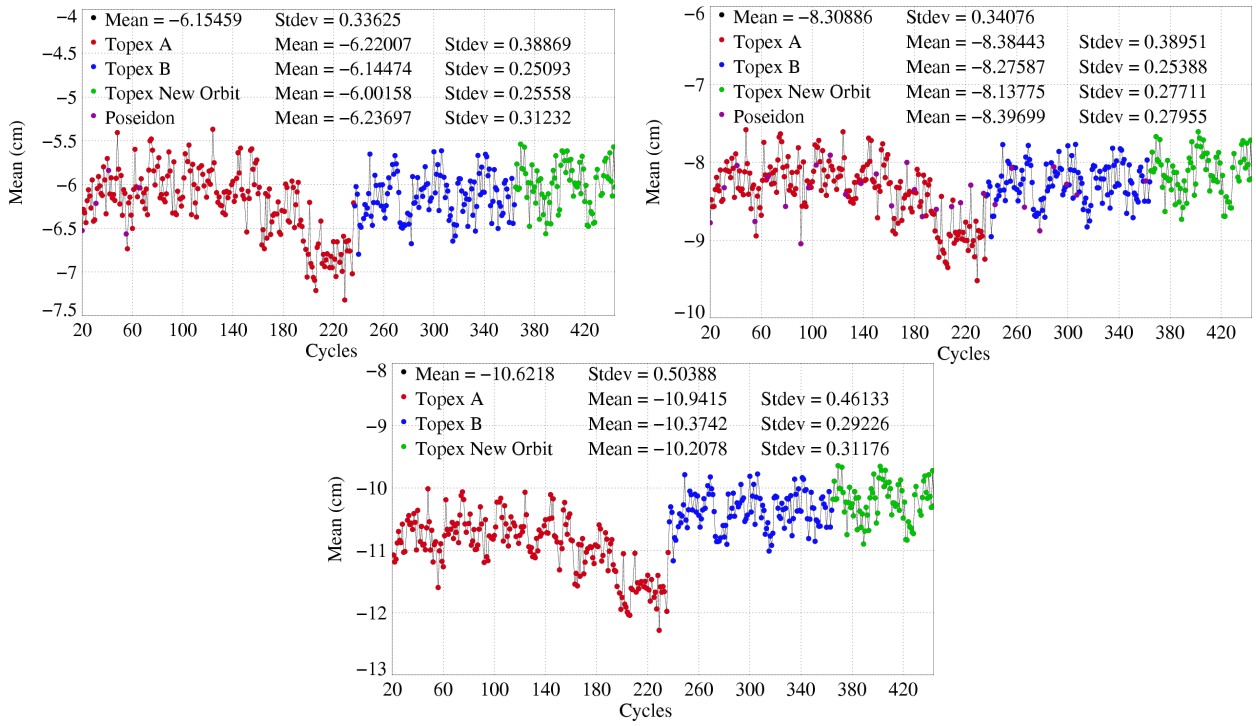

Figure 26: *Cycle means of BM3 SSB (top left), BM4 SSB (top right) and Non Parametric SSB correction (bottom)*

An annual cycle of about 1 cm amplitude is present in the cycle mean of the difference between BM4 and NASA BM3 models (Figure 27), because of sea state annual variations differently taken into account by the two models. But no drift can be detected from this figure, and the standard deviation of the difference remains lower than 1 cm RMS.

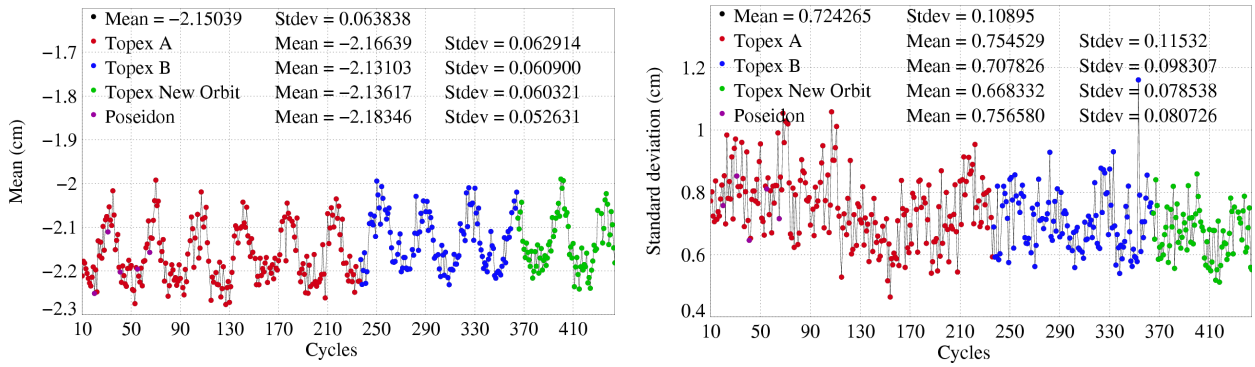

Figure 27: *Cycle mean (left) and standard deviation (right) of differences between BM3 and BM4 SSB corrections*

3.8.2 Non Parametric and BM4 SSB

The non-Parametric SSB (Gaspar et al, 2002 [19]) is computed for Alt-A and Alt-B data in order to compare with the BM4 SSB. Note that this Non Parametric SSB is not yet available for Poseidon1 data. The cycle mean of the correction has a similar shape as the BM4 or BM3 SSB (Figure 26). But due to wind and waves differently taken into account by the two models, a bias is observed on the cycle mean of the difference between the two corrections (Figure 28). This bias is about 25 mm during Alt-A period, and about 21 mm in the Alt-B period. It remains stable until the last cycles. It is not the same on the two periods because two different coefficient tables are used for the Non Parametric SSB, one has been computed from TOPEX crossovers on Alt-A period and the other from collinear passes on Alt-B period, while the BM4 SSB has been computed only on Alt-A cycles and is applied on the whole T/P period. Furthermore, the SWH trend observed during the last Alt-A cycles is differently taken into account by the two SSB model and this explains the drift observed on this period leading to a slightly rise of the bias from 25 mm to about 27 mm.

The cycle standard deviation of the difference between the two corrections (Figure 28) the same behavior than the cycle mean differences with higher values on the Alt-A period (about 9 mm) than on the Alt-B period (about 7.5 mm).

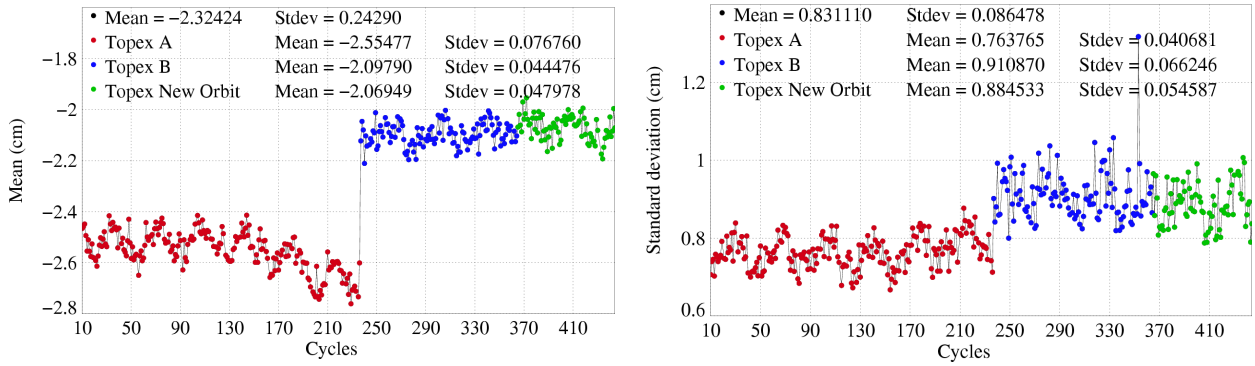

Figure 28: *Cycle mean (left) and standard deviation (right) of differences between BM4 and Non Parametric SSB corrections*

3.9 Waveform-deduced off-nadir angle

An estimation of the off-nadir angle is deduced from the shape of the waveforms themselves. Statistics of this parameter are plotted as a function of the cycle number on Figure 29. They show an increase of the mean parameter on Alt-A altimeter from cycle 130 to approximately cycle 210, with higher values for cycles 207 and 208. The Alt-A PTR change could be one candidate to explain this mean off-nadir angle rise. A small gap in the mean parameter is observed after cycle 213, which is the first AVISO MGDR cycle accounting for the version 6.3 SDPS software (Callahan, 1998 [5]).
There is no clear evidence of the difference between Alt-A and Alt-B estimations on this figure, even if the first Alt-B cycle (236) seems particular (maybe due to the time needed by the instrument or the processing to stabilize).
The cycle standard deviation shows a constant value (around seasonal variations) for A1t-A. The anomalous value obtained at cycle 193 is due to a pointing problem during an ASTRA SEU (Callahan 1998 [8] and Hancock, 1998 [22]). Values for Alt-B seem to be about 3.10-3 deg. RMS higher than Alt-A. Cycle 236 leads to the highest value showing that there is much more variability of this parameter for this first Alt-B cycle. Cycle 317 also exhibits a higher cycle standard deviation value for the attitude parameter. This is the result of a clock rollover that occurred during this cycle (Callahan, 2001 [8]). Indeed, even if no significant impact on data quality can be detected, some waveform deduced attitude values between 0.2 and 0.3 degrees are observed during this cycle.
The mispointing values are higher than usual from cycle 433 to 437 due to a pitch wheel event linked to the T/P safehold mode occurred from cycle 430 to 432 (see electonic communication : T/P Daily Status (26/07/2004). Consequently, the satellite had a strong mispointing during this period.

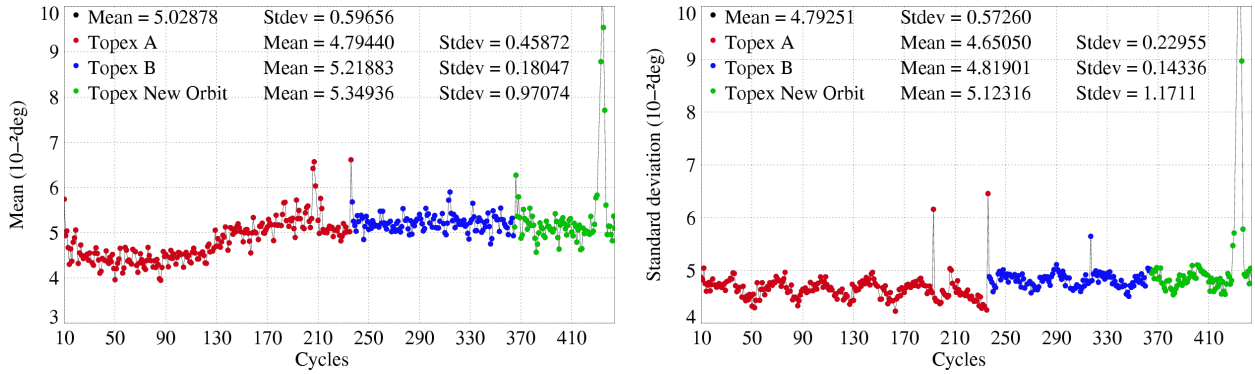

Figure 29: *Cycle mean (left) and standard deviation (right) of waveform-deduced offnadir angle values*

4 Crossover analysis

Crossover differences are systematically analyzed to estimate data quality and to assess the effectiveness of different corrections applied to Sea Surface Height (SSH). The main SSH calculation, used as a reference, is defined as follows:

$$SSH = Orbit - Altimeter\ Range - \sum_{i=1}^{n} Correction_i$$

with $T/P\ Orbit = NASA\ JGM3\ orbit$ and

$$\begin{aligned}
\sum_{i=1}^{n} Correction_i \quad = \quad & Dry\ troposphere\ correction \\
+ \quad & Inverse\ barometer\ correction\ (Time\ variable\ reference\ pressure) \\
+ \quad & Radiometer\ wet\ troposhere\ correction\ (TMR\ corrected\ from\ Ruf\ 2002). \\
+ \quad & Dual\ frequency\ ionospheric\ correction\ (DORIS\ for\ Poseidon) \\
+ \quad & Non\ Parametric\ SSB\ (BM4\ for\ Poseidon) \\
+ \quad & GOT99\ ocean\ tide\ correction \\
+ \quad & Earth\ tide\ correction \\
+ \quad & Polar\ tide\ correction
\end{aligned}$$

Except the updated Inverted barometer and the GOT99 tide correction, all the parameters are extracted from the M-GDR (Aviso User Handbook [1]). The Results presented below are based on a crossover data set from which only SSH differences lower than 30 cm are selected, in order to avoid contamination by spurious measurements, for instance near the coastlines.

4.1 Overall results

Data quality can be monitored from the cycle-by-cycle standard deviation crossover differences which are computed using the main analysis defined above. Figure 30 shows the trend in the standard deviation according to the cycle number. Some general features can be deduced from this figure:

- The standard deviation is between 6.5 and 7.5 cm, showing the excellent quality of the data.
- The crossover standard deviation tends to decrease in the first part of the mission.
- An annual cycle appears on this figure, with maximum values of the global crossover standard deviation in summer (northern hemisphere summer).
- The Side-A altimeter problems, detected for example in the Alt-A SWH parameter, seem to have no quantifiable impact on the crossover standard deviation.
- Higher values are obtained from Poseidon cycles, particularly in the last years (cycles 243 to 299).

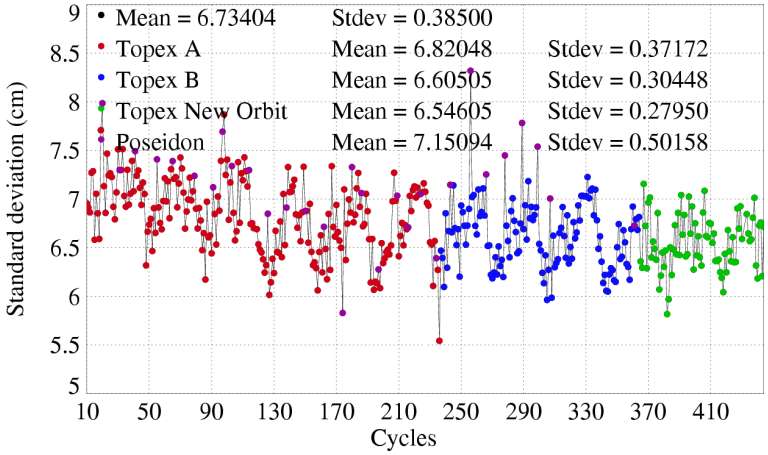

Figure 30: *TOPEX/Poseidon crossover cycle standard deviation, from cycle 11 to cycle 444. Only crossover differences less than 30 cm are selected*

- The ground track change after cycle 365 seems to have no impact on the crossover standard deviation.

In order to better assess the system performances, the same analysis has been performed selecting deep ocean areas ($oceandepth < -1000m$), with low ocean variability ($< 20cmrms$), excluding high latitudes to avoid contamination by ice. The results are plotted on Figure 31. The overall standard deviation is lower than 6 cm RMS. No trend and no seasonal signal can be detected, showing the impact of crossover selection and the influence of high latitudes in the previous figure (Figure 30), given the great number of crossovers in these zones.

A dedicated study was performed in a previous annual report (Dorandeu et al., 2001 [14]) to analyze the variance of crossover differences by latitude bins. The study showed that the decreasing trend was particularly located at high latitudes in the Southern hemisphere (below 60S): the crossover variance decreases by about 15 cm2 in these areas which count, on average, for almost $\frac{1}{4}$ of the total number of crossover points. As these zones are known to be the most impacted by atmospheric pressure variations, the same analysis was performed without applying any pressure induced correction (neither dry tropospheric nor inverse barometer corrections were applied). Comparing the two results allowed computing the variance explained by atmospheric corrections at crossovers. The study showed that the variance explained by pressure induced corrections particularly increases for latitudes below 60S, with the same order of magnitude (15 cm2) as the fall in the variance of fully corrected SSH crossover differences.

Thus the decreasing trend in the TOPEX/Poseidon crossover variance seems to be mainly due to pressure corrections, maybe because of improvements in the ECMWF meteorological model (see Figure 16). The impact of these corrections is largely located at high latitudes, explaining why no trend can be detected from crossover analysis excluding these zones. The analysis by latitude bands also showed annual cycles at hemispheric scale essentially located in high latitude areas. In the southern hemisphere, at these latitudes (higher than 40 degrees), the number of crossover points is about 3 times greater than in the northern hemisphere, because of much more ocean surface. This basically explains why an annual cycle appears at global scale, in phase with the southern hemisphere annual cycle.

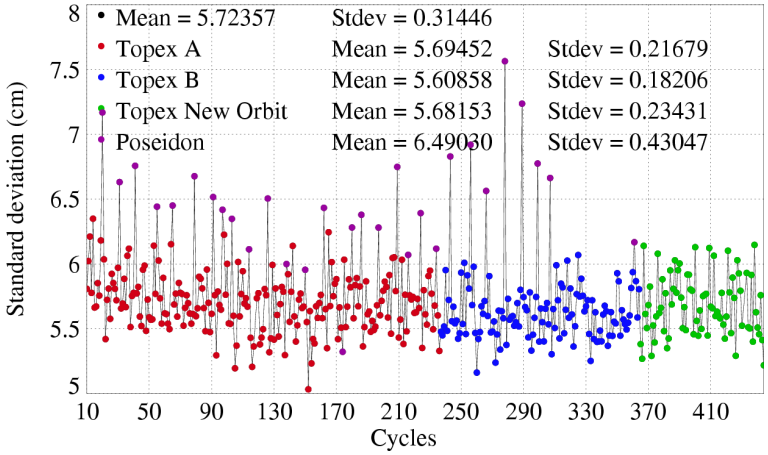

Figure 31: *TOPEX/Poseidon crossover standard deviation, when selecting:latitudes between 50S and +50N; low ocean variability areas (ocean variability* $< 20cm$*); open ocean areas (depth* $< -1000m$*)*

The quality of Poseidon cycles, showed as red dots on Figure 30, can be compared to that of TOPEX. A difference in the crossover variance is observed between the two altimeters, and this difference tends to increase in the last cycles (except cycle 361). Since among all the corrections used to compute the SSH only the ionospheric correction differs between the two kinds of data, it is interesting to use the DORIS correction for both altimeters and to compare the results (Figure 32). Using the DORIS ionospheric correction makes the results from TOPEX and Poseidon altimeters much more consistent. Thus it shows that the DORIS ionosphere correction degrades the crossover variability, essentially in the second part of the mission and explains why higher differences are found between TOPEX and Poseidon in the last years (Figure 31). The crossover variances using TOPEX dual frequency and DORIS corrections will be specifically analyzed in the dedicated section 4.5.

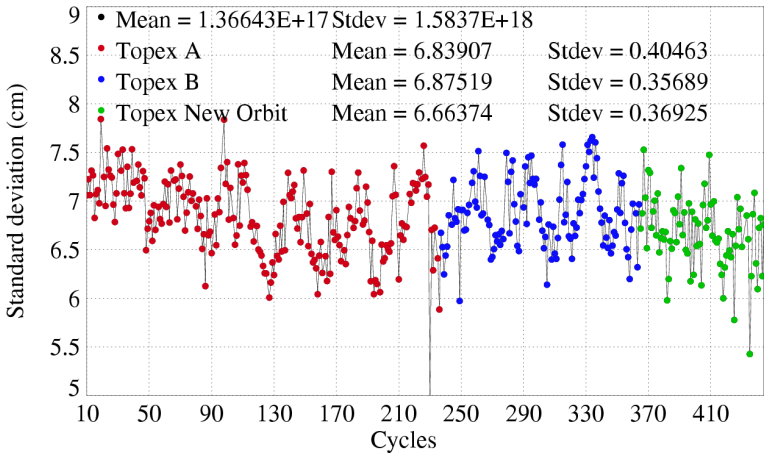

Figure 32: *TOPEX/Poseidon crossover standard deviation when using the DORIS ionosphere correction (same as Figure 30 but with DORIS instead of TOPEX ionosphere correction)*

However, differences of about 2 cm^2 remain between TOPEX and Poseidon after applying the same ionosphere correction. It is known that TOPEX data are somewhat filtered due to the altimeter processing (tracker processing instead of retracking), which explains the noise difference with Poseidon (Le Traon et al, 1994 [31]). This can translate into different crossover variance from the two altimeters.

Figure 33 shows the geographical pattern of the crossover standard deviation computed from cycle 11 to cycle 444 and averaged over bins of 4x4 degrees. In some high-latitude areas of the northern hemisphere, e.g. the Bering Strait and Hudson Bay, the standard deviation is always high (over 13 cm RMS), probably because of bad ocean tide modeling. Deficient tide models degrade also the results in some coastal areas and enclosed seas. The map also gives "conventional" information on the high variability of the major ocean currents (Gulf Stream, Kuroshio, Confluence zone, Agulhas Current), with higher variability in the western parts of the basins. The standard deviation of the crossover differences clearly increases with latitude. This is related to the high pressure variability at high latitudes (Le Traon et al., 1996 [32]) which is imperfectly accounted for in the inverse barometer correction.

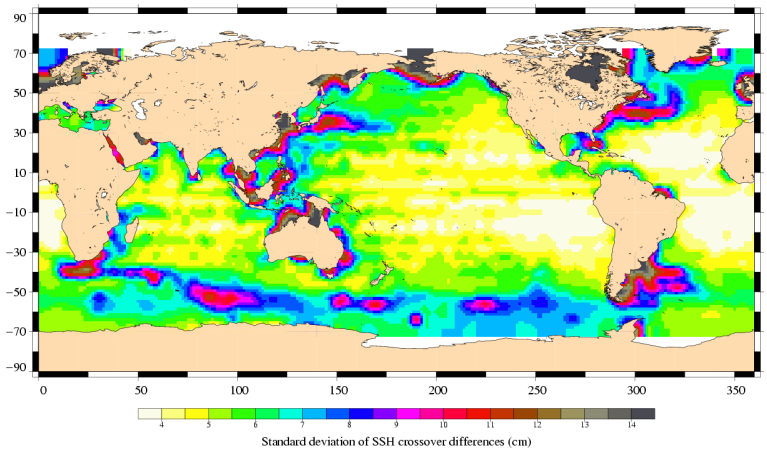

Figure 33: *Geographical pattern (4x4 degree bins) of TOPEX/Poseidon crossover standard deviation (cm), from cycle 11 to cycle 444*

From this map, the system accuracy can be estimated: the sea surface height (SSH) variance can be split into a component due to ocean variability, and a component due to residual orbit errors and errors in both instrumental and geophysical altimeter corrections. If there was an area with zero ocean variability, we could derive an estimate of the absolute system performance. Areas of weakest variability (which increase errors due to the system) yield a crossover standard deviation lower than 3-4 cm. Since crossovers are differences between ascending and descending passes, the result needs dividing by 2 to estimate the precision (assuming errors between two crossing passes are not correlated). However, this estimate does not include geographically-correlated orbit error, which cancels out at crossovers. This analysis therefore shows that system precision is better than 3 cm for isolated measurements.

The same type of map can be produced for the averaged crossover differences. In some areas, Figure 34 shows systematic differences between ascending and descending passes, on the order of 3-6 cm, which are probably due to geographically-correlated orbit errors.

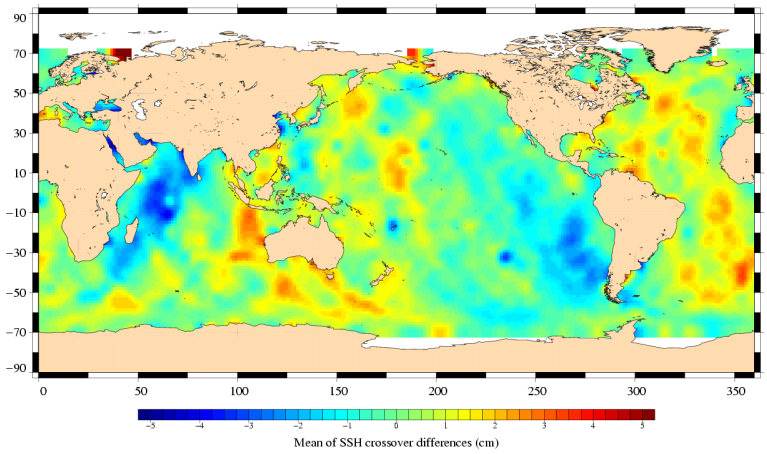

Figure 34: *Geographical pattern (4x4 degree bins) of the mean of crossover differences, from cycle 11 to cycle 444.*

4.2 Comparison of NASA and CNES orbits

The two orbit fields present in the M-GDRs can be compared in terms of crossover variance. Computing the cycle by cycle difference between the variance using the CNES orbit and the variance using the NASA orbit leads to the results plotted in figure 35. The CNES orbit globally increases the variance by about 2.1 cm2 relative to the NASA orbit but the degradation is particularly high from cycle 100 to cycle 246. As mentioned before (section 3.2), during this period the DORIS station coordinates have not been updated in the CNES orbit computation. This of course impacts the global orbit quality in the long-term. The difference in crossover variance is clearly reduced since the use of the IRTF97 reference frame for the CNES orbit starting at cycle 247. The CNES orbit performance at crossovers has been even more improved after introducing the ITRF2000 reference frame and the albedo model at cycle 320. The crossover variance difference between NASA and CNES orbits is now very close to zero except during the orbit transition from cycle 365 to cycle 368.

The four plates of Figure 36 respectively show the geographical pattern of the difference in crossover variance between CNES and NASA orbits before cycle 246 (top left), from cycle 247 to cycle 319 (top and right), from cycle 320 to cycle 364 before the orbit change (bottom and left) and after cycle 369 after the orbit change (bottom and right). The 4 periods correspond to the changes in the CNES orbit calculation (ITRF97 at cycle 247, ITRF2000, albedo model at cycle 320 and the orbit change from cycle 365 to 368). The figure shows the improvements made to the CNES orbit calculation by changing the reference frame. From cycle 320 onwards, the relative performances of the two orbits are globally balanced and in the last period, after the orbit change, the CNES orbit seems slightly better. Indeed, in order to improve the CNES orbit calculation, the Hill force has been adjusted since September 2002 over a period of 1 day instead of 3 days. Moreover ITRF2000 has been applied in the NASA orbit calculation from cycle 360 onwards. As a result, the consistency between 2 orbits is better.

Differences between ascending passes and descending passes have been computed for the two orbits and averaged in geographical bins for the whole T/P mission. The local means are then compared on

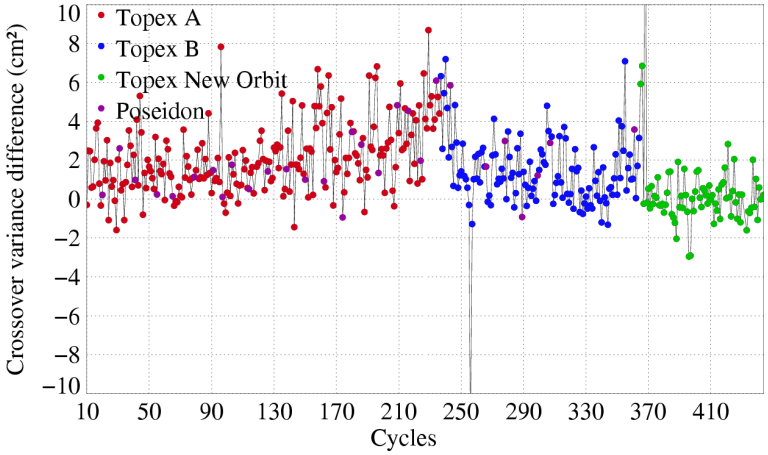

Figure 35: *Gain in crossover variance (cm2) when using NASA orbit rather than CNES orbit*

Figure 36. Systematic differences in the crossover mean, along the satellite track, are as large as 2 cm. These long wavelength signals may be due to geographically correlated orbit errors.

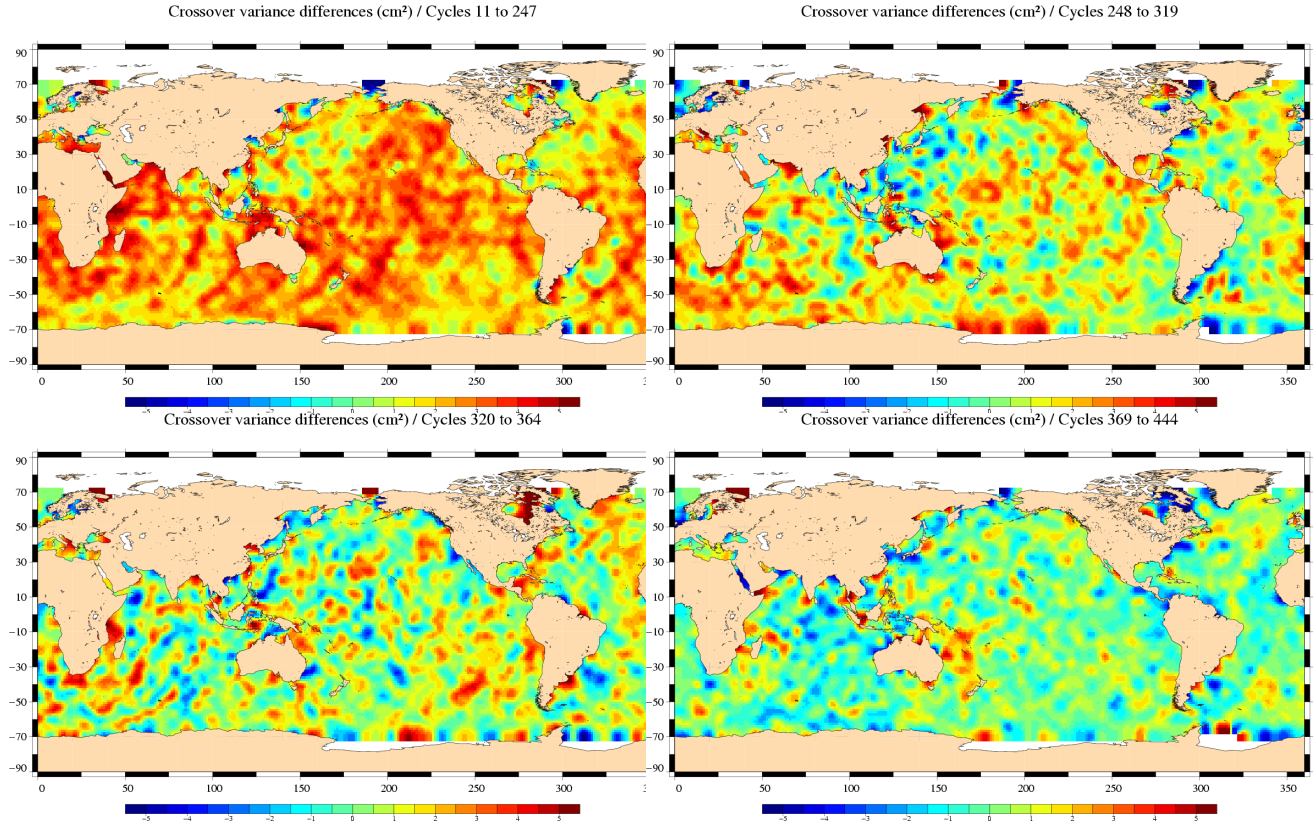

Figure 36: *Difference in crossover variance (cm2) when using NASA orbit rather than CNES orbit, before use of the ITRF97 set of coordinates in the CNES orbit (top left), with the use of ITRF97 (top right) and with ITRF2000 before (bottom left) and after the orbit change (bottom right)*

4.3 Comparison of tidal models

4.3.1 CSR3.0 and FES95.2

Since no changes have been made to the tidal models used in the M-GDRs, no difference relative to the results presented in the T/P annual report from 2001 (Dorandeu et al., 2001 [14]) are expected. One should thus refer to this previous report for a comparison of CSR3.0 and FES95.2 performances at crossovers.

4.3.2 GOT99 and CSR3.0

Figure 38 shows the crossover variance difference when using the GOT99 tidal correction rather than the CSR3.0 tidal correction. The gain in variance is about 2 cm2. The GOT99 tidal correction yields the best performances particularly near to the coasts (Figure 38) and in semi-enclosed seas, but the improvements provided by this model are also significant in deep ocean areas.

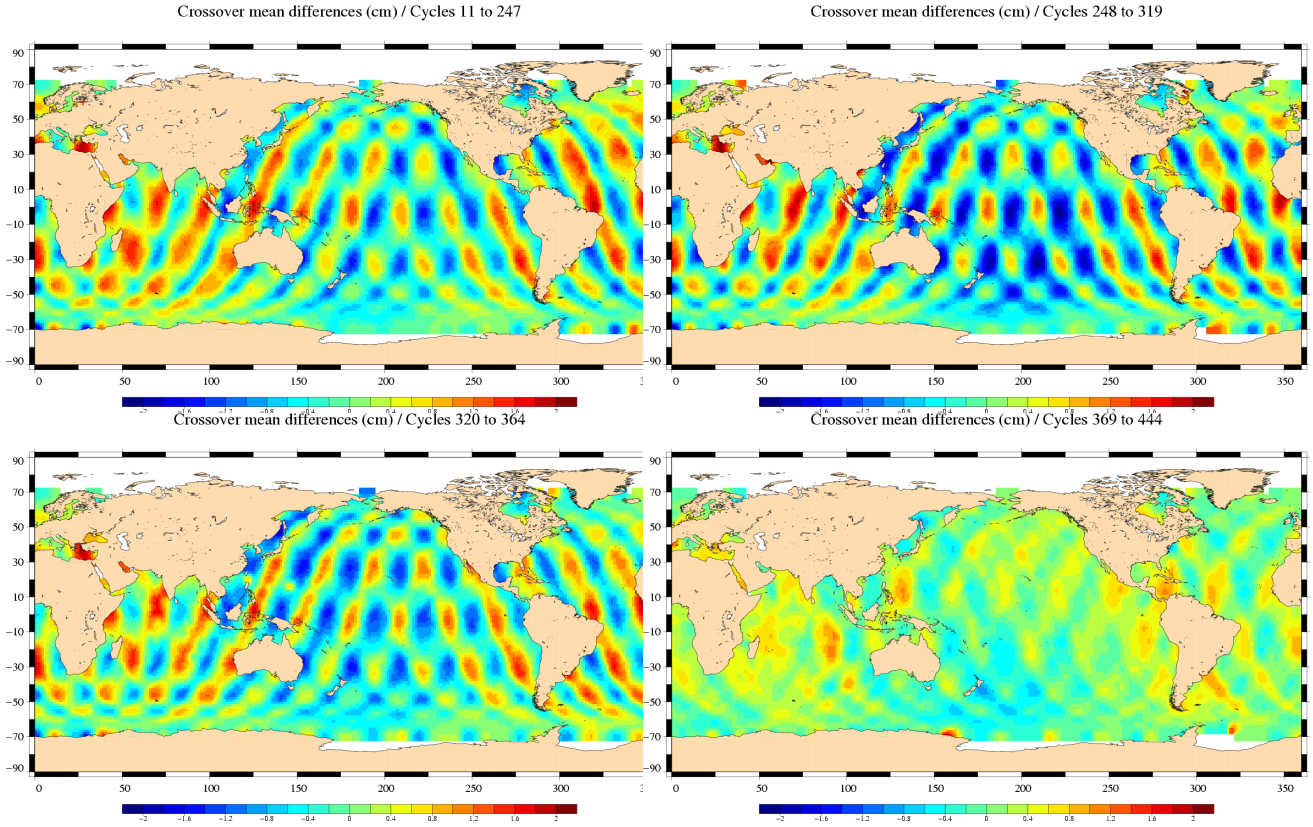

Figure 37: *Difference in crossover means obtained when using NASA and CNES orbits*

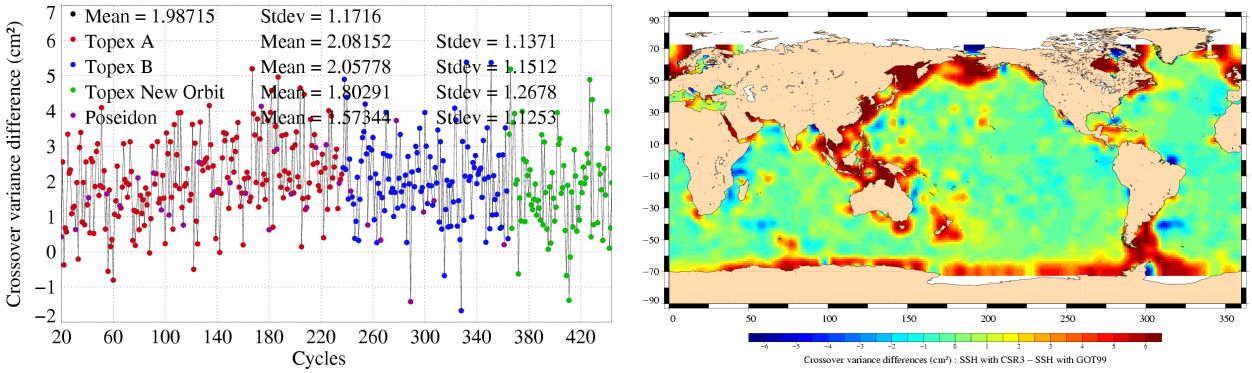

Figure 38: *Gain in crossover variance (cm2) when using the GOT99 tidal correction rather than the CSR3 tidal correction*

4.4 Comparison of radiometer (TMR) and model (ECMWF) wet troposphere corrections

Figure 39 shows the crossover variance difference when using the ECMWF troposphere model rather than the TMR correction. The extra variance obtained is about 5 cm^2. But the improvements made to

the model (see section 3.4.3) result in a decreasing variance relative to the TMR correction. A gain in crossover variance of about 2 cm2 is obtained in the last cycles by the ECWMF model relative to the first part of the mission.

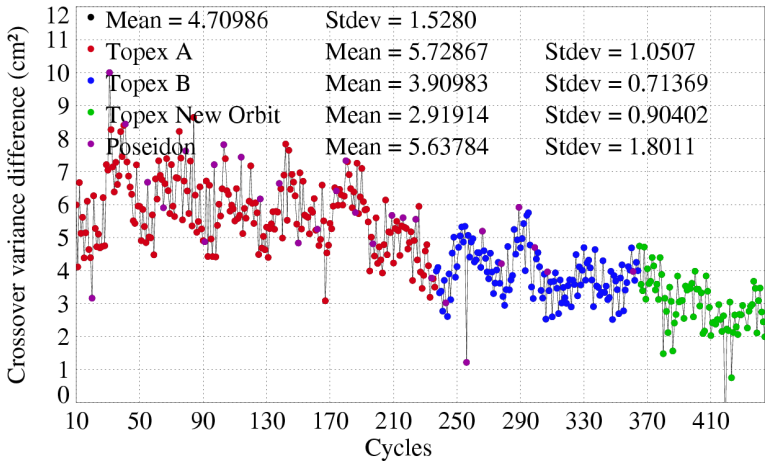

Figure 39: *Gain in crossover variance (cm2) when using the TMR wet troposphere correction rather than the ECMWF correction*

The gain in variance when using the TMR correction rather than the ECMWF correction is higher in the wettest areas (Figure 40).

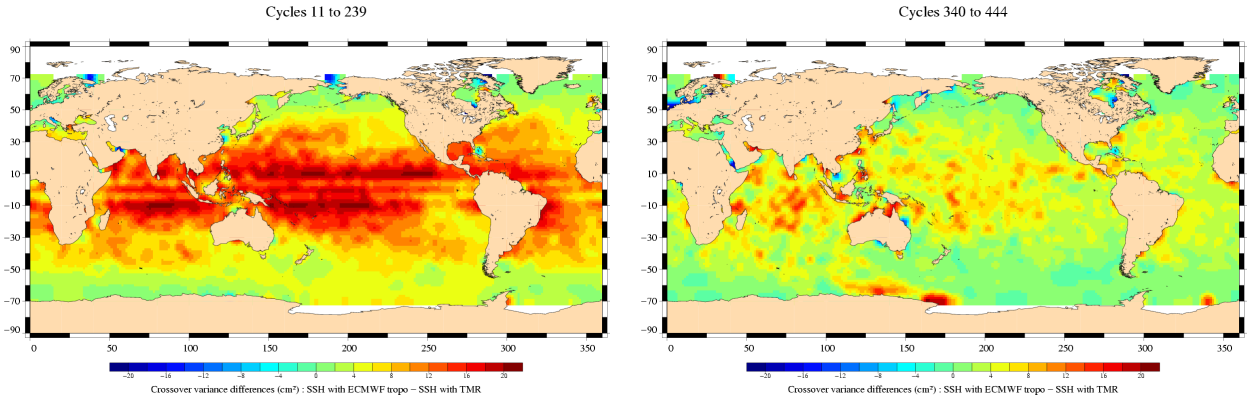

Figure 40: *Gain in crossover variance (cm2) when using the TMR wet troposphere correction rather than the ECMWF correction*

4.5 Comparison of Topex dual-frequency and Doris ionosphere corrections

Taking the dual-frequency ionosphere correction as a reference and using only TOPEX crossover points, the same type of analysis as above has been achieved. The dual frequency ionosphere correction was first filtered using a low-pass Lanczos filter and a cutoff wavelength of 300 km.

The crossover variances obtained using respectively DORIS and TOPEX corrections are 47.01 and 45.30 cm2 (Figure 41 on the left). Thus, the dual frequency correction yields the best performances, particularly in the last cycles, when the solar activity reaches its maximum over the TOPEX/Poseidon mission. In the last period, the difference between DORIS and TOPEX crossover variances is as large as 5 cm2. It explains the major part of the greater variance obtained with Poseidon data relative to TOPEX in the last years.

The results are clearly degraded by the use of the DORIS correction around the geomagnetic equator (Figure 41 on the right). In these areas the DORIS correction poorly retrieves the equatorial ionosphere spikes and often lowers the crest of them. But in some high SWH areas, up to 1-2 cm2 of variance is added by the dual frequency correction relative to DORIS. We will see in the next section that the 3-parameter SSB correction, used to correct TOPEX data before deriving the ionosphere correction, has poor performances in high SWH areas. Moreover, instrumental drifts and losses of accuracy in Alt-A SWH estimation may also impact the results.

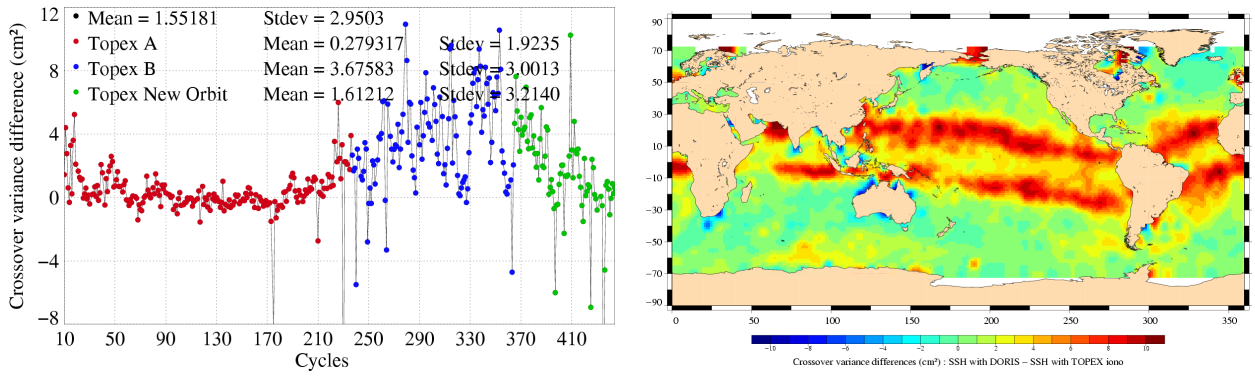

Figure 41: *Difference in terms of crossover variance (cm2) when using the TOPEX ionosphere correction rather than DORIS*

Figure 42 compares the crossover mean differences obtained using DORIS and TOPEX ionosphere corrections. The figure thus compares differences between ascending and descending passes computed respectively with DORIS and TOPEX corrections. Using only Alt-A measurements (i.e. cycles 11 to 235), a slight difference on the order of a few millimeters is observed between the two hemispheres. The same type of map is obtained when comparing the BENT model and the dual-frequency correction (not shown here). One hypothesis could be that the altimeter processing causes this kind of behavior, due to hemispheric corrections.

When using only Alt-B measurements (i.e. cycles 236 to 444), the results are dramatically different. On the one hand, differences are much more contrasted maybe because of the high solar activity through

the considered period. On the other hand, differences at hemispheric scale are from the opposite relative to those obtained with Alt-A. Therefore this change seems to be due to the altimeter processing.

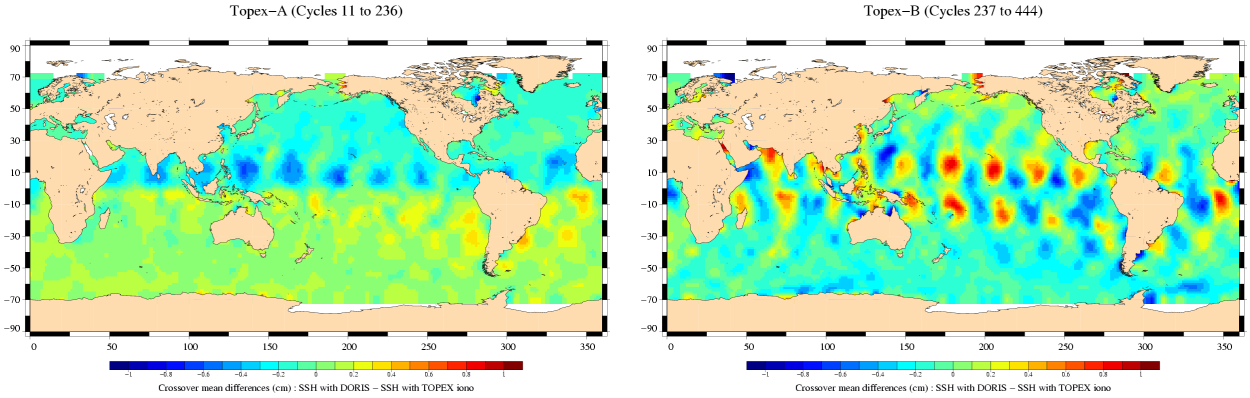

Figure 42: *Comparison of mean crossover differences obtained when using DORIS and TOPEX ionosphere corrections (DORIS TOPEX), with Alt-A cycles (left) and Alt-B cycles (right)*

4.6 Comparison of sea state bias corrections (SSB)

4.6.1 BM3 and BM4 SSB

The three-parameter (Chelton, 1994, [10]) and the four-parameter (Gaspar et al., 1994, [18]) Sea State Bias (SSB) corrections have also been compared in terms of crossover variance (Figure 43), only for TOPEX data, since the NASA SSB is not available for Poseidon.

The gain in variance using BM4 rather than BM3 is of about 0.6 cm2. Figure 43 (on the left) also shows that the extra variance using BM3 relative to BM4 decreases with time. In fact, from the shape of the curve, it seems that a change happens around cycles 120-130. The period after these cycles is characterized by lower explained variance of BM4 relative to BM3 and less seasonal signal in the difference of variance. On Alt-A cycles, some part of this trend may be due to the evolution of Alt-A SWH estimation. Nearly the same results are obtained with last Alt-A and Alt-B estimations. Note that both models were fitted on the first part of the T/P Mission.

The geographical pattern of the gain in variance using BM4 rather than BM3 is presented on Figure 43 (on the right). A latitude dependency is clearly visible, with a gain in variance higher than $1 cm^2$ in almost all areas at latitudes higher than 30 degrees. The results are much more balanced at low latitudes: the effect of the additional SWH-dependent term only appears in regions where large waves are usually observed (Gaspar et al., 1994 [18]).

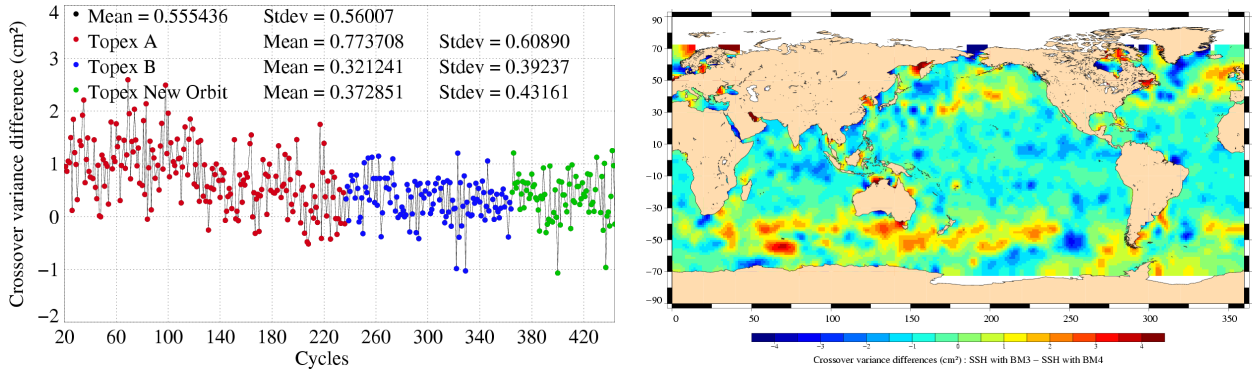

Figure 43: *Gain in crossover variance (cm2) when using BM4 SSB correction rather than BM3*

4.6.2 BM4 and Non-Parametric SSB

The four-parameter (Gaspar et al., 1994, [18]) and the Non-Parametric (Gaspar et al., 2002, [19]) Sea State Bias (SSB) corrections have also been compared in terms of crossover variance (Figure 44 bottom), only for TOPEX data, since the Non-Parametric SSB is not available for Poseidon. The gain in variance using the non-parametric model rather than BM4 is about 0.5 cm2 for Alt-A cycles (until cycle 236) and 1.2 cm2 for Alt-B cycles. The BM4 SSB has been computed using only Alt-A cycles contrary to the Non-Parametric SSB which uses two different coefficient tables: the first has been computed on the Alt-A period and the second on the Alt-B period. This explains the significant difference of performance between the two SSB models from cycle 237 onwards (Alt-B cycles).

The geographical pattern of the gain in variance using non parametric model rather than BM4 is presented on Figure 44 (top) with two maps in order to distinguish Alt-A cycles (on the left) from Alt-B cycles (on the right). The significant gain obtained on Alt-B cycles is clearly visible in regions where large waves are usually observed, at latitudes higher than 30 degrees.

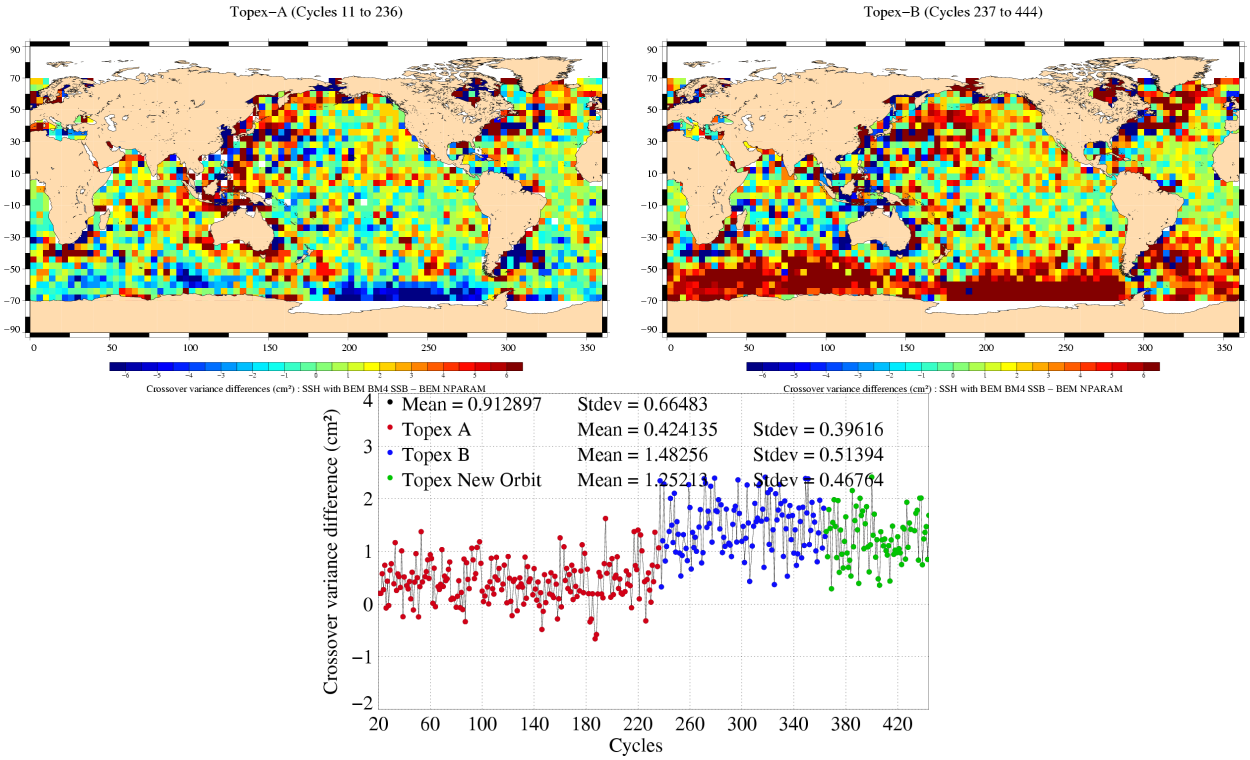

Figure 44: *Gain in crossover variance (bottom) when using non-parametric SSB correction rather than BM4 SSB with Alt-A cycles (left) and Alt-B cycles (right)*

5 Topex/Poseidon / ERS cross-calibration

ERS OPR ([17]) produced by CERSAT (French Processing and Archiving Facility for ERS-1 and ERS-2) at IFREMER have been used to achieve this study. ERS-1 and ERS-2 OPR data quality assessment and cross-calibration relative to TOPEX/Poseidon are routinely performed at CLS under IFREMER contract. Dual crossovers are computed from TOPEX/Poseidon M-GDR data and ERS data allowing comparisons of both altimeter and radiometer parameters.
For more informations, the ERS-2 annual report from 2004 about calval activities is avaible at: http://www.jason.oceanobs.com/documents/calval/validation_report/tp/annual_report_e2_2004.pdf.

5.1 SWH cross-calibration

Both ERS-1 and ERS-2 data sets have been used to compute statistics of the differences between TOPEX/Poseidon and ERS SWH estimations (figure 45). Only SWH crossover differences with a maximum time lag of 1 hour are selected to limit sea state variability. The differences are then averaged over 12 TOPEX cycles to get homogeneous sampling. This could not be done with Poseidon for which the mean is computed over only 1 cycle, explaining the noisier (ERS-Poseidon) differences.
For ERS-1 and TOPEX/Poseidon comparisons, phases C (1^{st} 35-day repeat mission, October 1992 - December 1993) and G (2^{nd} 35-day repeat mission, March 1995 - June 1996) of ERS-1 have been reprocessed in version 6, phases E-F (geodetic mission, April 1994 - March 1995) are still in version 3. The differences obtained between the three time series can be explained by the following reasons: a bias of 12 cm is obtained between version 6 and version 3 (the two last time series), and the mean SWH is impacted in the long-term by the IF filter drift (Mertz et al., 2002 [35]).
The Side-A TOPEX SWH drift is clearly evidenced on figure 45, since differences between ERS-2 and Poseidon remain almost constant during the same period. A variation as large as 35 cm in the Alt-A SWH can be deduced from these results. The gap between Alt-A and Alt-B can also be easily estimated and it is confirmed by the results of TOPEX-alone statistical monitoring (Figure 22). Notice that the Alt-B SWH mean level is about 5 cm lower than the one of Alt-A around cycles 110-120.
The last Alt-B estimates seem steadier than the Alt-A estimations, even though around cycles 270 and 310, the mean differences relative to ERS-2 can increase to about 8 cm. These variations can be attributed to ERS-2 since during cycles 60 to 62, many problems occurred to ERS-2. From figure 45, no trend can be detected in (ERS Poseidon) SWH differences.

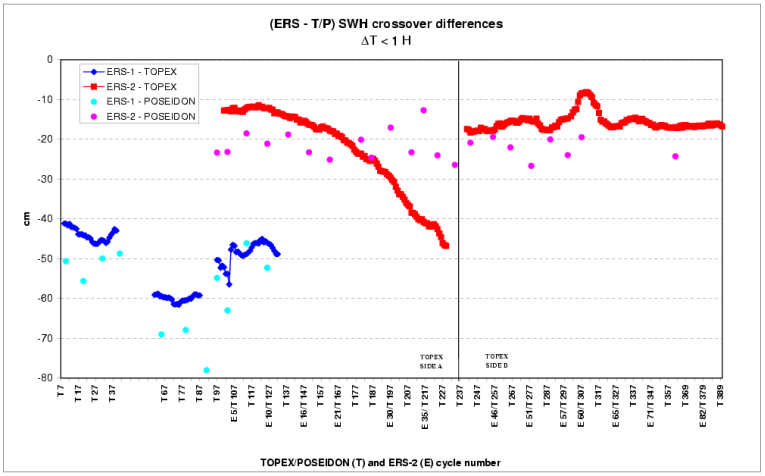

Figure 45: *Differences of SWH at 1 hour crossovers between ERS and TP. Except for Poseidon, each point is obtained averaging differences over 12 TOPEX cycles*

5.2 Sigma0 cross-calibration

Sigma0 differences between ERS and TOPEX (Ku band) measurements have also been processed as described above and plotted on figure 46. Major variations in the (ERS-2 TOPEX) mean differences up to TOPEX cycle 270 seem to be due to TOPEX and can be correlated to what is observed in the Sigma0 statistical monitoring (figure 24). For instance, the increasing mean difference between ERS-2 and TOPEX backscatter coefficients form cycle 160 to cycle 220 can be attributed to TOPEX, since this variation is also observed in the TOPEX-alone trend. After cycle 270, one should be less confident on ERS-2 Sigma0 estimations. In fact, large drops in ERS-2 Sigma0 occurred during the year 2000 (Dorandeu et al., 2000 [15]). Although the ERS-2 Sigma0 drops have been corrected in the results presented on figure 46, according to the recommendations from this study, large degradation in the ERS-2 measurement due to mispointing explains the bell shape observed in (ERS-2 T/P) differences between cycles 260 and 300. Moreover, many problems occurred in cycles 60 to 62 ERS-2 (Mertz et al., 2002 [33]), leading to a large decrease around cycle 313.

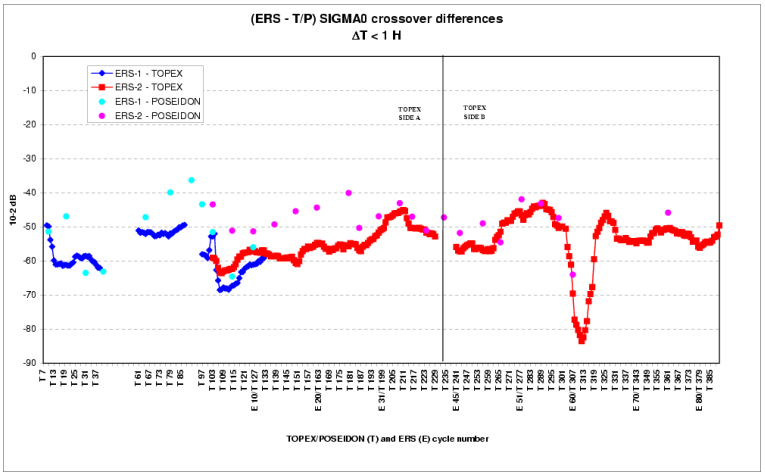

Figure 46: *Differences of Sigma0 at 1 hour crossovers between ERS and TP. Except for Poseidon, each point is obtained averaging differences over 12 TOPEX cycles*

5.3 Topex / ERS radiometer cross-calibration

Comparison between the TOPEX microwave radiometer (TMR) and the ERS-2 microwave radiometer (MWR) has been carried out following the method detailed in Stum, 1998 [41]. It consists in comparing the measurements of the two satellites at TP/ERS crossover points with less than 1-hour time lag. Estimates of the differences are made over time periods of 12 TP cycles, to get homogenous and repeatable sampling of the atmosphere. The mean value of the (TMR ERS ATSR/M) wet tropospheric correction difference at these crossovers is computed. Studies have been carried out to calculate the drift over time of the TMR path delay (Ruf, 2002 [39]). The data set has been corrected for in this study. Figure 47 shows the (T/P ERS-2) crossover mean wet tropospheric correction difference versus the series of 12 T/P cycles time periods. The TMR path delay was corrected for the drift in this figure. The abscissa of each reported value is referred to the end of the 12-cycle period (e.g. for the 12-cycle period 2 to 13, the abscissa is 13, and so on). The values obtained for ERS-2 data may not be confident: indeed, a drift appears in the 23.8 GHz brightness temperature (see Obligis et al., 2003, [37]) and may be reevaluated. A new correction was proposed by Scharroo et al., 2004 ([42]) to take into account the gain fall, the drift, and the stop of the drift in April 2000. An evaluation of those corrections is under investigation at CLS and will be presented in the annual report of ERS-2 (Mertz et al., 2005 [34]). The most prominent feature of figure 47 is the increase of the difference after T/P cycle 157 (December 1996). The small oscillations with a one-year time period are probably due to annual variation of the crossovers sampling: during summer, less crossovers with dry atmospheres are sampled, because of the sea ice extension in the Southern hemisphere, and this leads to a higher mean of the T/P-ERS path delay difference.

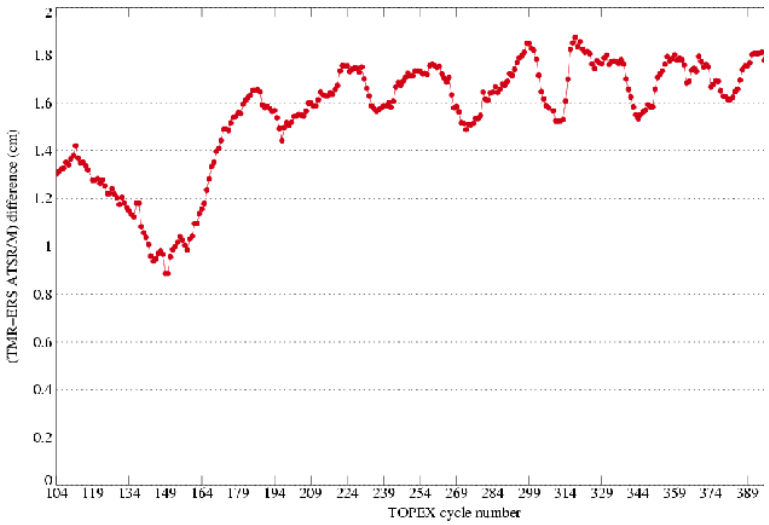

Figure 47: *Differences of Sigma0 at 1 hour crossovers between ERS and TP. Except for Poseidon, each point is obtained averaging differences over 12 TOPEX cycles*

6 Repeat-track analysis

This analysis is used to compute Sea Level Anomalies, variability and thus to estimate data quality, but also to determine the trend in the Mean Sea Level (MSL) and the relative bias between Alt-A, Alt-B and POSEIDON altimeters.

A mean profile was estimated from seven years of TOPEX/Poseidon data, to integrate ocean signals over a representative period. This reference point can thus be used to compute Sea Level Anomalies (SLA) until cycle 364. Due to the orbit change between cycles 365 and 368, the T/P orbit is not repetitive and no nominal track is available during this period. Therefore it is not possible to compute SLA. On the new ground track, there are too few repeat cycles to allow computing a significant reference profile. Thus SLA are computed relative to the CLS01 Mean Sea Surface (Hernandez et al, 2001) (CLS01 MSS) also estimated from the same seven years of T/P data.

6.1 Ocean variability

The sea-surface variability map for the period covering cycles 11 to 444(Figure 48) is obtained by geographically calculating the standard deviation of the altimeter residuals relative to the mean profile (or to the MSS).

This variability can be split into a component due to ocean signal itself (notice the very high variability in the area of the major ocean currents) and also into other components including residual orbit errors and errors due to altimeter corrections. In the repeat-track method, most of the orbit error (the component due to errors in the geopotential model) cancels out. The geographical areas with lowest variability yield standard deviation values on the order of 3 to 4 cm, which can be taken as an estimate of the system precision. This analysis therefore confirms the results derived from crossover analysis.

Apart from major currents areas (Gulf Stream, Kuroshio, Agulhas current, Confluence zone, circumpolar current), high variability is observed near the coastlines and in enclosed seas where tidal models are less efficient. Higher variability is also observed near the equator: the "El Niño" and "La Niña" events (eg. 1997-1998) increase the variability in the equatorial Pacific.

The cycle-by-cycle SLA standard deviation has been computed and plotted on Figure 49. It shows the large impact of the 1997 El Niño event increasing the ocean variability by about 1 cm rms at global scale. After 1999, higher variability is obtained because the reference 7-year mean profile does not include all particular ocean signals of the last years. The variability increases in October 2002 due to another "El Niño" situation. In addition, with T/P on its new ground track, one should expect higher SLA variability just because the MSS is less precise outside the nominal track (Hernandez et al).

In terms of measurement quality, this study confirms crossover analysis results: there is no difference between Alt-A and Alt-B. Higher variance is obtained for some very incomplete Poseidon cycles (e.g. cycles 256 and 278).

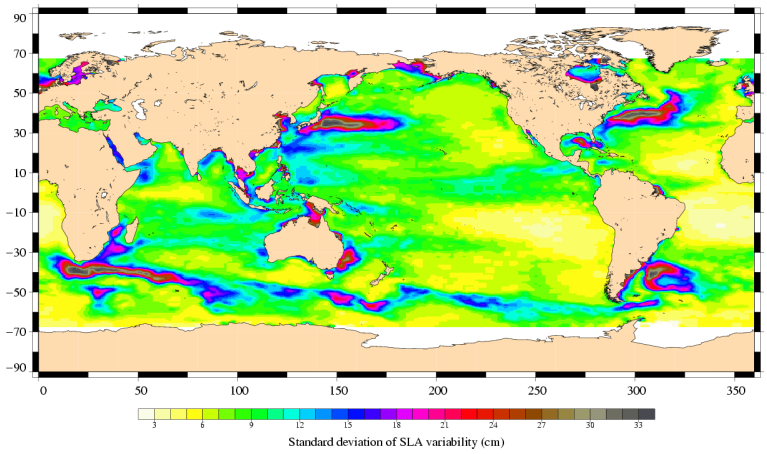

Figure 48: *Map of SLA variability (cm) from collinear analysis of T/P data from cycles 11 to 444.*

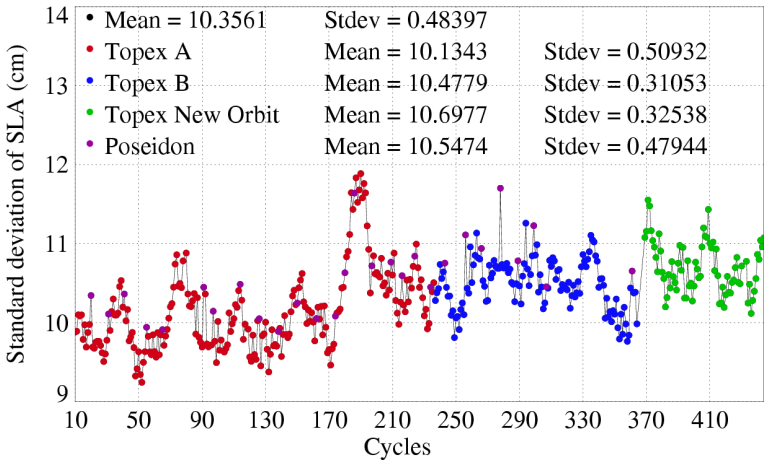

Figure 49: *Cycle per cycle monitoring of SLA variability (cm) from collinear analysis of T/P data from cycles 11 to 444.*

6.2 Mean sea level variations

6.2.1 Main results

The cycle-by-cycle mean of the residual heights can be used to estimate the trend in the MSL as observed by TOPEX/Poseidon. The value for each cycle is calculated from averaging over 2° by 3° bins, then weighting by latitude to take account of the relative geographical area represented by the bin. Moreover the annual, semi-annual and 60 day variations have been removed.

The relative bias between TOPEX and Poseidon, clearly marked in the last Alt-A cycles, has been

taken into account. Furthermore, as already shown in the comparison between TOPEX and DORIS ionosphere corrections (section 3.5.2), the drift between the two corrections has been corrected for on Poseidon cycles.

Based on the studies from several authors (e.g. Ruf, 2000 [40], Kheim et al., 2000 [30]), there is now a consensus among most of SWT members considering that a TMR drift correction should be applied to the TOPEX/Poseidon data for MSL estimations. A TMR drift of about 1-1.5 mm/year in the four first years of TOPEX/Poseidon has been evidenced in these works (see also section 3.4.1). In this study a drift of 1 mm/year has been applied until 1997 to derive MSL estimations.

Figure 50 shows the cycle-by-cycle MSL estimations from cycle 11 to cycle 444 for Alt-A, Alt-B and Poseidon using the NASA orbit and the inverse barometer correction.

- The last 1997 "El Niño" event leads to an unprecedented MSL rise (since the beginning of the mission), showing that long time series are needed to infer climate change conclusions from MSL estimates at the level of precision of 1 mm/year
- After El Niño, the MSL falls down back, but again rises in the last Alt-A cycles. We know that, via the SSB correction (SWH increase), the impact of the Alt-A instrumental changes on MSL estimations is non-negligible, even though effects on the range measurement tends to compensate the effect of SSB. This may explain the higher MSL for the last Alt-A cycles.
- The Alt-B MSL estimations lead to a gap between 0.5 and 1 cm relative to the last Alt-A cycles, but they seem to be more consistent to Alt-A data before El Niño.
- Estimates from cycles 300 onward are lower, even though from this figure, the MSL rise seems faster during the Alt-B time period.

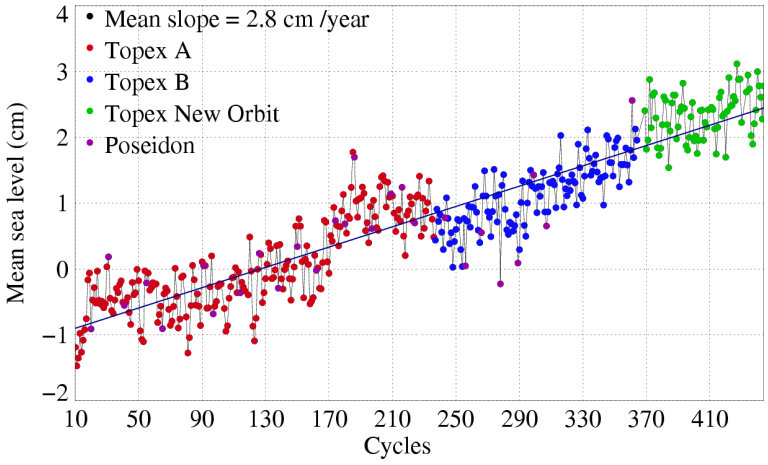

Figure 50: *Mean Sea Level obtained from AVISO M-GDR data (with additive correction). Inverse barometer correction is applied. TMR drift up to beginning of 1997: 1.0 mm/year; Additive Alt-A/B bias value: 0.5 cm; Correction for (DORIS-TOPEX) ionosphere correction drift, for Poseidon cycles after cycle 209*

Many authors do not use the inverted barometer correction, to estimate MSL because the correction from the M-GDR products uses a constant reference pressure. Indeed such a correction would lead to unrealistic ocean mass variations. Thus the time-varying reference mean pressure from ECMWF fields has been used to compute the inverted barometer correction (Dorandeu and Le Traon, 1999 [16]). In order to estimate the effect of this correction on previous results, the same calculation has been performed without applying the inverted barometer correction (Figure 51). This leads to similar results. However, Figure 51 shows much less noise compared to the case without IB correction but annual variations slightly larger due to differences between the global mean pressure from meteorological fields and the mean pressure sampled by TOPEX/Poseidon (Dorandeu et al., 1999).

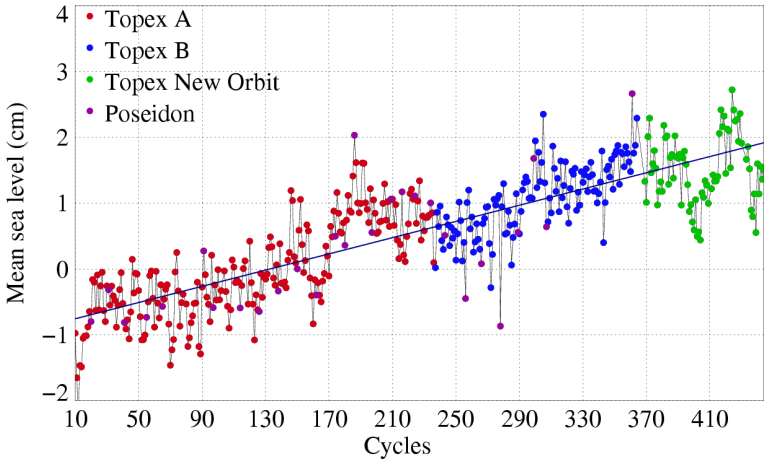

Figure 51: *Mean Sea Level obtained from AVISO M-GDR data (with additive correction). Inverse barometer correction is not applied. TMR drift up to beginning of 1997: 1.0 mm/year; Additive Alt-B/Alt-A bias value: 0.5 cm; Correction for (DORIS-TOPEX) ionosphere correction drift, for Poseidon cycles after cycle 209*

6.2.2 Impact of orbit calculation

As seen before (section 3.2), NASA and CNES terrestrial reference frames used in the precise orbit determination are not the same and cause radial differences at the level of a few millimeters. The impact of these discrepancies has been estimated in terms of Mean Sea Level variations and plotted on Figure 52. Dramatic differences, as large as 1 cm at hemispheric scale, are obtained between the two MSL estimations after cycle 170. As northern and southern hemispheres are not equally sampled, a trend is also observed in global MSL estimations. The figure shows a definite change in differences between the two orbits at cycle 247 when the ITRF97 reference frame was used in the CNES orbit calculation. This led to less difference between the two MSL estimations. As already mentioned, other important changes occurred in the CNES orbit calculation at cycle 320, with the use of the ITRF2000 reference frame and the albedo model. Moreover ITRF2000 has been applied in the NASA orbit calculation from cycle 360 onwards. As a result, the consistency between 2 orbits is better. Differences are reduced to very close to zero values at both global and hemispheric scales.

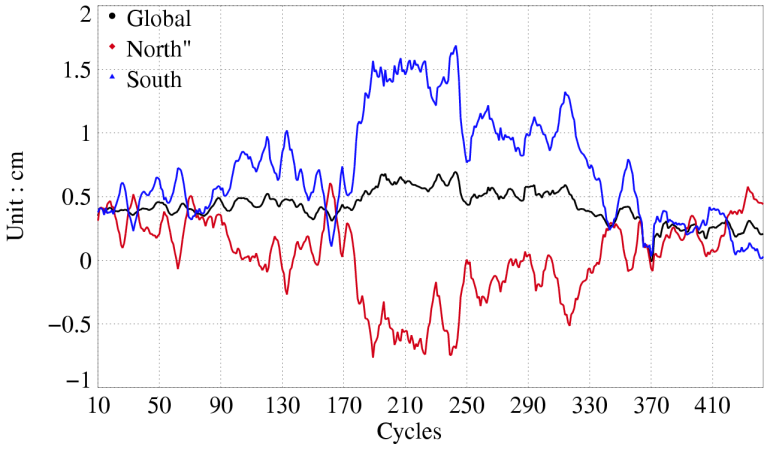

Figure 52: *Difference in MSL estimations using respectively CNES and NASA orbits*

6.3 Topex/Poseidon relative altimeter bias

Collinear differences are also used to compute the (TOPEX Poseidon) relative bias. Each Poseidon cycle is compared to the two adjacent TOPEX cycles, leading to a mean relative bias estimate.
Figure 53 shows the values of the mean (TOPEX Poseidon) SSH differences as a function of Poseidon cycles. The figure is split into three parts defined by Poseidon data retracking and the switch from Alt-A to Alt-B.

After Poseidon data retracking, the relative bias was about 1 cm higher than before, even though a dedicated bias value had been applied in the AVISO processing to account for the impact of retracking. In addition, the relative bias value has increased during the last Alt-A cycles, maybe due to Alt-A changes.

After the Alt-B switching on, the TOPEX/Poseidon relative bias has been reduced to very low values because of remaining Alt-A/alt-B bias. Moreover, the last estimates are directly impacted by the (TOPEX - DORIS) ionosphere correction difference which leads to overestimate the relative bias by about 0.5 cm in the last cycles.

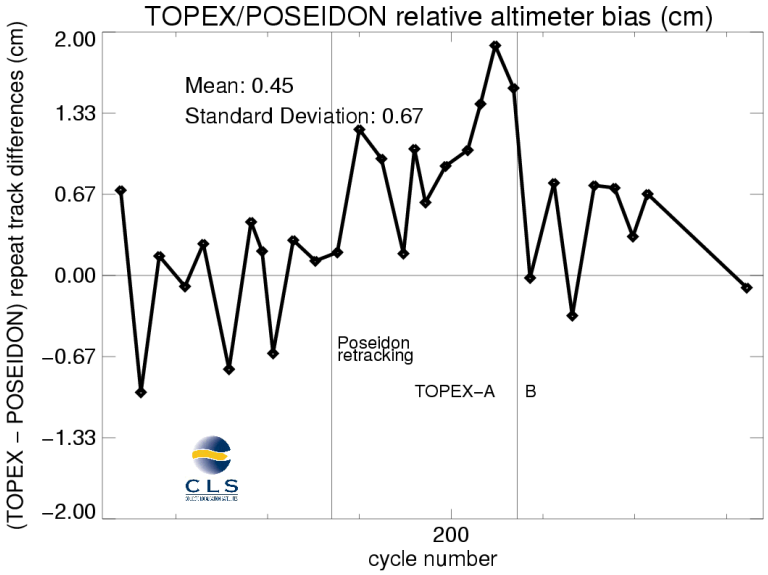

Figure 53: *(TOPEX Poseidon) SSH relative bias from AVISO M-GDRs (no other correction applied)*

6.4 Sea level seasonal variations

A short description of major oceanic signals is given here, in order to assess the data quality for oceanographic applications.
The large scale seasonal variations in the surface-topography (e.g. steric effect due to heat flux variations, seasonal an inter-annual variability of the equatorial currents) are clearly evidenced on this figure.
Important inter-annual signals can be observed in the steric effect which is characterized by the contrast between Northern and Southern hemispheres, according to seasons. It is larger, for example, during winter and spring 1996 relative to 1993. Seasonal variations in west boundary currents, and therefore in the associated transports, are also exposed to inter-annual variations: the winter cooling of both Gulf Stream and Kuroshio currents and their extensions is weaker in 1994 and particularly great in 1996 and 1998.

The most important changes are observed in the equatorial band. Though El Niño events have already occurred (e.g. fall 94/winter 95), the 1997 El Niño is the major feature in these regions since the beginning of the mission, because of its amplitude and duration. Due to Kelvin waves eastward propagation, it creates large positive anomalies in the eastern part of the Pacific ocean. Warmer water masses reach the California coasts in summer/fall 1997. At the same time, negative anomalies affect the western part of the basin.

At the end of 1997 and winter 1998, large anomalies are also observed around the equator in the Indian Ocean. After El Niño events, trade winds forcing acts again to create westward propagation of water masses. Surface-topography anomalies, respectively positive and negative at the western and eastern parts of the Pacific, lead to "La Niña" situation in 1999 and 2000. During Summer 2001, eastward propagations seem to begin in the equatorial zone.

At the end of 2002, another El Niño situation occurs. It has been noticed in terms of SLA variability (section 6.1). Then the equatorial Pacific Ocean comes back to La Niña situation in Spring 2003.

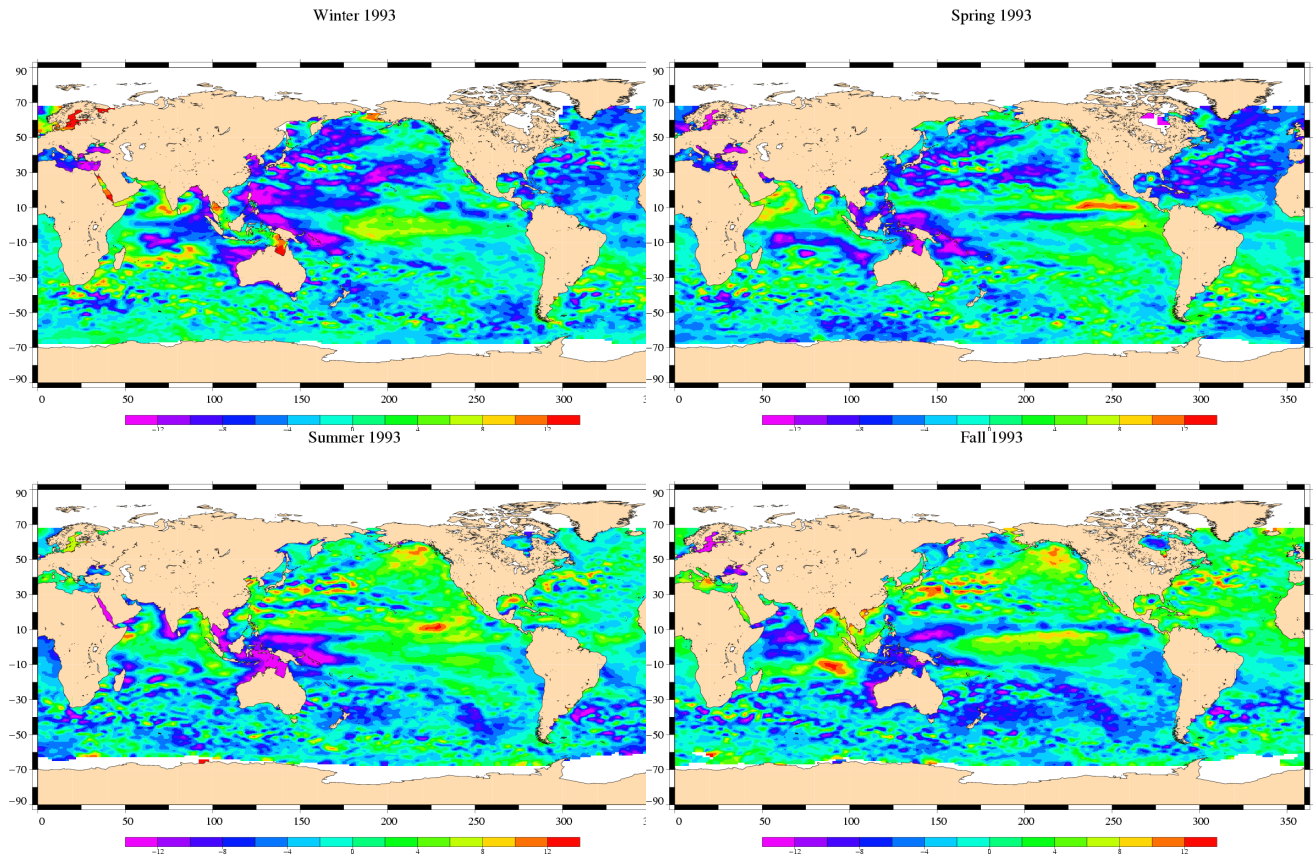

Figure 54: *Seasonal variations of Jason SLA (cm) for year 1993 relative to a MSS CLS 2001*

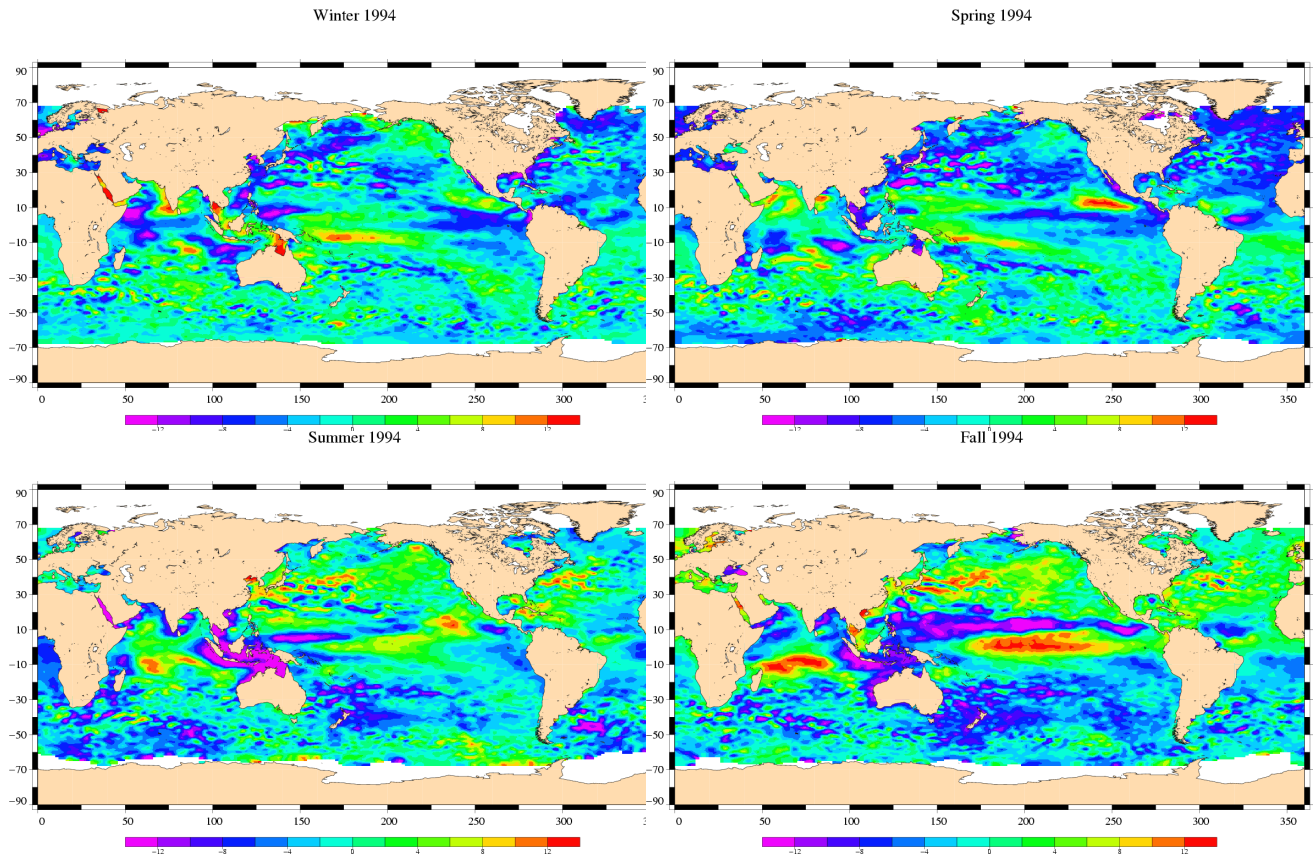

Figure 55: *Seasonal variations of Jason SLA (cm) for year 1994 relative to a MSS CLS 2001*

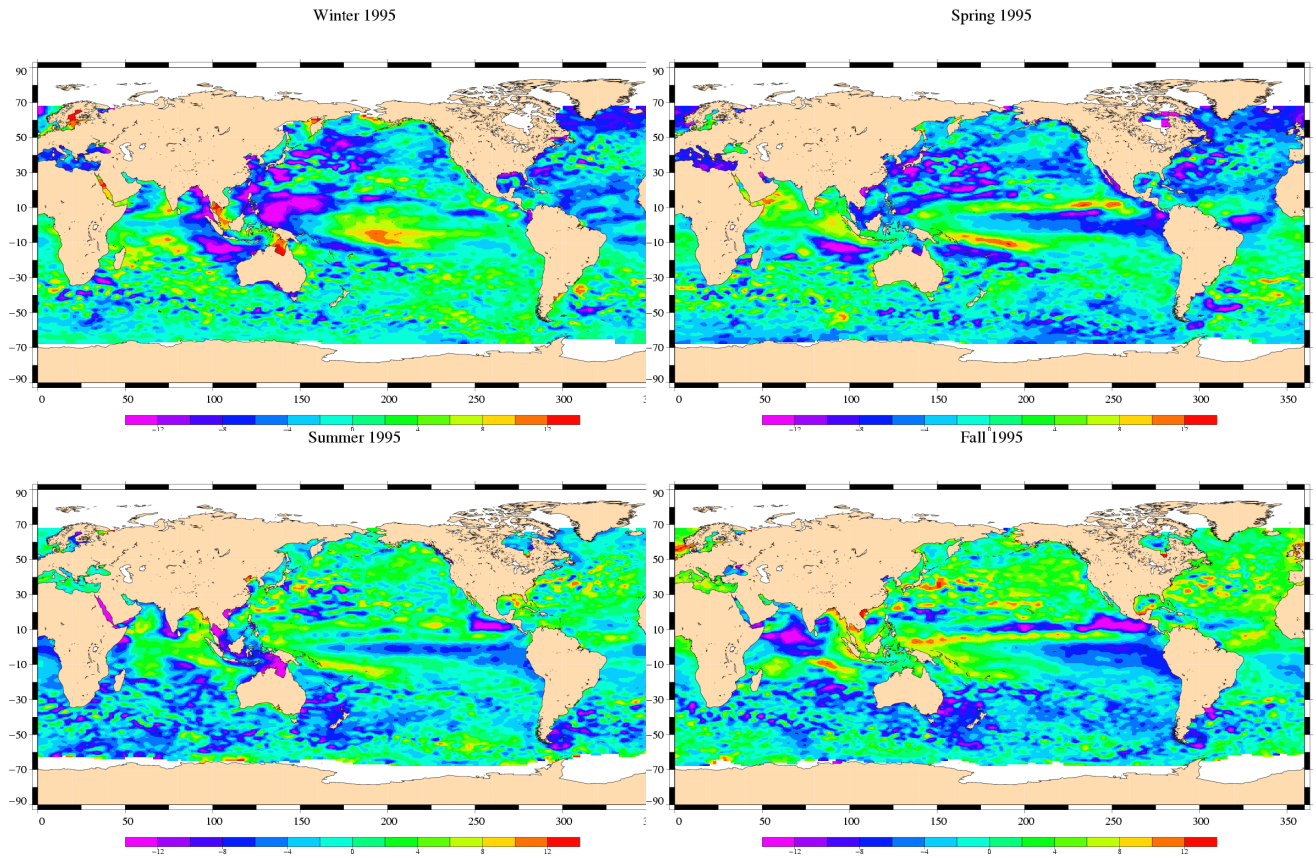

Figure 56: *Seasonal variations of Jason SLA (cm) for year 1995 relative to a MSS CLS 2001*

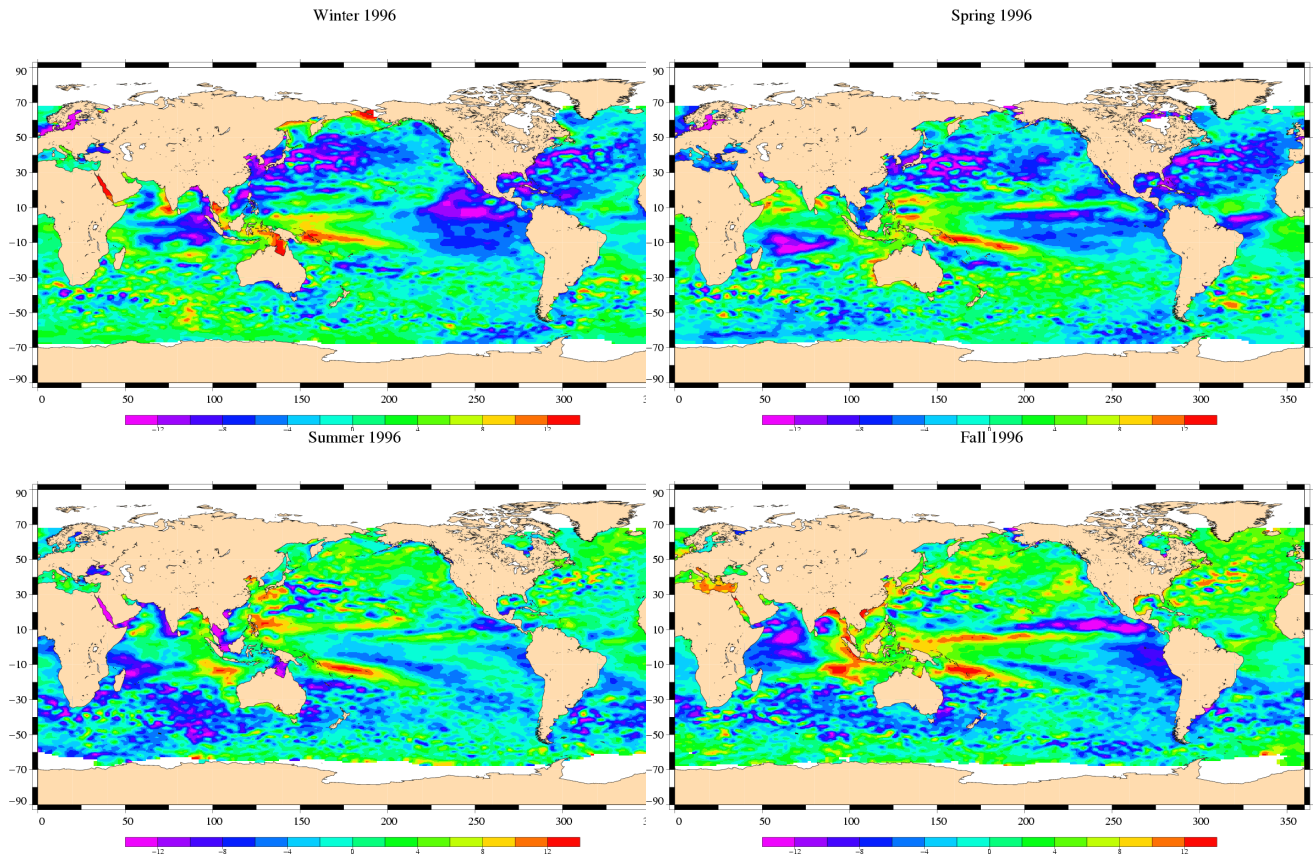

Figure 57: *Seasonal variations of Jason SLA (cm) for year 1996 relative to a MSS CLS 2001*

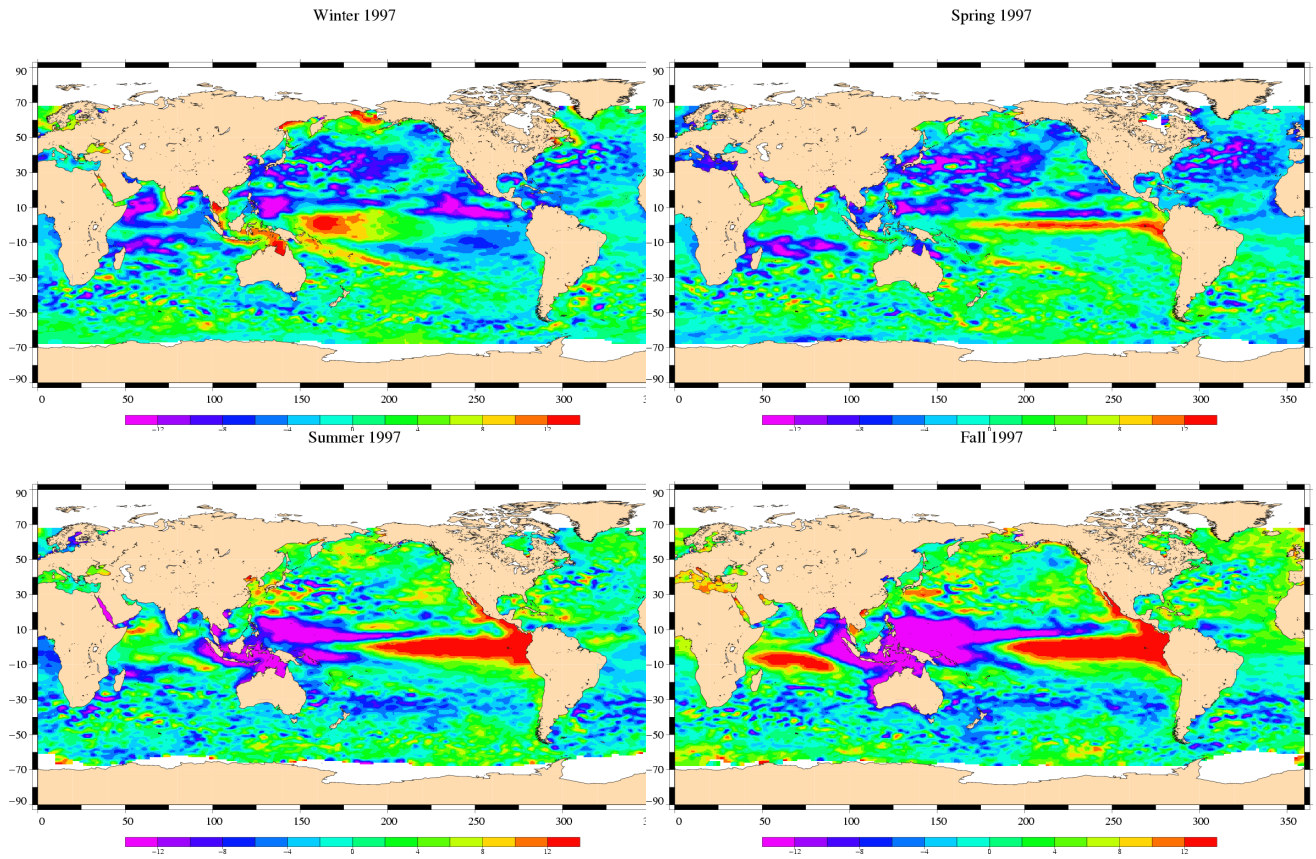

Figure 58: *Seasonal variations of Jason SLA (cm) for year 1997 relative to a MSS CLS 2001*

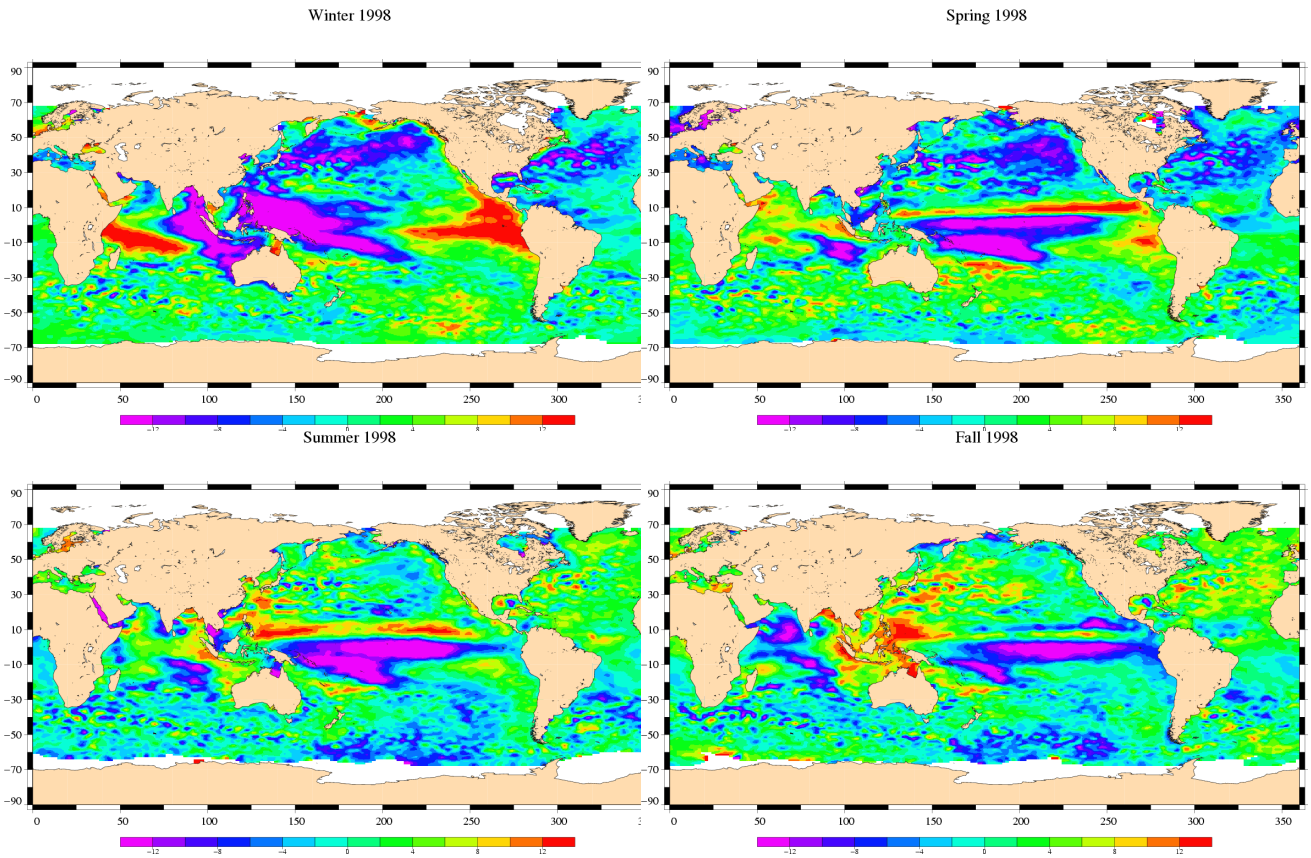

Figure 59: *Seasonal variations of Jason SLA (cm) for year 1998 relative to a MSS CLS 2001*

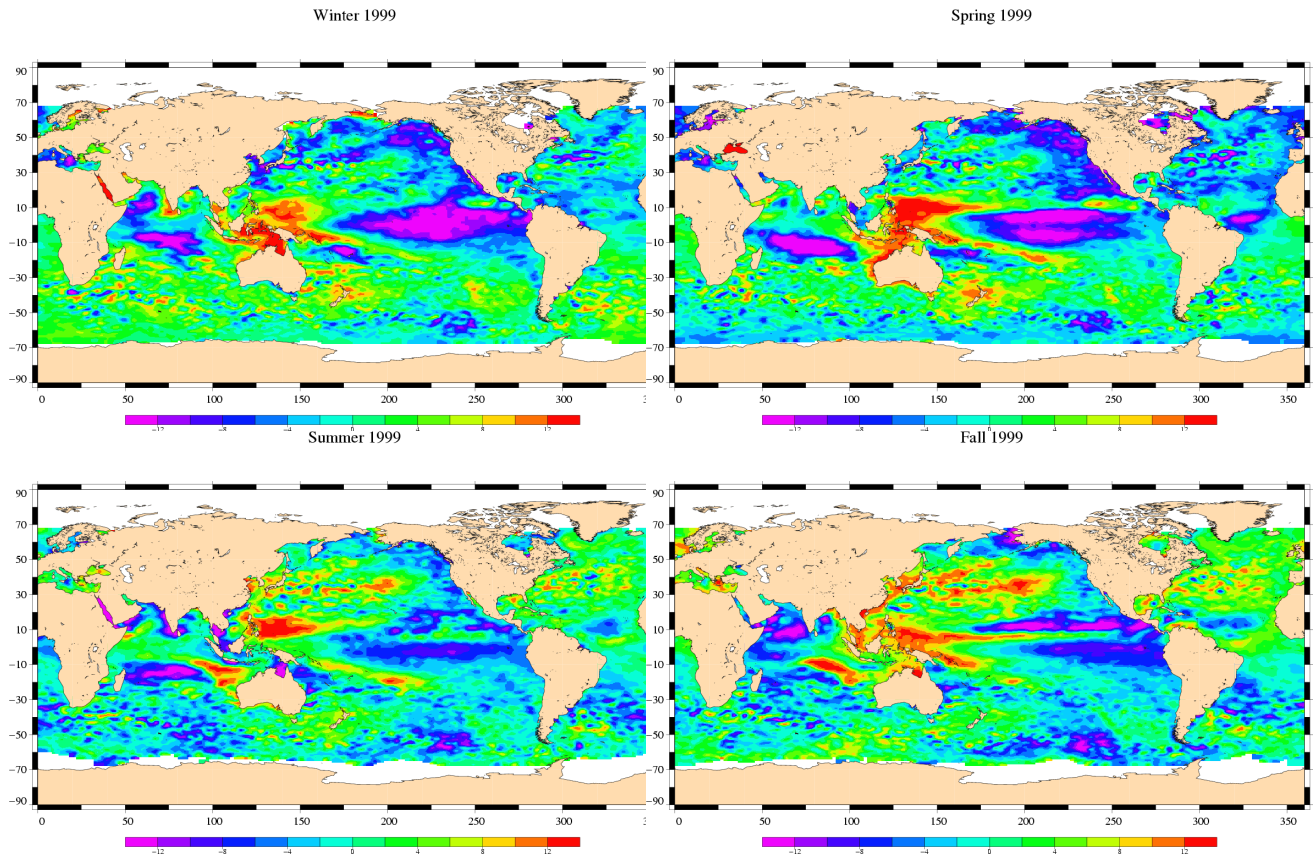

Figure 60: *Seasonal variations of Jason SLA (cm) for year 1999 relative to a MSS CLS 2001*

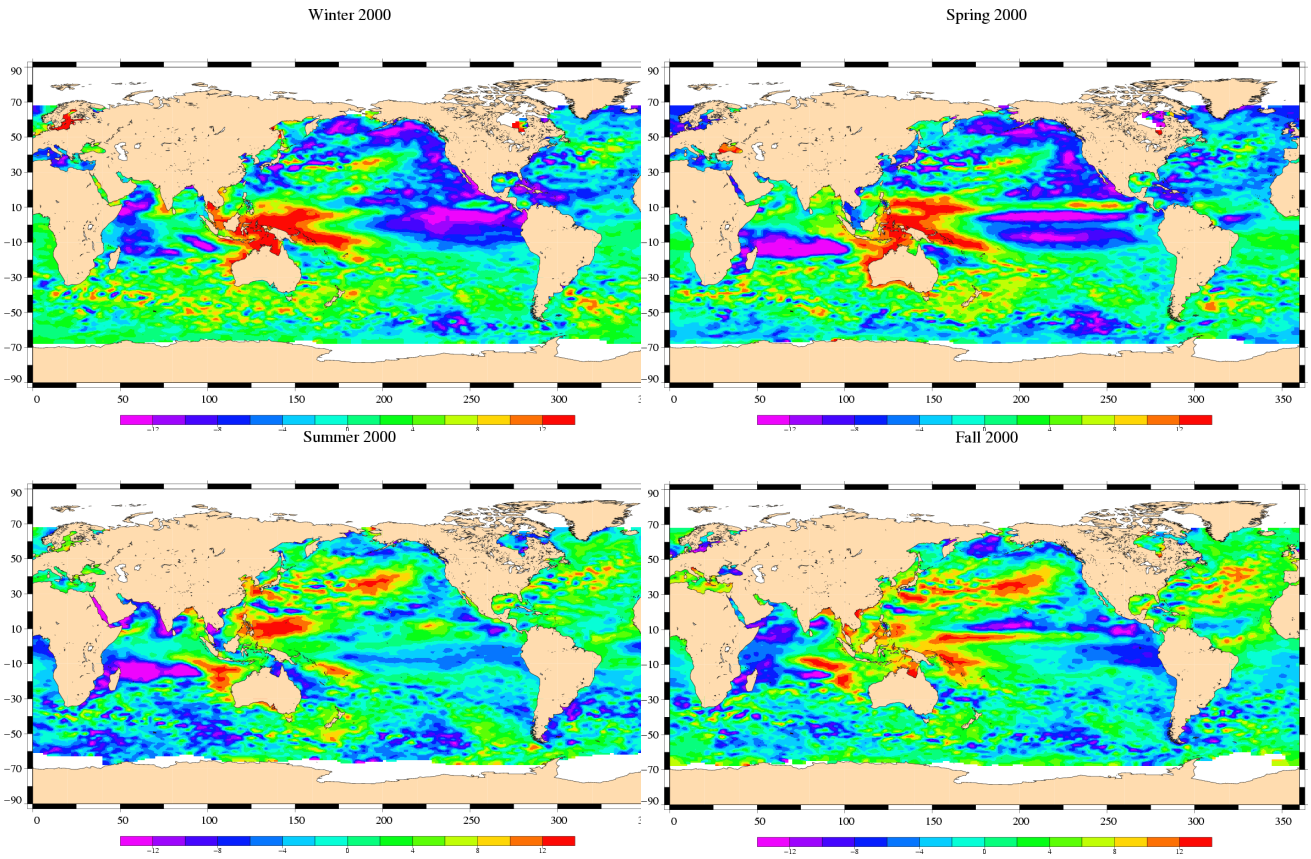

Figure 61: *Seasonal variations of Jason SLA (cm) for year 2000 relative to a MSS CLS 2001*

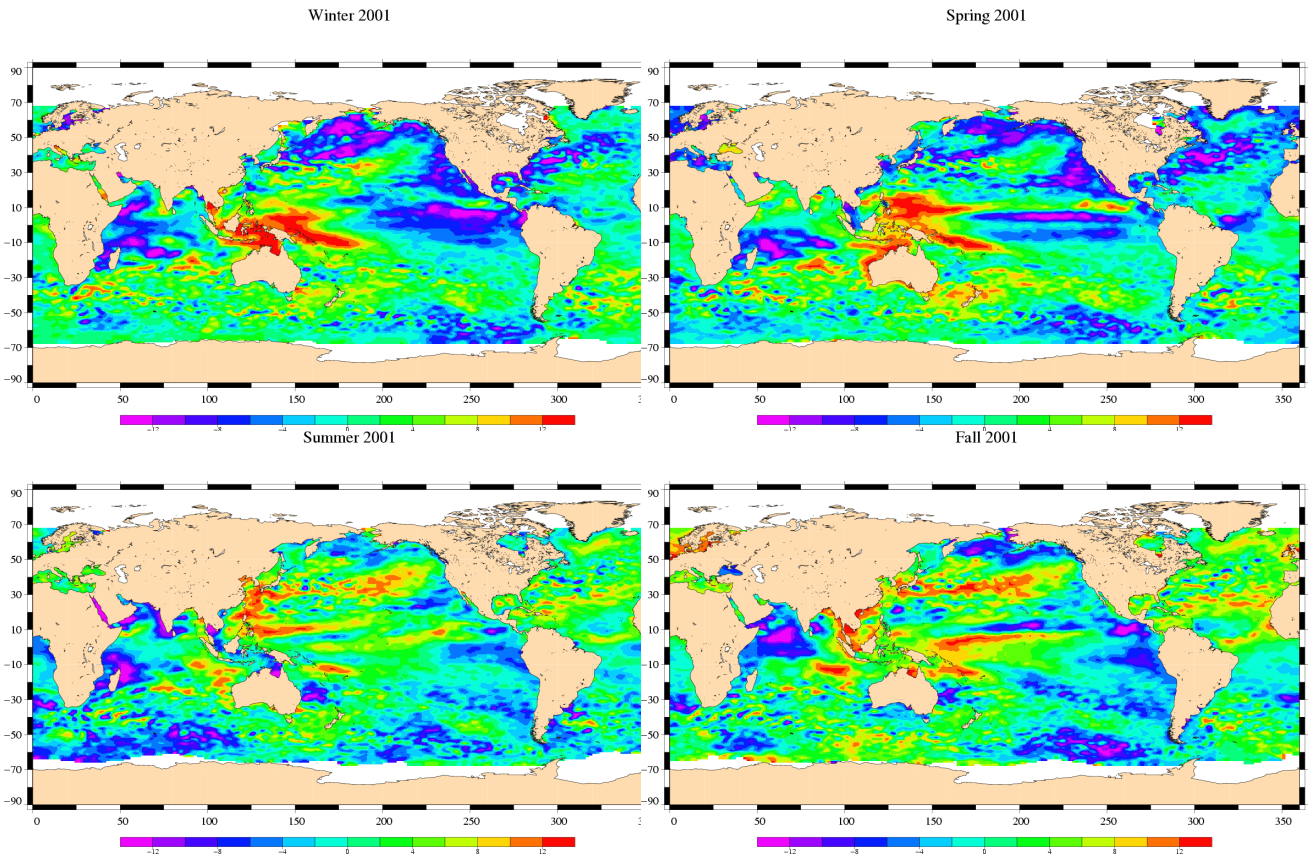

Figure 62: *Seasonal variations of Jason SLA (cm) for year 2001 relative to a MSS CLS 2001*

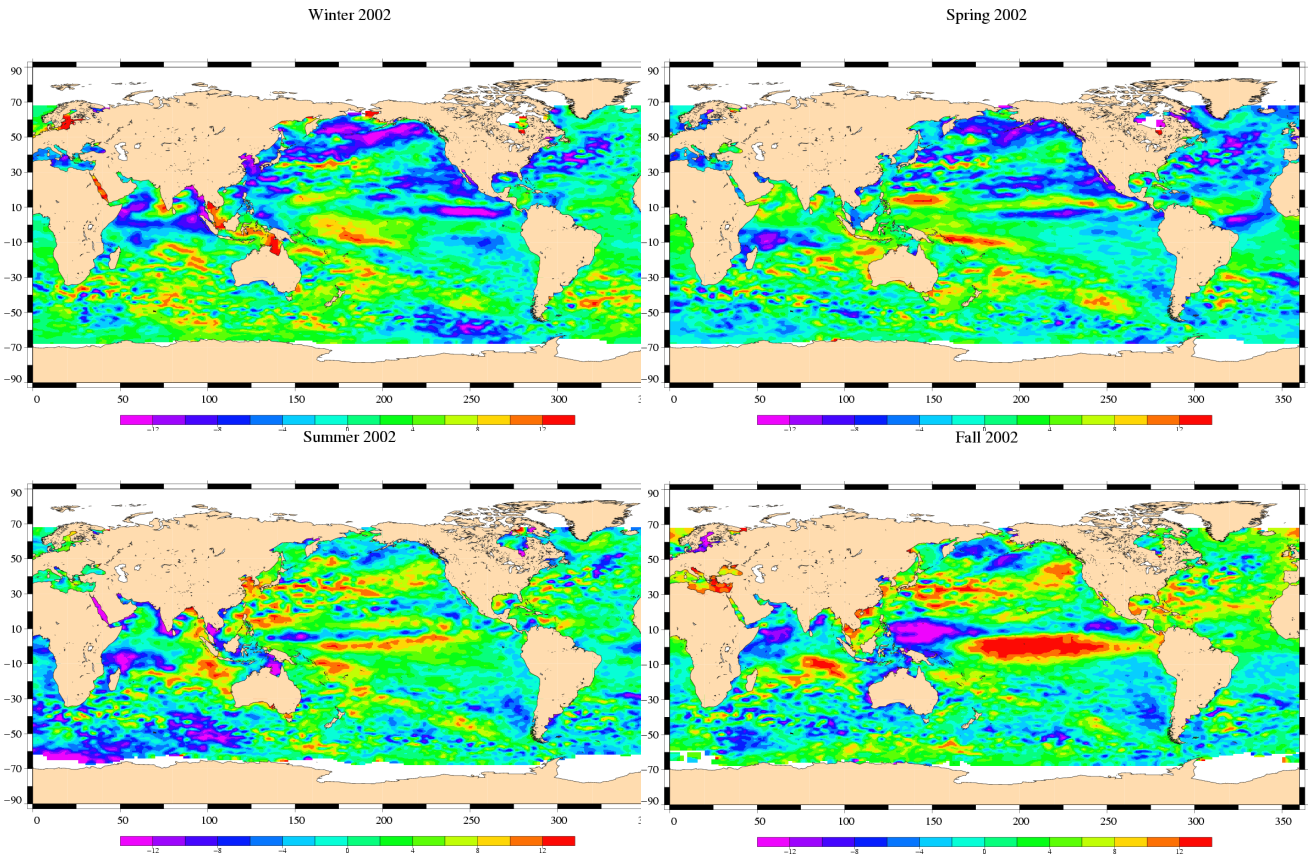

Figure 63: *Seasonal variations of Jason SLA (cm) for year 2002 relative to a MSS CLS 2001*

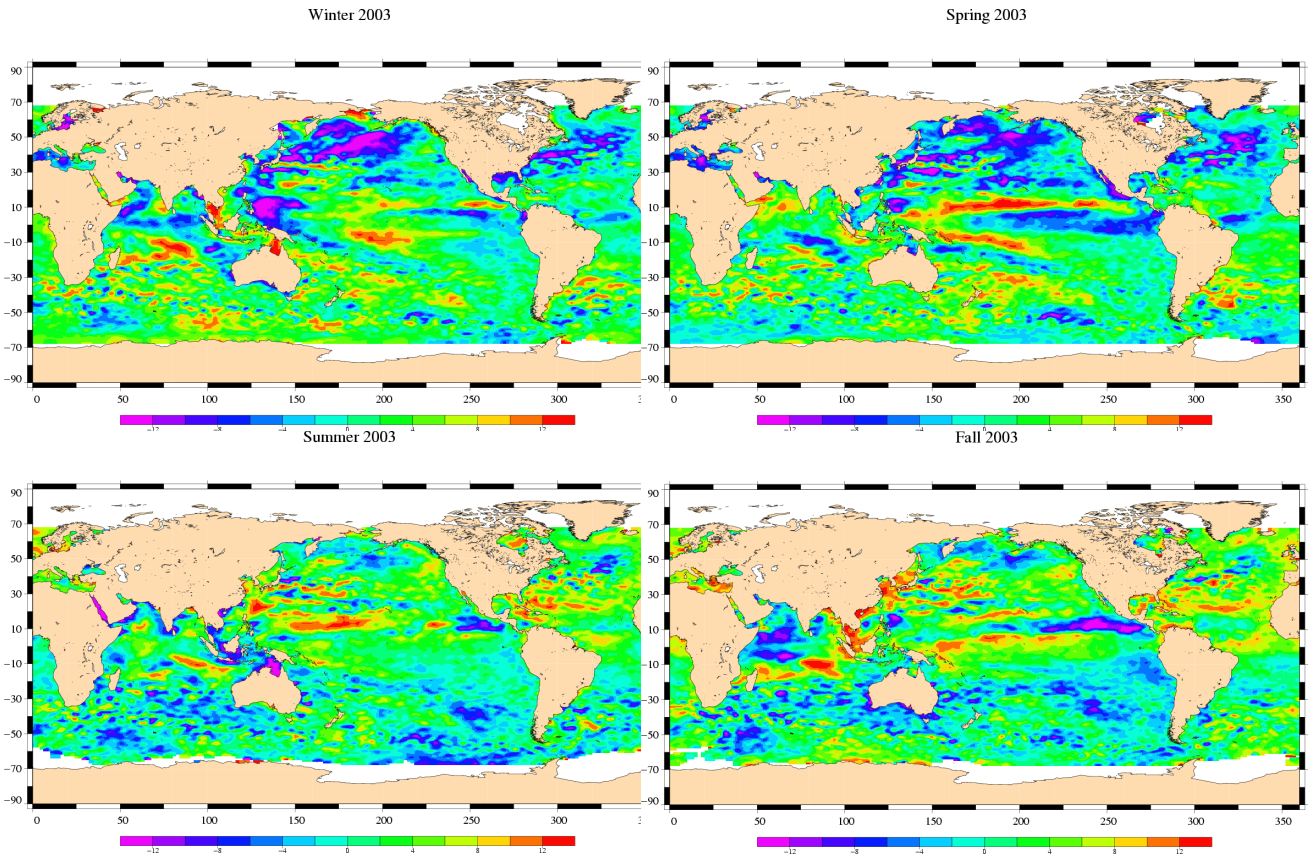

Figure 64: *Seasonal variations of Jason SLA (cm) for year 2003 relative to a MSS CLS 2001*

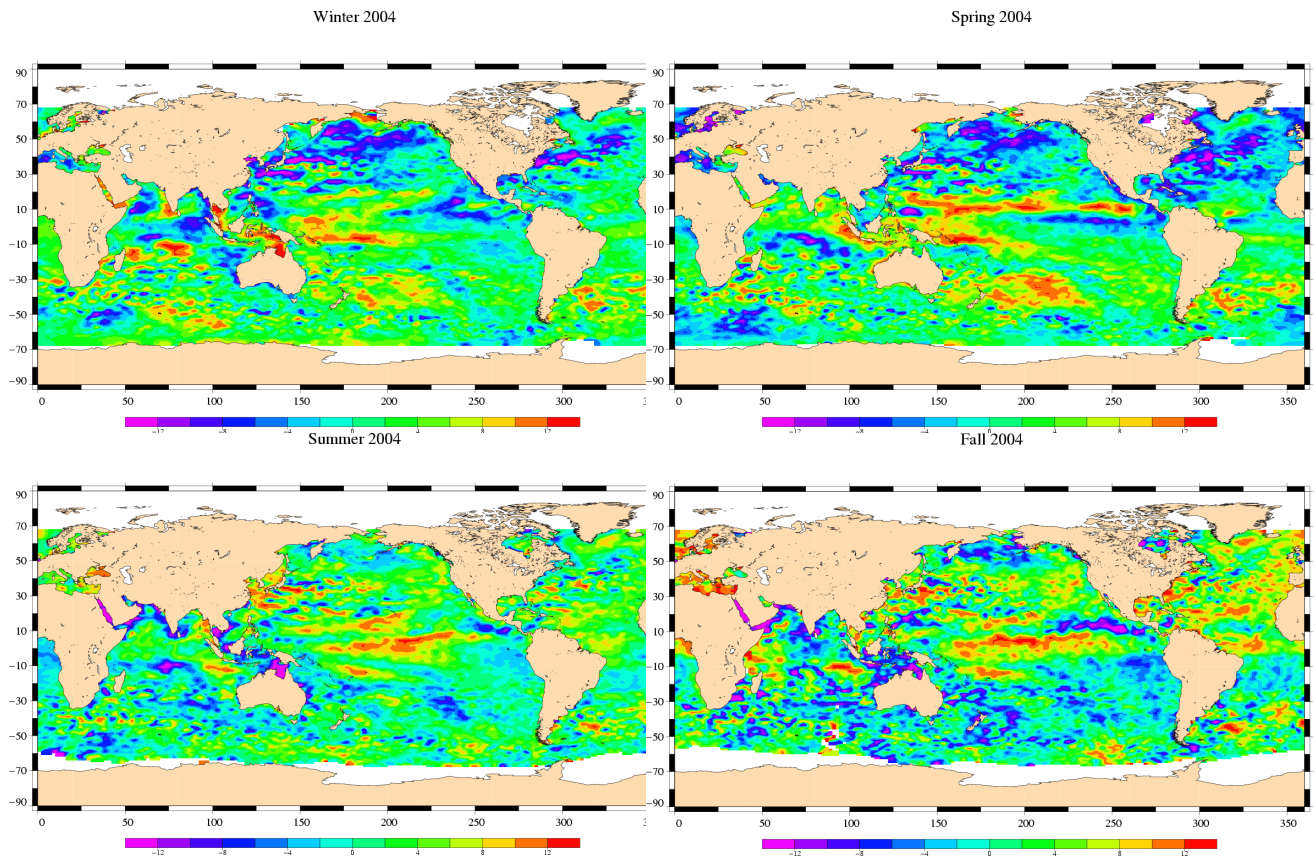

Figure 65: *Seasonal variations of Jason SLA (cm) for year 2004 relative to a MSS CLS 2001*

7 Mean Sea Level (MSL) and Sea Surface Temperature (SST) comparisons

This study has been carried out in order to monitor the MSL seen by all the operational altimeter missions. Long-term MSL change is a variable of considerable interest in the studies of global climate change. Then the objective here is on the one hand to survey the mean sea level trends and on the other hand to assess the consistency between all the MSL. Besides, the Reynolds SST is used to compare the MSL with an external data source. The mean SST is calculated as the same way as the MSL.
The following missions have been used : TOPEX/Poseïdon (T/P), Jason-1 (J1), Geosat Follow-On (GFO) and Envisat. The MSL and SST time series have been plotted over global ocean and over main oceanic areas. This allows us to correlate the MSL trends seen by each mission and to compare them with the SST.
In addition to this analysis, the maps of regional MSL change and SST change have been plotted for each mission over the Jason-1 period and the Envisat period. The differences of these maps has been performed; this is a way to display eventual local drifts.
This study is still on going and the analysis of the plots presented here is very preliminary. Basically, it allows us to give an overview of results which can be achieved.

7.1 SSH definition for each mission

The main SSH calculation are defined for all the satelites as defined below as of the GDR products (Jason-1, Envisat) or MGDRs products (T/P) :

$$SSH = Orbit - Altimeter\ Range - \sum_{i=1}^{n} Correction_i$$

with :

$$\begin{aligned}
\sum_{i=1}^{n} Correction_i &= Dry\ troposhere\ correction \\
&+ Inverse\ barometer\ correction \\
&+ RadiometerWet\ troposhere\ correction \\
&+ AltimeterIonospheric\ correction \\
&+ Sea\ state\ bias\ correction \\
&+ Ocean\ tide\ correction \\
&+ Earth\ tide\ correction \\
&+ Polar\ tide\ correction
\end{aligned}$$

But some exceptions or additionnal corrections have been applied :

- For Jason-1 and Envisat the wet troposhere correction has been changed by the ECMWF model in order to remove the effects of abnormal changes or trends observed on the radiometer wet troposhere correction.
- For Envisat, the USO drift has been applied.
- For T/P, the radiometer wet troposhere correction has been corrected from Ruf correction (Ruf, 2002b [40])
- For T/P, the relative bias between TOPEX and Poseidon and between TOPEX A and TOPEX B has been taken into account
- For T/P, the drift between the TOPEX and DORIS ionosphere corrections has been corrected for on Poseidon cycles.
- For Geosat Follow-On, the GIM model has been used for the ionospheric correction.

7.2 MSL and SST time series over main oceanic areas

7.2.1 Methodology

The MSL and the Reynolds SST have been computed cycle per cycle according to the main oceanic areas for each altimeter mission. For each plot, the MSL scale is described on the left and the SST scale on the right. The MSL and the SST don't have the same unit ("cm" and "degree"), thus to compare the 2 quantities, the SST scale is adjusted on the MSL scale so that the SST trend and the MSL trend are visually the same. Thus the SST and the MSL dynamics can be compared.
For each area, 2 charts have been plotted: only the MSL have been plotted on the right whereas the SST has been plotted on the left in addition. For each plot, the 60-day signal has been smoothed. Notice that an articial MSL bias has been applied in order to not superimpose each curve.

7.2.2 Global ocean

MSL and SST have been monitored over global ocean in figure 66 over T/P period and in figure 67 over Jason-1 period.

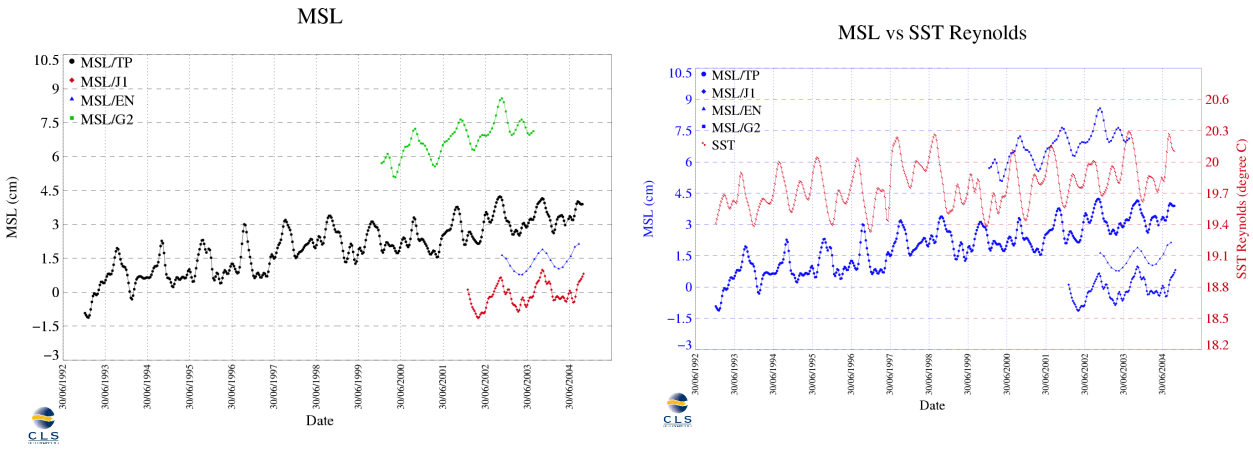

Figure 66: *MSL and SST over global ocean and over the T/P period*

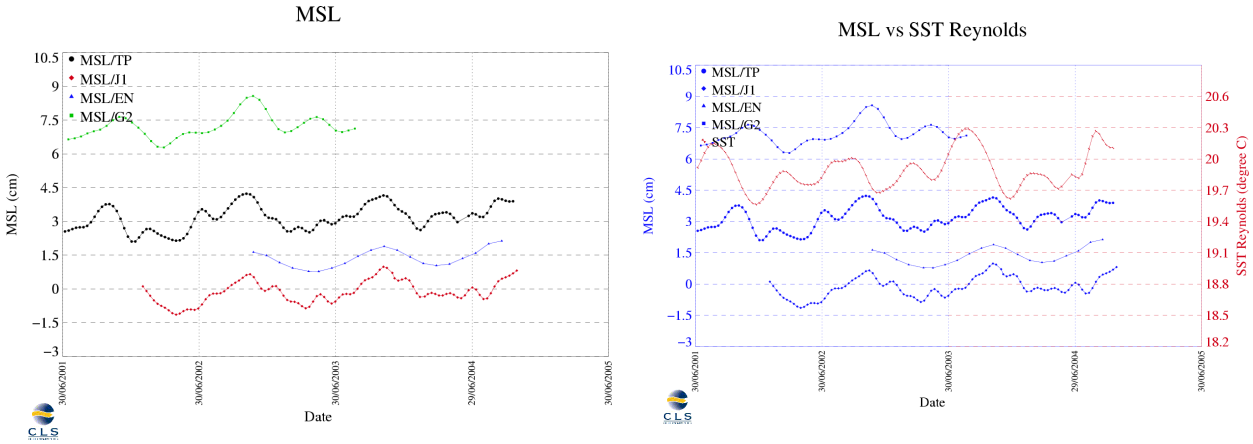

Figure 67: *MSL and SST over global ocean and over the Jason-1 period*

7.2.3 Monitoring over the Indian Ocean

Figure 68 and figure 69 are the same as in section 7.2.2 over the Indian Ocean.

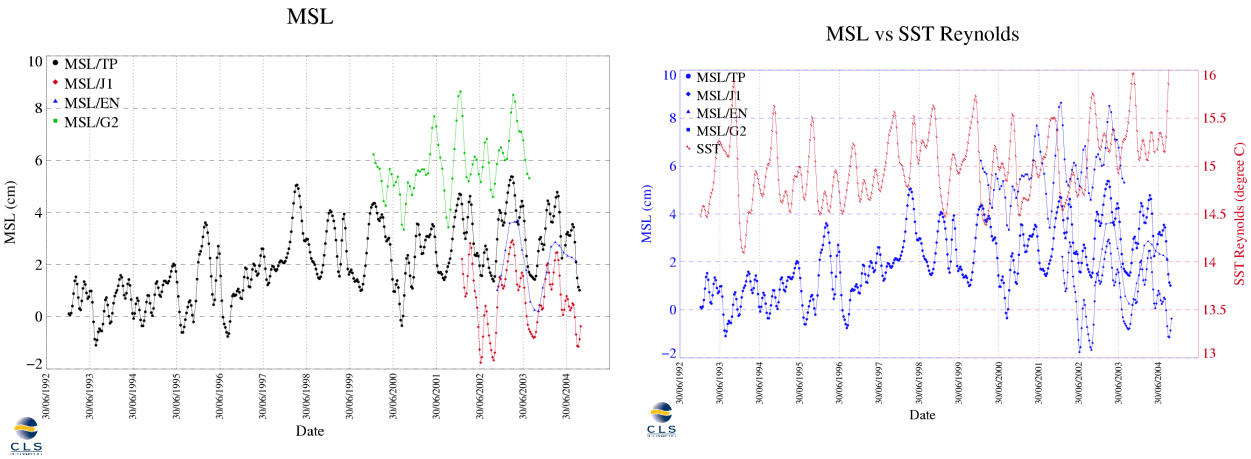

Figure 68: *MSL and SST over the Indian Ocean and over the T/P period*

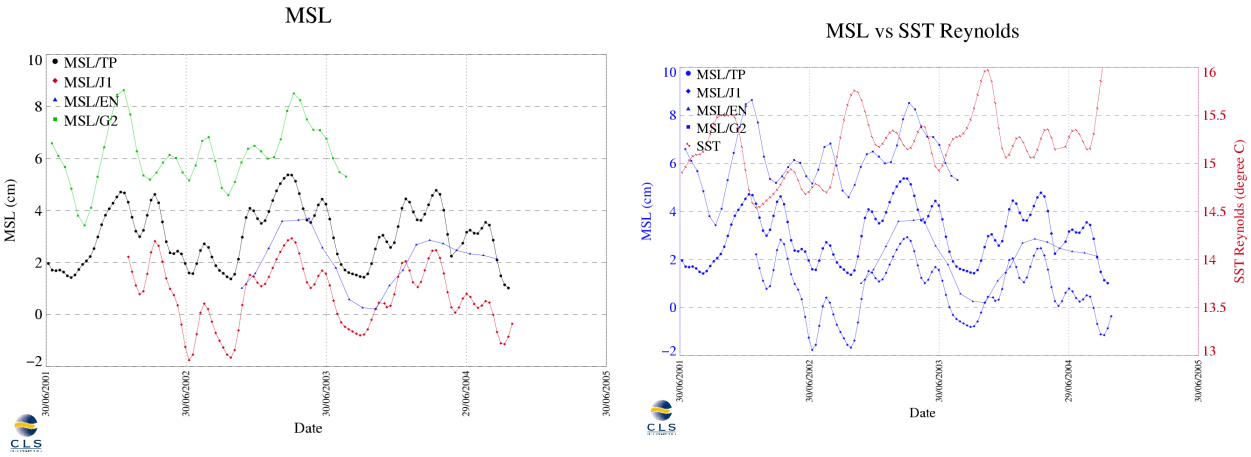

Figure 69: *MSL and SST over the Indian Ocean and over the Jason-1 period*

7.2.4 Monitoring on the Northern hemisphere

Figure 70 and figure 71 are the same as in section 7.2.2 on the Northern hemisphere.

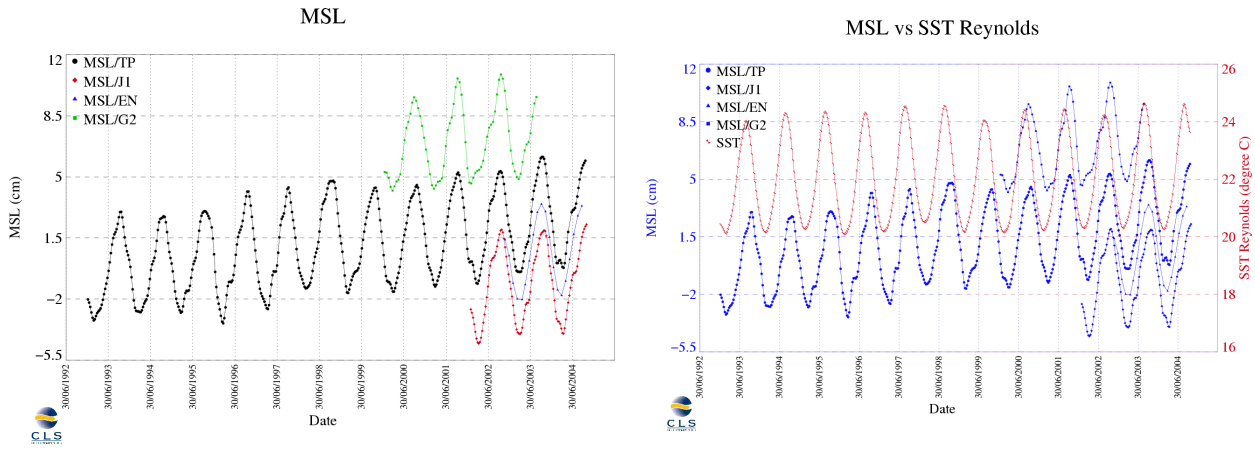

Figure 70: *MSL and SST on the Northern hemisphere and over the T/P period*

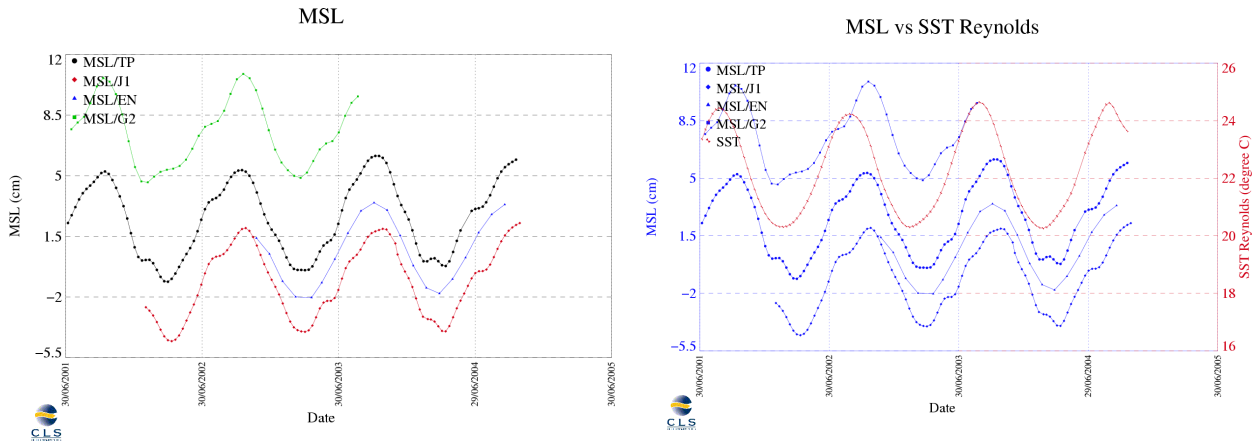

Figure 71: *MSL and SST on the Northern hemisphere and over the Jason-1 period*

7.2.5 Monitoring on Southern hemisphere

Figure 72 and figure 73 are the same as in section 7.2.2 on the Southern hemisphere.

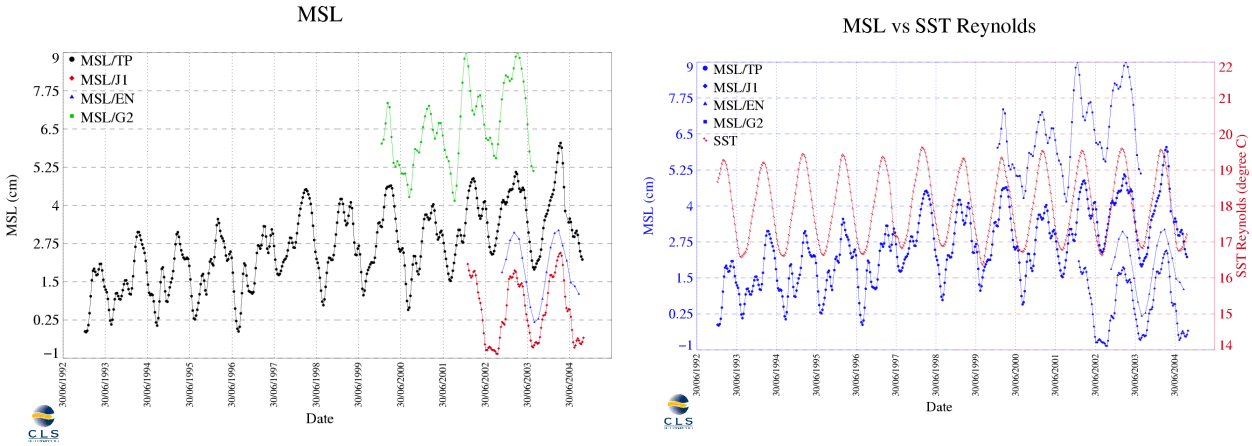

Figure 72: *MSL and SST on the Southern hemisphere and over the T/P period*

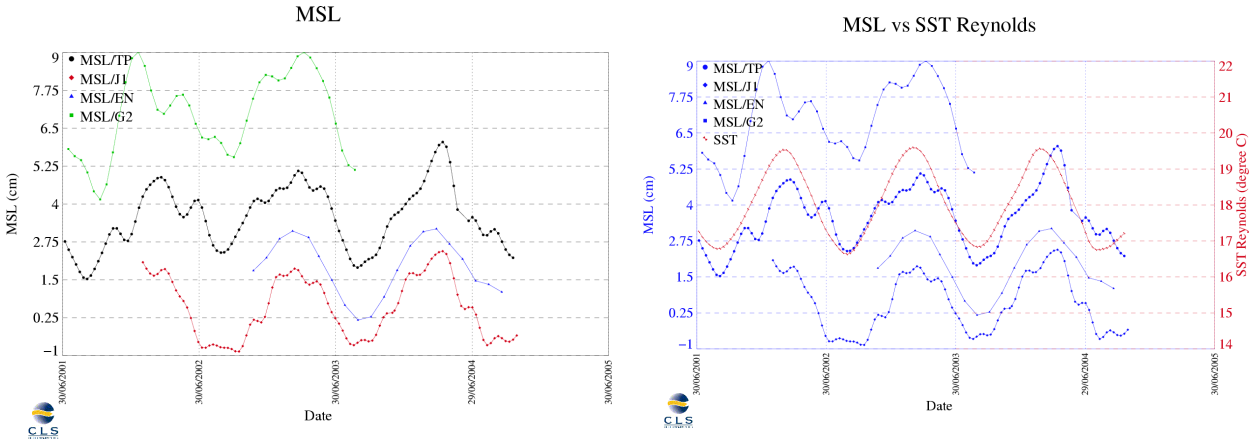

Figure 73: *MSL and SST on the Southern hemisphere and over the Jason-1 period*

7.2.6 Monitoring over the North Atlantic Ocean

Figure 74 and figure 75 are the same as in section 7.2.2 over the North Atlantic Ocean.

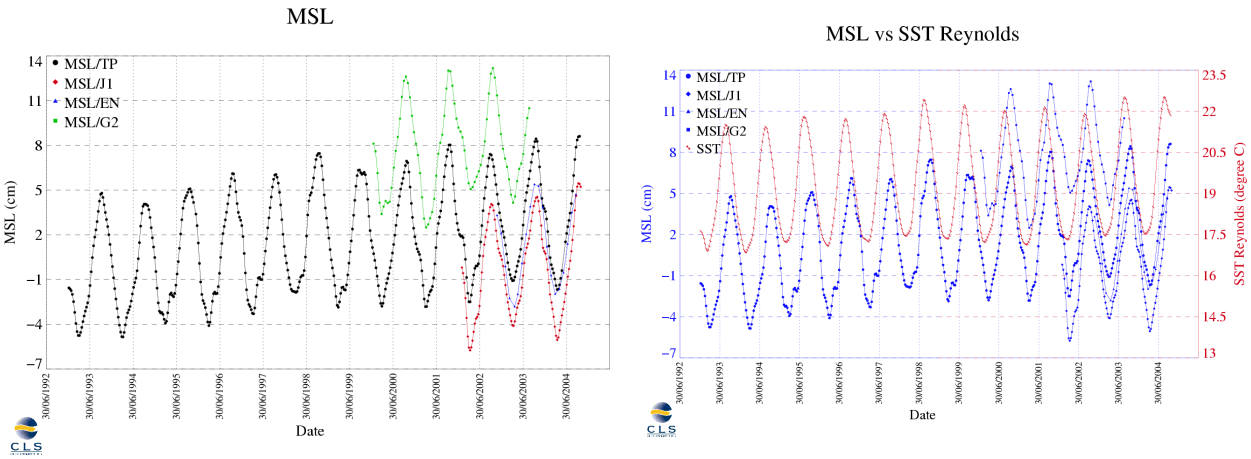

Figure 74: *MSL and SST over the North Atlantic Ocean and over the T/P period*

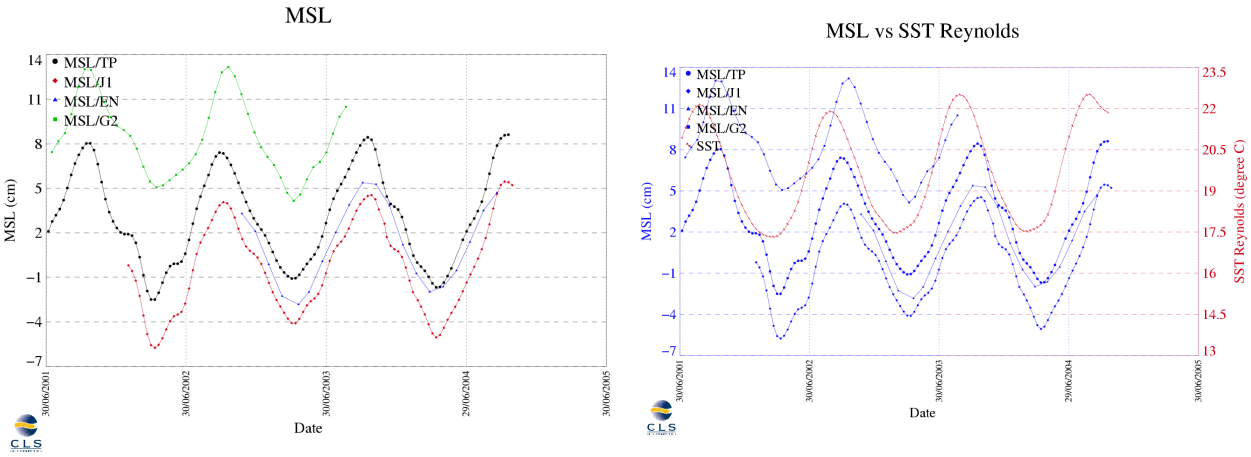

Figure 75: *MSL and SST over the North Atlantic Ocean and over the Jason-1 period*

7.2.7 Monitoring over the South Atlantic Ocean

Figure 76 and figure 77 are the same as in section 7.2.2 over the South Atlantic Ocean.

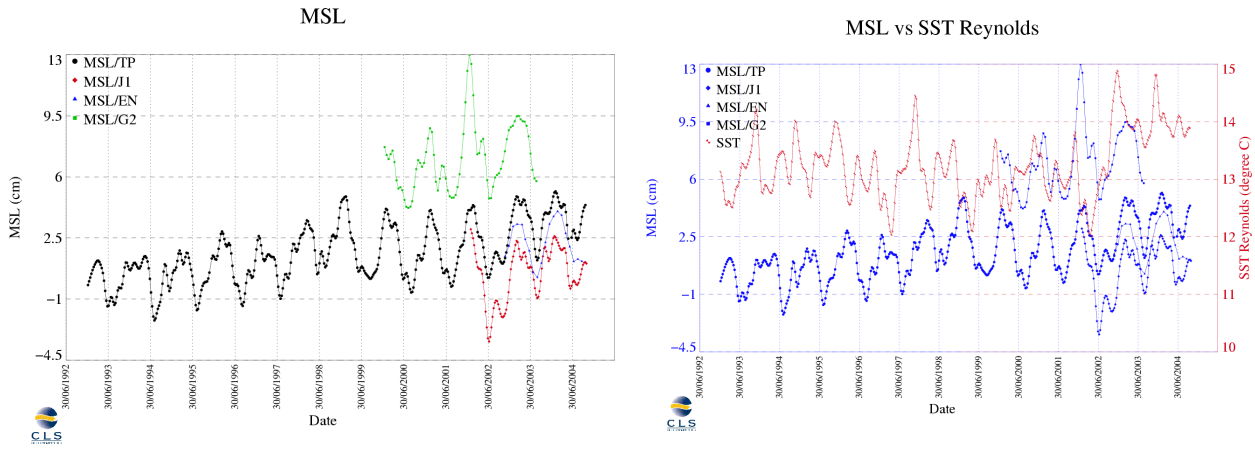

Figure 76: *MSL and SST over the South Atlantic Ocean and over the T/P period*

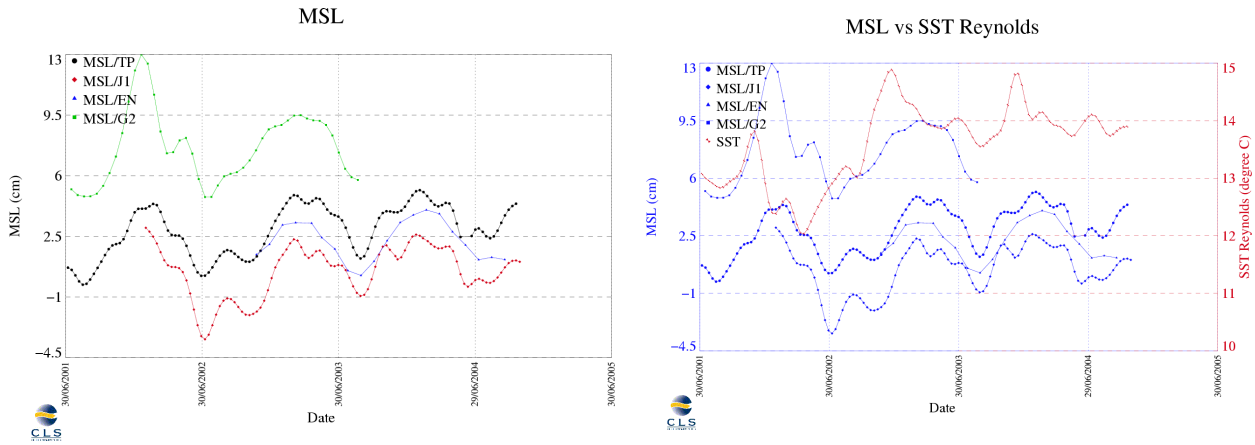

Figure 77: *MSL and SST over the South Atlantic Ocean and over the Jason-1 period*

7.2.8 Monitoring over the North Pacific Ocean

Figure 78 and figure 79 are the same as in section 7.2.2 over the North Pacific Ocean.

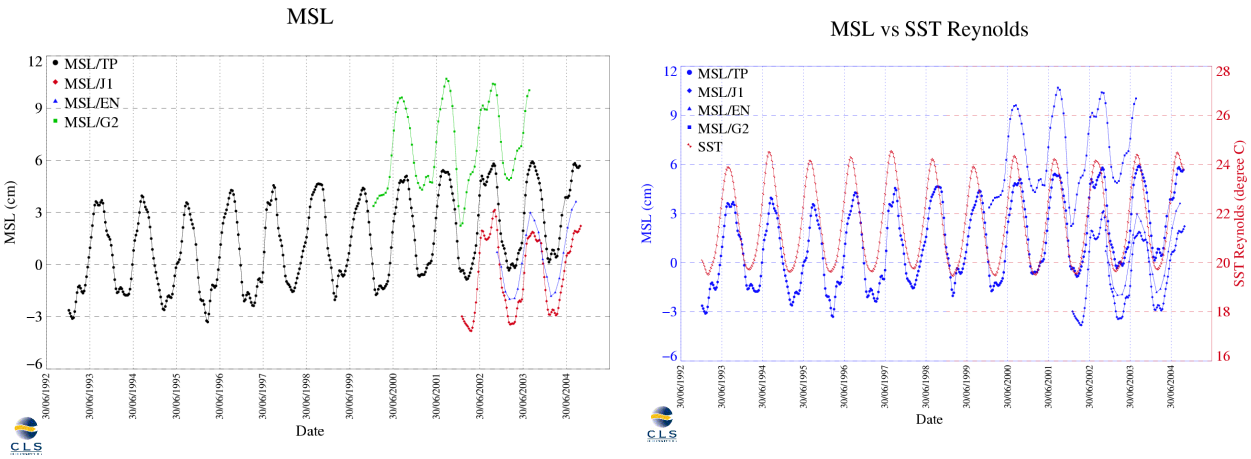

Figure 78: *MSL and SST over the North Pacific Ocean and over the T/P period*

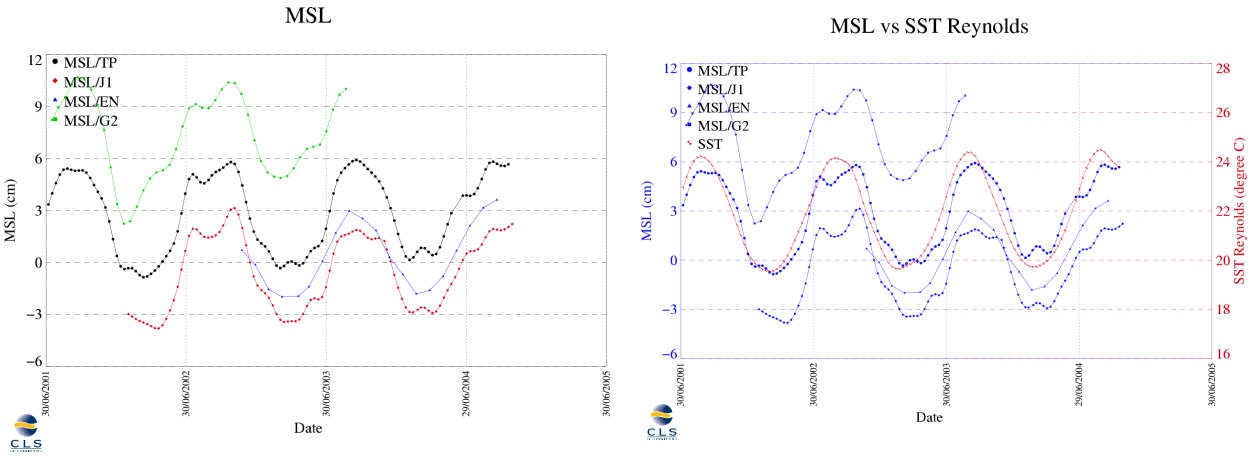

Figure 79: *MSL and SST over the North Pacific Ocean and over the Jason-1 period*

7.2.9 Monitoring over the South Pacific Ocean

Figure 80 and figure 81 are the same as in section 7.2.2 over the South Pacific Ocean.

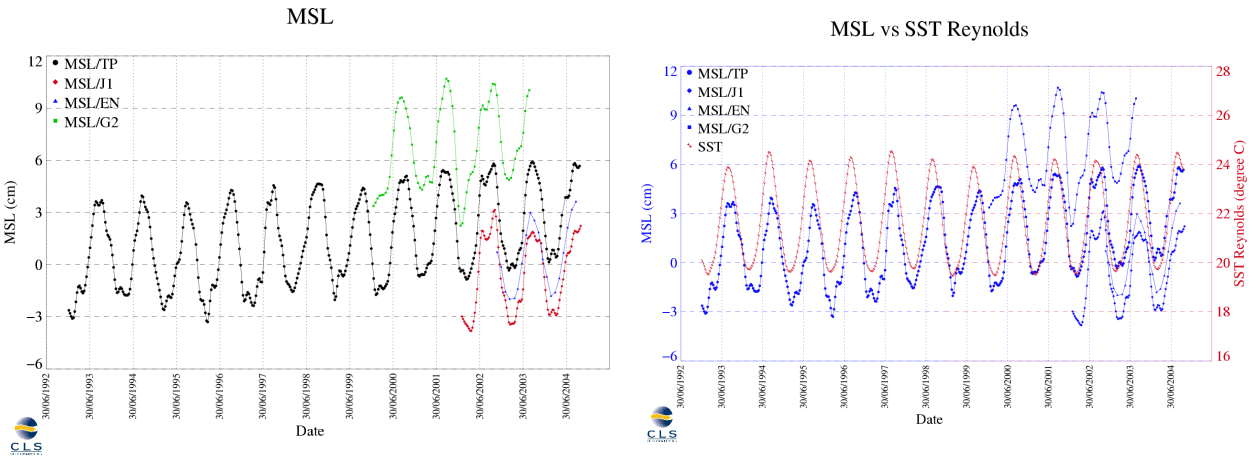

Figure 80: *MSL and SST over the South Pacific Ocean and over the T/P period*

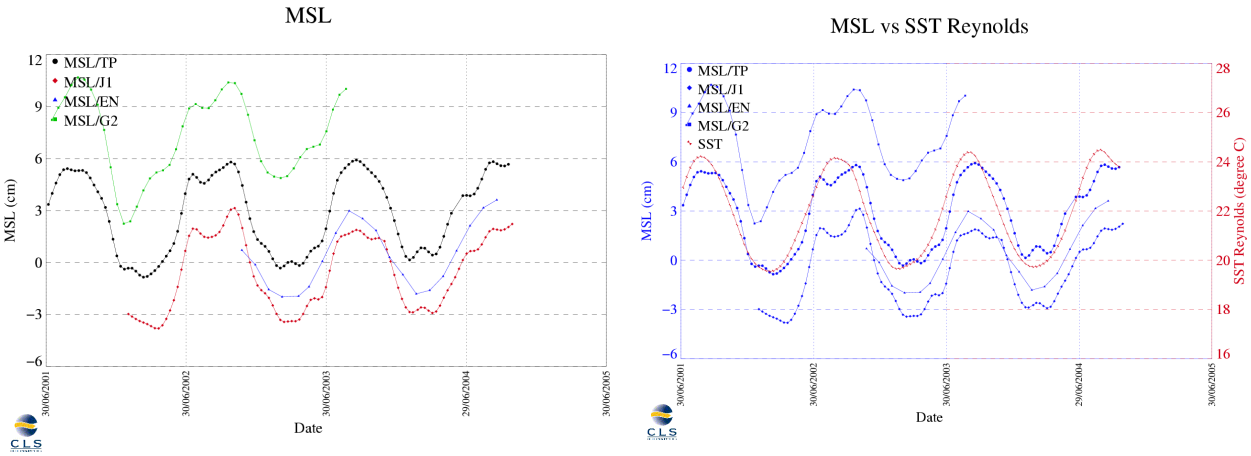

Figure 81: *MSL and SST over the South Pacific Ocean and over the Jason-1 period*

7.2.10 Monitoring over the Mediterranean Sea

Figure 82 and figure 83 are the same as in section 7.2.2 over the Mediterranean Sea.

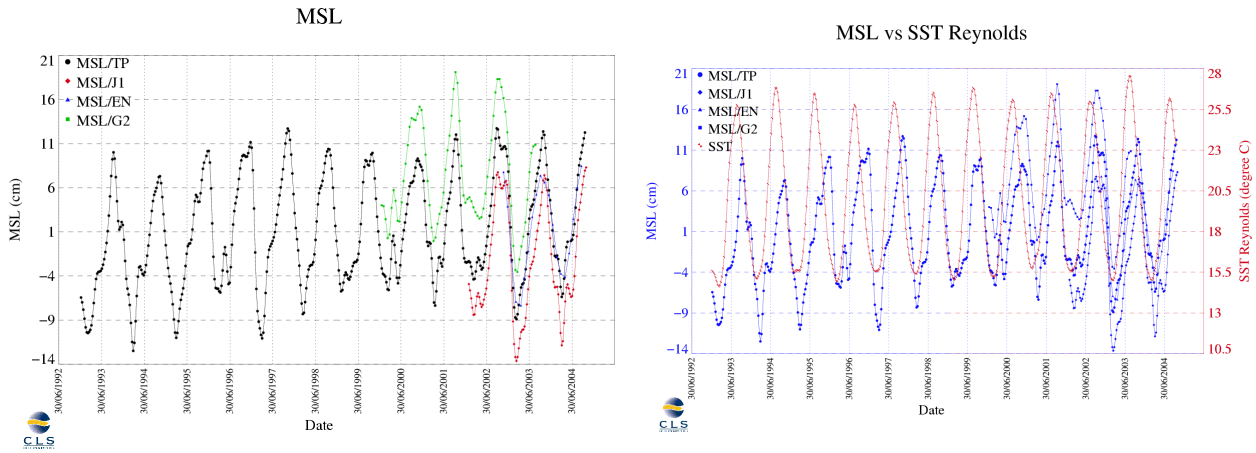

Figure 82: *MSL and SST over the Mediterranean Sea and over the T/P period*

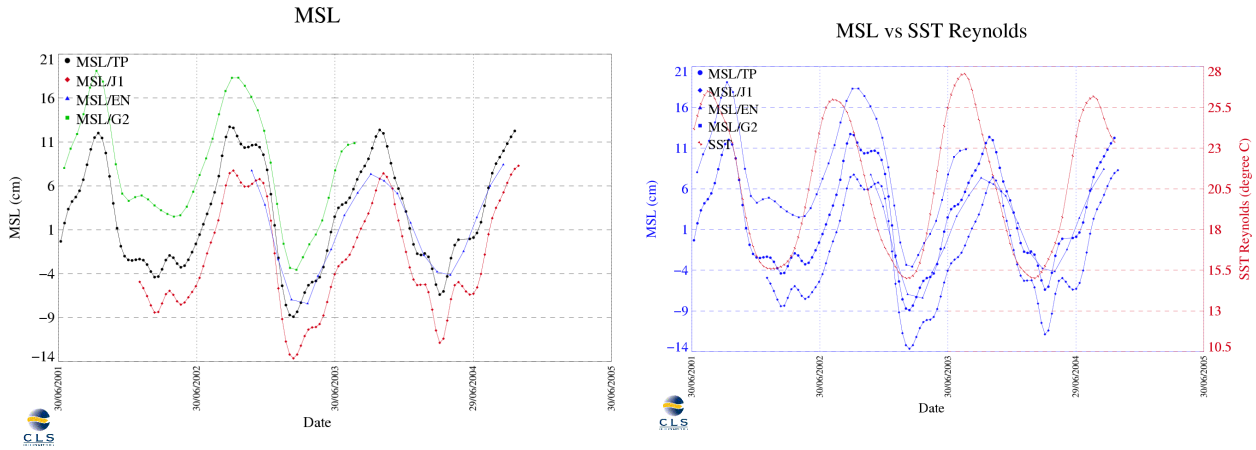

Figure 83: *MSL and SST over the Mediterranean Sea and over the Jason-1 period*

7.2.11 Monitoring over the Black Sea

Figure 84 and figure 85 are the same as in section 7.2.2 over the Black Sea.

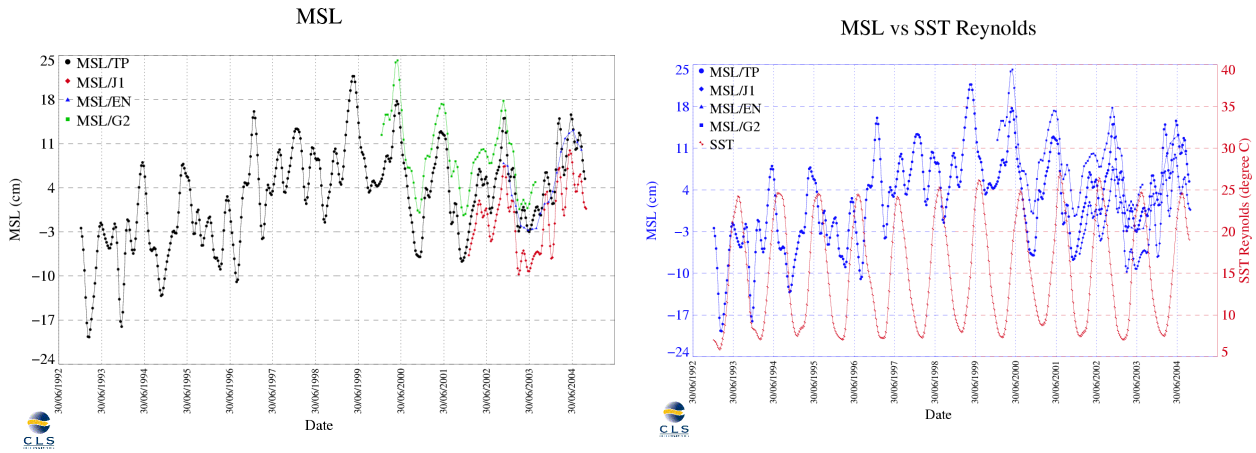

Figure 84: *MSL and SST over the Black Sea and over the T/P period*

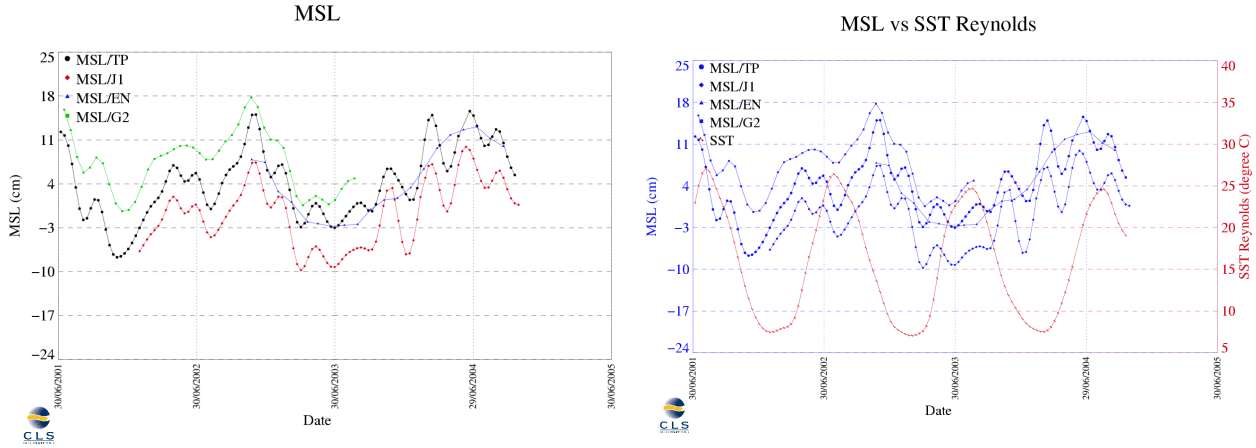

Figure 85: *MSL and SST over the Black Sea and over the Jason-1 period*

7.3 Spatial MSL and SST slopes

7.3.1 Methodology

In order to monitor the MSL, the spatial MSL slopes have been calculated. The SLA grids (2x2 degree bins) have been computed cycle per cycle, and the slope has been performed on each grid point. As for time analysis, 60 day, semi-annual and annual signals have been removed before estimating the slopes. Then, the MSL slopes have been mapped for each mission. These maps are used to compare the MSL slopes between each altimetrer mission. This allows us to detect potential local drifts.
Besides the SST slopes has been computed in a same way in order to correlate them with the MSL slopes.

7.3.2 Spatial MSL slopes over Jason-1 period

The MSL slopes has been plotted for Jason-1 (on the right) and T/P (on the left) over Jason-1 period in figure 86. The MSL trends seen by the two satellites seem very homogenous that is shown by the bottom map where the difference between the 2 previous maps have been plotted. However, differences can be observed in some areas: they are under investigation.

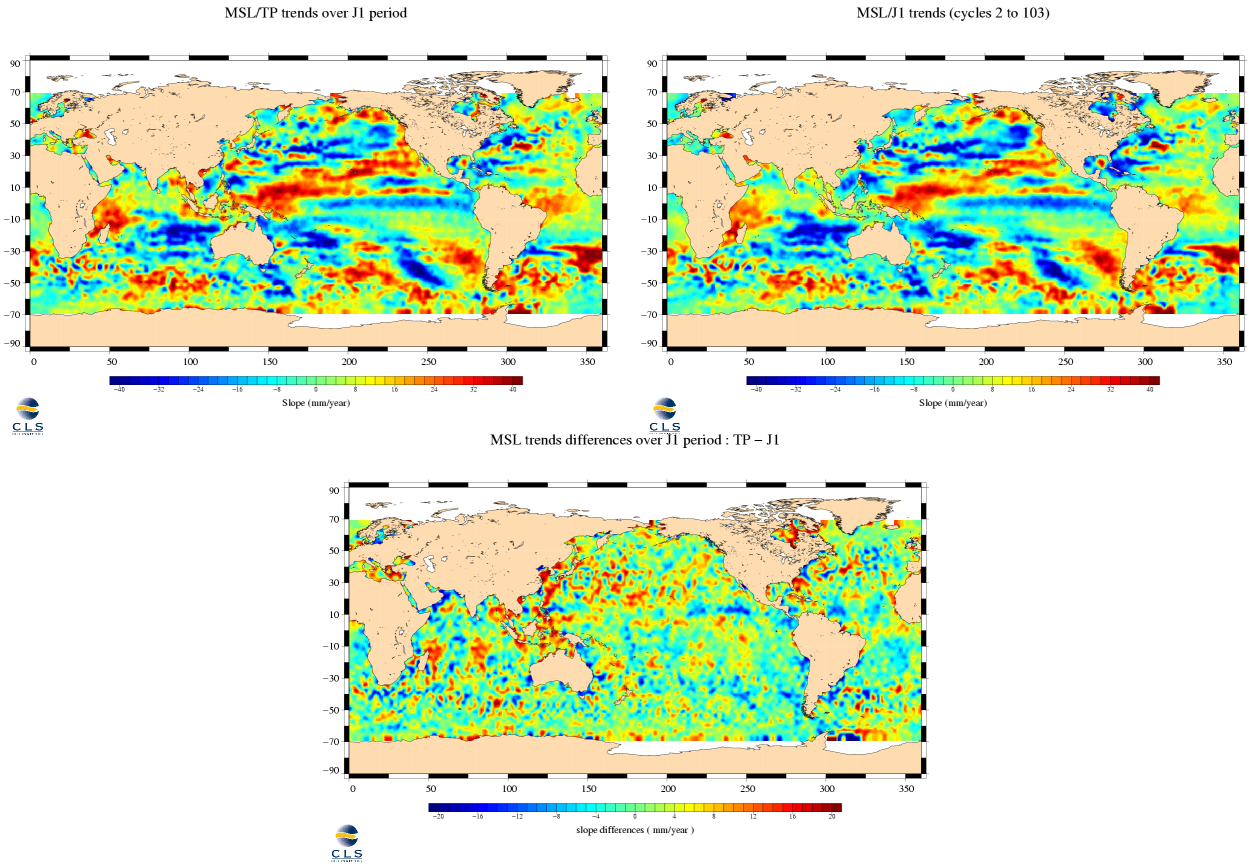

Figure 86: *MSL slopes over Jason-1 period for T/P (left) and Jason-1 (right), MSL slope differences between Jason-1 and T/P (bottom)*

7.3.3 Spatial MSL slopes over Envisat period

Same work has been performed over Envisat period using Envisat data in figure 87. The 3 maps seem very homogenous.
In figure 88, the slope differences between each mission have been plotted. They allow us to observe differences in equatorial area between T/P and Envisat, and between T/P and Jason-1. These differences are not visible between Envisat and Jason-1. Investigations are on-going to understand the reasons of this observation.

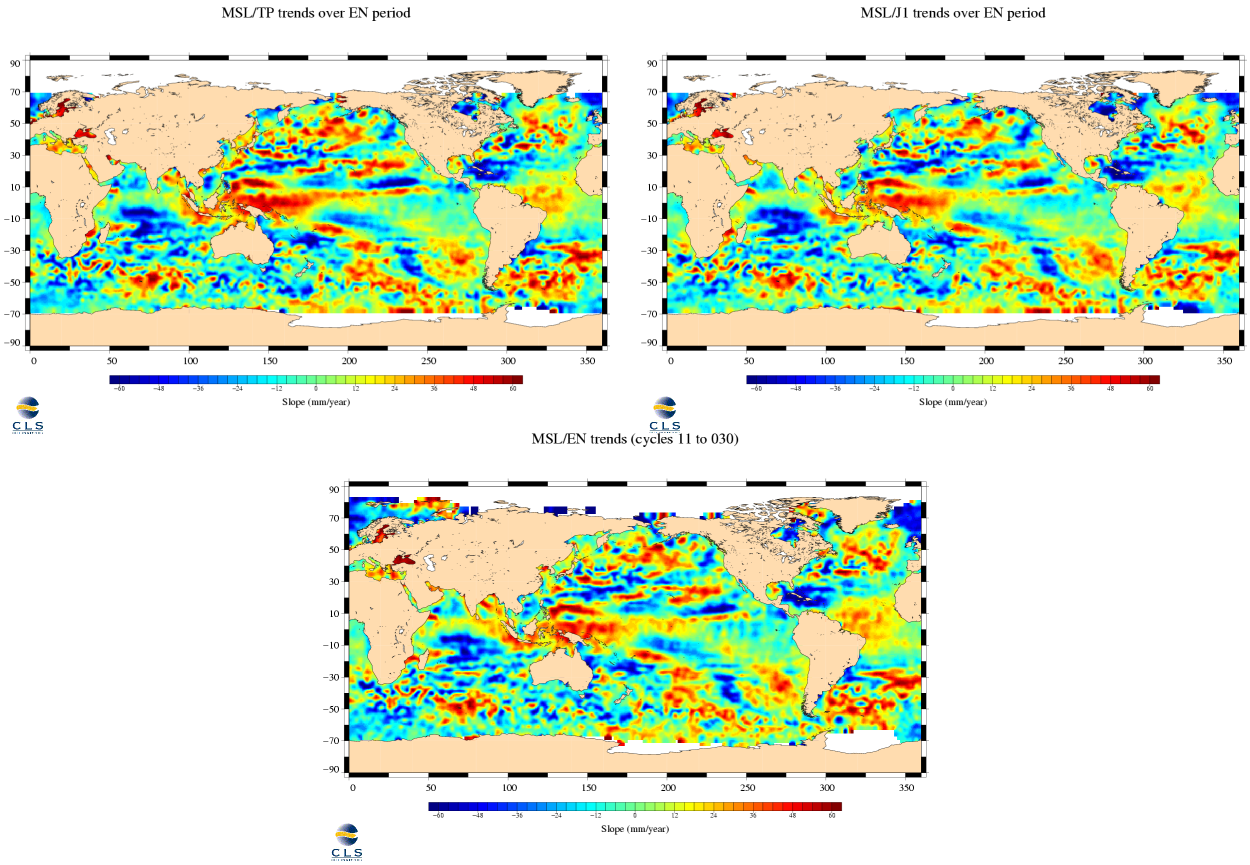

Figure 87: *MSL slopes over Envisat period for T/P (left), Jason-1 (right) and Envisat (bottom)*

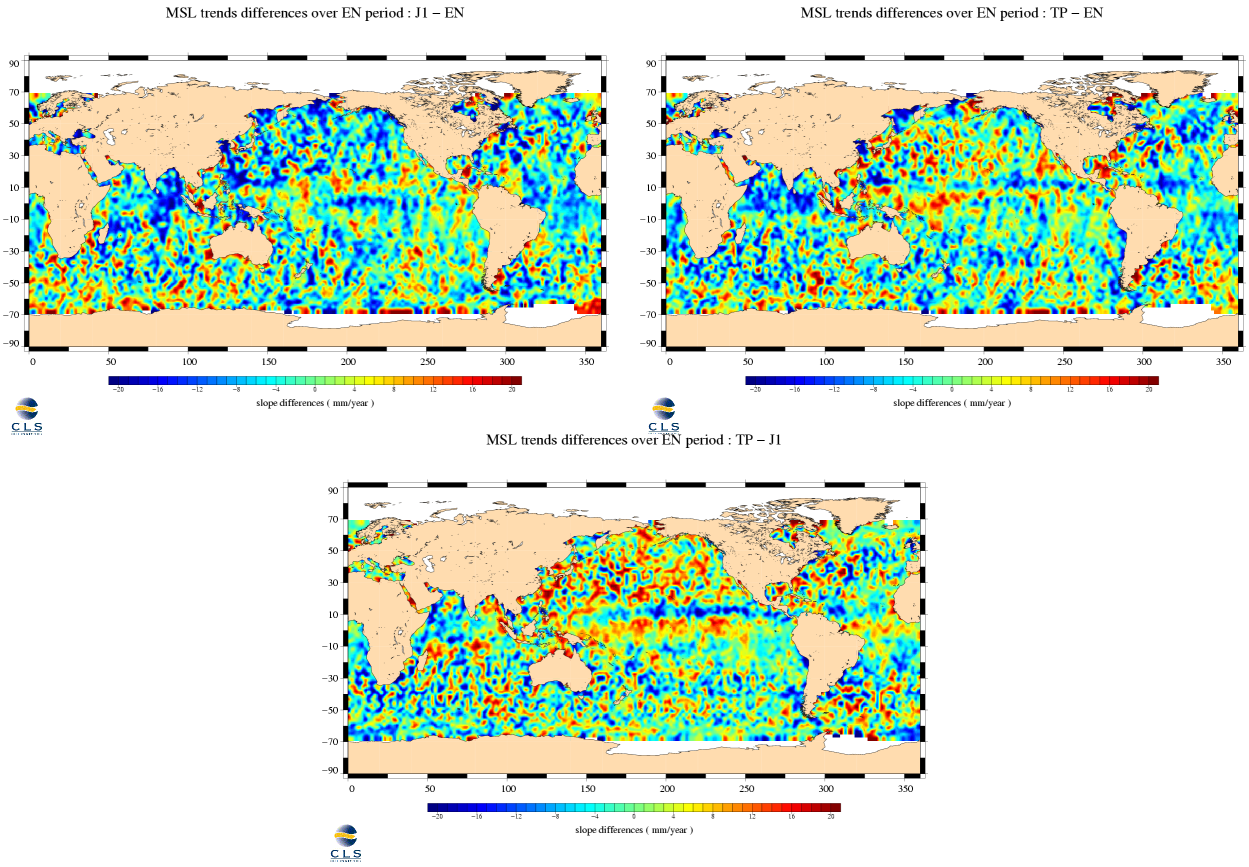

Figure 88: *MSL slopes differences over Envisat period between Jason-1 and Envisat (left), T/P and Envisat (right) and T/P and Jason-1 (bottom)*

7.3.4 Spatial SST and MSL slopes for T/P

The T/P MSL slopes have been mapped in figure 89 on the left. In order to correlate the MSL and the SST, the SST slopes have been plotted in the same figure on the right.
12 years of T/P data have been used to estimate the slopes; this allows us to have a good estimation of the local MSL trends. The adjustment errors of the MSL and the SST slopes are mapped in the figure 90.

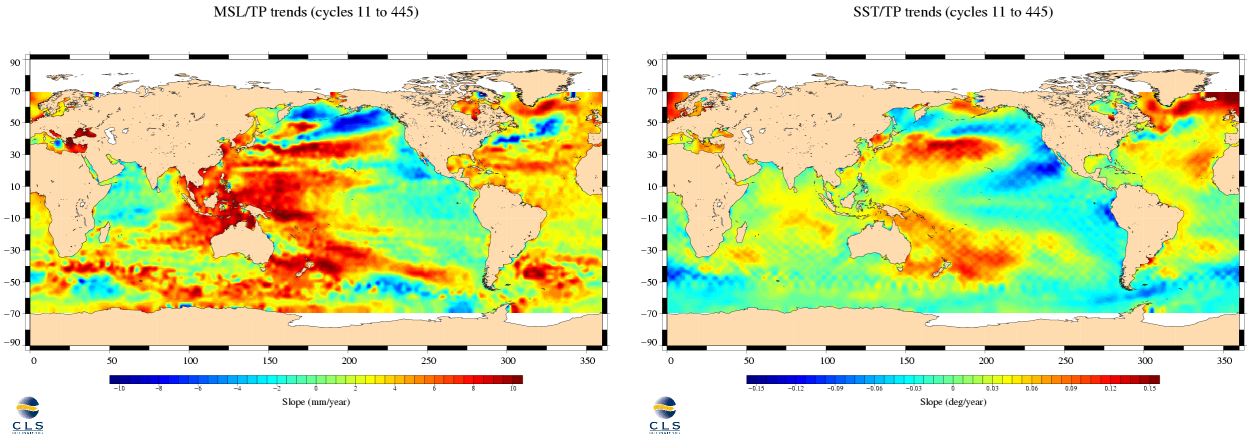

Figure 89: *T/P MSL and SST slopes over 12 years*

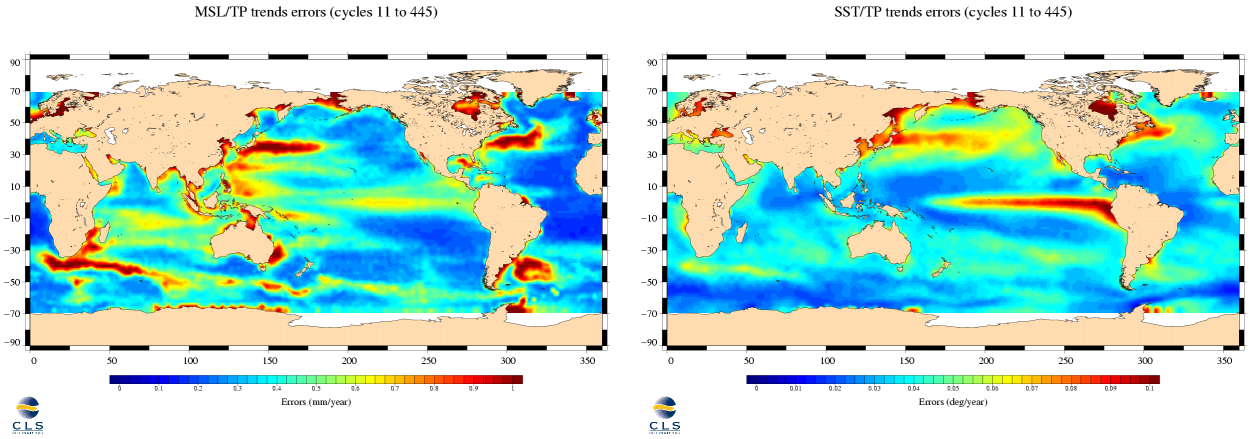

Figure 90: *Adjustment errors of T/P MSL and SST slopes over 12 years*

8 Conclusion

Since the beginning of the TOPEX/Poseidon mission, constant efforts have been made in all the TOPEX/Poseidon system components to reach the major goals in terms of mesoscale study and SSH long term monitoring. Data quality and precision have been maintained thanks to instrumental survey, precise orbit determination, updated ground processing and careful data analysis. Calibration and validation activities, operated in line with the data production but also as a long term survey, represent a valuable contribution to the data quality maintenance and improvement.

The TOPEX/Poseidon mission thus provides an unprecedented long altimeter measurement series, allowing long term mean sea level trends determination and climate change studies. Continuity in data quality and precision is mandatory to achieve these goals.

TOPEX Side-A altimeter troubles, due to instrument aging, were detected. But switching to the Side-B redundant altimeter allowed to carry on with the mission, even if it produced two discontinuous time series. However, precise calibration activities give means to link A and B series with the needed accuracy, as it is done between TOPEX and Poseidon altimeters. Other sources of error have risen during the mission (e.g. TMR troposphere correction drift, DORIS ionosphere correction for Poseidon). Each individual parameter has thus to be carefully verified in the long term as part of the global system accuracy. For the last years, the tape recorder performances has continued to decline. Thus it was decided on cycle 444 to remove from service the tape recorder. Science data recovery requirements will now be met through increased TDRSS (Data relay Satellite System) real-time contacts.

During more than 12 years, continuous data quality assessment has proven to be essential to detect potential system errors or drifts and to maintain the TOPEX/Poseidon usefulness for oceanography. Now it also allows linking TOPEX/Poseidon measurements to the Jason-1 mission and this way to ensure the continuity of precise altimetry. The cross-calibration exercise has been performed during the Jason-1 verification phase. From that, is has been decided to move the TOPEX/Poseidon ground track westward at one half the nominal track intervals. This highly improved ocean sampling opens a new area of precise altimeter measurements, with large expected improvements for instance, in ocean studies, tide modeling, or coastal applications.

References

[1] AVISO User Handbook. Merged Topex/Poseidon Products (GDR-Ms), AVINT-02-101-CN.

[2] AVISO/CALVAL. Validation du cycle 267. CLS.OC/NT/98.60. Version 267, 14 Janvier 2000.

[3] Berthias, J.P., Transition to ITRF2000, internet communication, 16 May 2001.

[4] Blusson, A, personal communication, March 2002.

[5] Callahan, P.S., New TOPEX Science Processing, internet communication to topex-poseidon@omnet.com, 2 September 1998.

[6] Callahan, P.S., Revised GDRs coming, internet communication to topexposeidon@omnet.com, 19 January 2000.

[7] Callahan, P.S., Change in Sigma0 and Reprocessing Cycles 277-284, internet communication to topex-poseidon@omnet.com, 3 August 2000.

[8] Callahan, P.S., Cycle 193 (Day 349) data, internet communication to topexposeidon@omnet.com. 20 January 1998.

[9] Callahan, P.S., TOPEX clock rollover, Internet communication to TOPEX/Poseidon@omnet.com, 29 April 2001.

[10] Chelton, D.B.. The Sea State Bias in altimeter estimates of sea level from collinear analysis of TOPEX data. *J. Geophys. Res.*, **99, 24995-25008**, 1994.

[11] Dorandeu, J., Impact sur le niveau moyen des mers d'un "biais en z" appliqué sur l'orbite. AVISO/CALVAL report. CLS.DOS/NT/98.89, 1998.

[12] Dorandeu, J., P.Y Le Traon, M.H. Calvez, P. Gaspar, F. Ogor. Validating TOPEX/Poseidon Data, AVISO/CALVAL yearly report. CLS/DOS/NT/97.042/2, 1997.

[13] Dorandeu, J., AVISO, "Side-B TOPEX Altimeter evaluation", AVI-NT011-317-CN, Edition 1.0, 1999.

[14] Dorandeu, J., M-H De Launay, F. Mertz and J. Stum, AVISO/CALVAL yearly report, 8 years of TOPEX/Poseidon data (M-GDRs), February 2001.

[15] Dorandeu, J., F. Mertz and J. Stum. Note on ERS-2 Sigma0 Variations since January 2000. CLS.DOS/NT/00.286, 2000.

[16] Dorandeu, J., and P-Y. Le Traon, Effects of Global Mean Atmospheric Pressure variations on Mean Sea Level Changes from TOPEX/Poseidon, *J. Atmos. Oceanic technology*, **1279-1283**, 1999.

[17] CERSAT Altimeter & Microwave Radiometer ERS Products User Manual. C2MUT-A-01-1F, version 2.2, 1996.

[18] Gaspar, P., F. Ogor, P-Y. Le Traon and O-Z. Zanife, Estimating the Sea State Bias of the TOPEX and POSEIDON altimeters from crossover differences, *J. Geophys. Res.*, **99, C12, 24981-24994**, 1994.

[19] Gaspar, P., S. Labroue and F. Ogor. Improving nonparametric estimates of the sea state bias in radar altimeter measurements of sea level, *J. Atmos. Oceanic Technology*, **19, 1690-1707**, October 2002.

[20] Hancock, D.W., Alt-B bad measurements, Internet communication to TOPEX Side-B CAL/VAL group, 19 August 1999.

[21] Hancock, D.W., Alt-B bad measurements, Internet personal communication, 23 August 1999.

[22] Hancock, D.W., TOPEX Altimeter Performance 1997 Day 349 during ASTRA Outage, internet communication cited in [8], 20 January 1998.

[23] Hayne, G.S., and D.W. Hancock III, Observations from Long-Term Performance Monitoring of the TOPEX Radar Altimeter. TOPEX/Poseidon/Jason-1 Science Working Team Meeting, Keystone, Colorado, 1998.

[24] Hayne, G.S. and D.W. Hancock III, TOPEX Side B Calibration Table Adjustments, 7 November 2000.

[25] Hayne, G.S. and D.W. Hancock III, Observations from long-term Performance Monitoring of the TOPEX Radar Altimeter, TOPEX/Poseidon/Jason-1 Science Working Team Meeting, Keystone, Colorado, 1998.

[26] Hayne, G. S. and D.W. Hancock III, The TOPEX Sigma0 Calibration Table and its Updates, 14 March 1997.

[27] Hayne, G. S. and D.W. Hancock III, TOPEX Sigma0 Calibration Table History for all Side A Data, 27 July 1999. Available on the internet at http://topex.wff.nasa.gov/Sigma0Cal_A_All.pdf

[28] Hayne, G. S. and D.W. Hancock III, TOPEX Side B Calibration Table Adjustments : March 2002 Update, 08 March 2002. Available on internet at http://topex.wff.nasa.gov/mar_02_update_sig0_cal_tbl.pdf

[29] Hayne, G.S., TOPEX Side-B Sigma0, etc, personal communication, 15 June 2000.

[30] Keihm, S.J., V. Zlotniki and C.S. Ruf, TOPEX Microwave Radiometer Performance Evaluation, 1992-1998. *IEEE Trans. Geosci. Remote Sensing*, **Vol. 38, pp. 1396-1386**, May 2000.

[31] Le Traon, P.-Y., J. Stum, J. Dorandeu, P. Gaspar and P. Vincent. Global statistical analysis of TOPEX and POSEIDON data. *J.Geophys. Res.*, **99 : 24619-24631**, 1994.

[32] Le Traon, P.-Y., P. Gaspar, J. Dorandeu, F. Ogor. Amélioration des performances des altimètres TOPEX/POSEIDON et ERS. Contrat 856/CNES/95/1523/01, 1996.

[33] Mertz, F., J. Dorandeu and J. Stum, Long term monitoring of the OPR altimeter data quality. Report of IFREMER contract n°01/2.210 374, January 2002.

[34] Mertz, F., N. Tran, S. Labroue, J. Dorandeu, V. Marrieu, J. Savaresse, ERS2 OPR data quality assessment (Long-term monitoring and particular investigations), Annual report 2004 of task 2 of IFREMER Contract No 04/2.210.714., CLS.DOS/NT/04.277, January 2005.

[35] Mertz F., J. Dorandeu, J. Stum, Validation and long-term monitoring of reprocessed (version 6) phase C ERS-1 OPR data. CLS.DOS/NT/02.539, March 2002.

[36] Morel, L., C. Boucher, P. Willis, J.P. Berthias. Terrestrial Reference Frame Differences for TOPEX POSEIDON, SWT Jason, Keystone, USA, 1998.

[37] Obligis, E., L. Eymard and N. Tran, ERS2/MWR drift evaluation and correction, CLS.DOS/NT/03.688, 2003.

[38] Queuffeulou P., P. Long-term comparison of ERS, TOPEX and Poseidon altimeter wind and wave measurements, 1998.

[39] Ruf, C.S., 2002. TMR Drift Correction to 18 GHz Brightness Temperatures, Revisited. Report to TOPEX Project, June 2002.

[40] Ruf, C.S. Detection of calibration drifts in spaceborne microwave radiometers using a vicarious cold reference. *IEEE Trans. Geosci. Remote Sensing*, **vol 38, pp 44-52**, Jan 2000.

[41] Stum, J., A comparison of brightness temperatures and water vapor path delays measured by the TOPEX, ERS-1 and ERS-2 microwave radiometers, *J. Atmos. Oceanic Technology*, **Vol 15, 987-994**, 1998.

[42] Scharroo R., J. L. Lillibridge, and W. H. F. Smith, Cross-Calibration and Long-term Monitoring of the Microwave Radiometers of ERS, TOPEX, GFO, Jason-1, and Envisat, **Marine Geodesy, 27:279-297**, 2004.

[43] TOPEX/POSEIDON daily status, internet communication for cycle 285, 12 Juny 2000.

[44] TOPEX/POSEIDON daily status, internet communication for cycle 304, 14 December 2000.

[45] TOPEX/POSEIDON daily status, internet communication for cycle 324, 2 July 2001.

[46] TOPEX/POSEIDON daily status, internet communication for cycle 332, 24 September 2001.